Determination of Dose Distribution of Ruthenium-106 Ophthalmic Applicators

Rungdham Takam, B.Sc.

Thesis submitted for the degree of
Master of Science (Medical Physics)
In the University of Adelaide
Department of Physics and Mathematical Physics

Supervisors:

Dr. Eva Bezak
Dr. John R. Patterson

August 2003

Contents

ABSTRACT.....vi

DECLARATION.....viii

ACKNOWLEDGMENTS.....ix

PREFACE.....xii

1. RUTHENIUM-106 OPHTHALMIC APPLICATORS.....1

1.1. Physical properties of ruthenium-106 ophthalmic applicators.....1

1.2. Nuclear properties of ruthenium-106 applicators.....4

1.3. Dosimetry of ruthenium-106 applicators.....7

1.4. Outline of the current project.....11

2. GENERAL PRINCIPLE OF THERMOLUMINESCENT DOSIMETER.....13

2.1. Introduction.....13

2.2. Basic phenomenon of thermoluminescence.....14

2.2.1. Characteristics of TLD phosphors.....15

2.2.2. Glow curves.....15

2.2.3. Sensitivity.....18

2.2.4. Dose response curves.....19

2.2.5. Energy response.....20

2.2.6. Thermal fading.....20

2.2.7. Annealing conditions.....21

2.3. Characteristics of commonly used TL phosphors.....21

2.3.1. LiF:Mg,Ti.....21

2.3.2. LiF:Mg,Cu,P.....23

2.3.3. BeO.....25

2.3.4. $CaSO_4$:Dy.....26

2.4. Thermoluminescence readout instrumentation.....28

2.4.1. Dosimeter heating system.....29

2.4.2. Light collection unit.....29

2.4.3. Light measuring systems.....29

2.5. Beta radiation dosimeter.....31

2.6. Conclusion.....32

3. STUDY OF BASIC CHARACTERISTICS OF $CaSO_4$:Dy TLD.....34

3.1. Introduction.....34

3.2. General properties of $CaSO_4$:Dy TLDs.....35

3.2.1. Reading reproducibility.....35

3.2.2. Dose response linearity.....35

3.2.3. Sensitivity.....36

3.2.4. Irradiation-orientation dependence and reading-orientation dependence.....36

3.3. Experimental instruments and procedures.....36

3.3.1. Experimental instruments.....36

3.3.1.1. $CaSO_4$:Dy TLDs.....36

3.3.1.2. Radiation sources.....37

3.3.1.3. TLD reader.....37

3.3.1.4. Annealing oven.....38

3.3.1.5. Effective point of measurement.....38

3.3.2. Experimental procedures.....39

3.3.2.1. Irradiation and reading of TLD samples.....39

3.3.2.2. Measurement of dose response sensitivity and reproducibility of $CaSO_4$:Dy TLDs.....40

3.3.2.3. Measurement of dose response linearity of $CaSO_4$:Dy TLDs.....42

3.3.2.4. Observation of orientation and reading dependence of $CaSO_4$:Dy TLDs.....43

3.4. Experimental results.....44

3.4.1. $CaSO_4$:Dy TLD dose response sensitivity.....44

3.4.2. $CaSO_4$:Dy TLD dose response reproducibility measurement results.....45

3.4.3. $CaSO_4$:Dy TLD dose response linearity measurement results.....46

3.4.4. Measurement results of irradiation-orientation and reading-orientation dependence of $CaSO_4$:Dy TLDs.....48

3.4.4.1. Results of irradiation-orientation dependence experiment.....48

3.4.4.2. Results of reading-orientation dependence experiment.....50

3.5. Discussion of experimental results.....51

3.5.1. Dose response sensitivity of $CaSO_4$:Dy TLDs.....51

3.5.2. Measurement of reproducibility of $CaSO_4$:Dy TLDs.....51

3.5.3. Measurement of $CaSO_4$:Dy TLD dose response linearity.....52

3.5.4. Measurement of irradiation-orientation and reading-orientation dependence of $CaSO_4$:Dy TLDs.....52

3.6. Conclusion.....53

4. MEASUREMENTS OF COB AND CCA TYPE RUTHENIUM-106 OPHTHALMIC APPLICATOR DOSE DISTRIBUTIONS.....55

4.1. Introduction.....55

4.2. Preparation and calibration of small $CaSO_4$:Dy TLDs.....56

4.3. Measurement of ruthenium-106 ophthalmic applicator dose distributions with small $CaSO_4$:Dy TLDs.....57

4.3.1. Measurement instrumentation.....57

4.3.2. Measurement procedures.....59

4.3.3. Calculation of depth dose from reading results.....64

4.4. Measurement results.....65

4.4.1. Calibration results of small CaSO4:Dy TLDs.....65

4.4.2. Results from measurements for dose distributions for a 20-mm ruthenium-106 ophthalmic applicator.....65

4.4.3. Results from the measurements for dose distribution of a 15-mm ruthenium-106 ophthalmic applicator.....69

4.5. Discussion of the experimental results.....75

4.5.1. Calibration of small $CaSO_4$:Dy TLDs.....75

4.5.2. Measurements of dose rate distribution of a 20-mm ruthenium-106 ophthalmic applicator.....75

4.6. Conclusion.....78

5. DETERMINATION OF THE DOSE RATE DISTRIBUTION USING A MOSFET DETECTOR.....79

5.1. Introduction.....79

5.2. Basic structure and principle of operation of MOSFET.....81

5.3. Experimental instrumentation.....84

5.3.1. MOSFET semiconductor dosimeter.....84

5.3.2. Eye phantom modification.....87

5.3.3. Ruthenium-106 ophthalmic applicator.....88

5.4. Experimental procedures.....88

5.5. Measurement results.....90

5.5.1. Measurement of dose response linearity.....90

5.5.2. Measurement of depth dose rate of ruthenium-106 applicator with MOSFET detector.....90

5.6. Discussion.....94

5.7. Conclusion.....95

6. SUMMARY AND CONCLUSION.....97

APPENDIX.....105

REFERENCES.....108

Abstract

Dose distributions of COB and CCA type ruthenium-106 ophthalmic applicators, of diameters 15 mm and 20 mm, respectively, were investigated using small $CaSO_4$:Dy thermoluminescent dosimeters. The $CaSO_4$:Dy TLD discs were irradiated with a 4MV linear accelerator (Varian Clinac 4/100) at the Royal Adelaide Hospital. A range of absorbed doses from 0.1 to 10 Gy was used to observe their reproducibility and linearity. This machine was selected because it provides an electron beam with an energy of approximately 1.3 MV that is close to the mean energy of beta particles produced by the decay of ruthenium-106. A TOLEDO Model 645D TLD Reader was used to readout the irradiated TLDs. It was found that these TLDs respond linearly to radiation doses up to 6 Gy above which supralinearity begins. A sensitivity factor for each TLD disc was measured and applied to subsequent readouts. Selected TLD discs were cut into small rectangular wafers with dimension of approximately 2 x 3 x 0.4 mm^3. The same method as described above was employed to obtain the sensitivity factor for each small TLD. Their relative dose response sensitivities ranged around the mean from approximately -20% to +17%.

Dose distributions of ruthenium plaques were observed by placing the small TLDs in different positions on an eye phantom. Eye phantoms were made of layers with different thicknesses and can be built up from 1 mm to 10 mm. The results showed that the radioactive layer was non-uniform on each plaque. Hot spots and cold spots were found in various positions throughout the plaques. In comparison to the depth dose values provided by the plaque manufacturer, the depth dose values measured by these small TLDs were

lower, and the percentage uncertainties were considerably improved. The highest uncertainty obtained was approximately ±10% compared with ±30% specified by the manufacturer. Determination of on-axis depth dose distributions of ruthenium-106 applicators was also conducted with the MOSFET semiconductor dosimeter. Its high sensitivity to radiation doses, instant readout and a simple measurement setup are some advantages of the MOSFET dosimeter. On-axis depth dose distributions measured with the MOSFET dosimeter were comparable with those measured with the small TLDs and those provided by the manufacturer (σ = 8%).

Declaration

This work contains no material which has been accepted for the award of any other degree or diploma in any university or other tertiary institution and, to the best of my knowledge and belief, contains no material previously published or written by another person, except where due reference has been made in the text.

I give consent to this copy of my thesis, when deposited in the University Library, being available for loan and photocopying.

SIGNED:_____ **DATE:** 1-8-2003

Acknowledgments

I wish to thank Australian Agency for International Development (AusAID), Australian Government, who gives me a great opportunity to come and study at University of Adelaide under the Australian Development Scholarship (ADS). Without their support and generosity, I would not be able to come this far to fulfill the dream of a mother to see her son getting as much education as possible.

I would like to also thank to my superiors, Mr. Poonsuk Pongpat, Director of Radiological Measurement Division (formerly Director of Health Physics Division), Mrs. Pentip Khunarak, Head of Radiological Hazard Analysis and Assessment Section, at the Office of Atomic Energy for Peace, to theirs support and help me in receiving this Australian Development Scholarship.

I am very grateful for the supervision and guidance of Dr. John R. Patterson, my supervisor. He was very helpful and supportive during my study at the University of Adelaide. In the passing two years that I have been studying at the university, I confronted several difficulties of being an overseas student. With his invaluable supervision and guidance, I can survive those hard times and be able to continue my studying. Furthermore, I also thank for his organizational and financial support in helping me to attend the conference and present my research findings and, in addition, proof reading this thesis.

I would like to thank the Royal Adelaide Hospital Departments of Radiation Oncology and Medical Physics for use of facilities. A year of completing my research project and writing my thesis would be very difficult without the supervision and guidance of Dr. Eva Bezak. With her experience and expertise in medical physics research that keep me in the right track and able to reach the aims of the research project. During this one year in doing my research project, I have gained a lot of knowledge in medical physics and research skills from Dr. Eva. Thank to her enthusiasm and willingness to provide her support and guidance in performing the experiments, writing this thesis and helping me to attend the conference and present my research report.

Thanks also to Mr. Kurt Byas for his expertise in TLD measurements. His supervision, guidance and support in performing experimental TLD measurements were invaluable. I am very appreciating for his enthusiasm and willingness to share his knowledge and friendship. The other staffs of the Medical Physics Department at the Royal Adelaide Hospital have all been very friendly and helpful, particularly Mr. Shane Hein who helped us in making the acrylic eye phantoms that were important instrument of this research experiments.

I wish to thank my colleagues at the Office of Atomic Energy for Peace, Siriluck Lumjiactas and Pennapa Kruakheo, who provide me the financial management. I would like to express my appreciate to my girlfriend, On-Anong Srasom, for giving me an inspiration, companionship and constant support from the beginning of the study until the last minute of finishing this thesis.

Finally, I would like to thank to my mother who always encourage her sons to obtain as much education as they can and become good and invaluable persons to community. I do really appreciate that and this thesis is dedicated to her.

Preface

Background

Ruthenium-106 ophthalmic applicators have been widely used for treatment of eye tumours and its clinical use has been developed for more than a decade (Taccini *et al.* 1997). It has been indicated in several reports that the treatment of those eye disorders with the ruthenium plaques (in selected cases), is an effective and reasonable method (Lim & Petrovich, 2000, and Gunduz *et al.*, 2000). Similar to other types of brachytherapy, the most important requirement for the use of ruthenium eye applicators is that the prescribed dose must be delivered to the target tissue with accuracy so an effective treatment is provided and the irradiation of healthy tissue is kept as low as possible. This important objective cannot be achieved without an understanding of the radiological characteristics of the ruthenium applicators such as dose distribution patterns in the eye ball and uniformity of the active layer (ruthenium-106) coated on the plaques. Hence, the determination of the dose distributions and uniformity of the active layer of the eye applicators should be carefully investigated. Although the radiological characteristics of the ruthenium applicators, such as absorbed dose rate and depth dose rate distribution, were provided with the purchase of the applicators, they have an uncertainty of ± 30% that is not acceptable for clinical use. Thus, an observation of the radiological characteristics of the applicators with an appropriate method providing an acceptable level of uncertainty is necessary.

Aims of the current research

Although improvements in the determination of the dose distributions of the ruthenium-106 ophthalmic applicators were achieved in previously published studies, evaluation of dose distribution characteristics of the ruthenium applicators needs be further investigated with the aim to obtain more accurate dose distribution patterns. Also, a simple and fast technique is needed to enable the routine measurement of radiation output of sources, for example to confirm the doses reported by the manufacturer (acceptance testing) or to check the integrity of the source after handling during treatments (quality assurance procedure). Some of the parameters to be investigated regularly may include the depth dose distribution (relative or absolute) along the central axis of the applicators, the horizontal dose distribution, and the homogeneity of the radioactive material distribution (ruthenium-106) in the applicators. Correspondingly, the specific aims of the presented research project include:

1. Determination of dose distribution characteristics of COB-494 and CCA-610 type ruthenium-106 applicators used for eye radiation treatments at the Royal Adelaide Hospital. Dose distribution patterns of these particular applicators in great details have not been reported previously.

2. Determination of dose distribution values (central depth dose and off-axis dose) for both mentioned ruthenium-106 applicators with an uncertainty acceptable (below 10%) for clinical use.

3. Development of a standard dosimetry method that can be used for evaluation of the dose distributions of ruthenium-106 applicators for routine quality assurance purposes.

In order to achieve this, two dosimetry methods were employed in the current work: small $CaSO_4$:Dy thermoluminescence dosimeters and a semiconductor MOSFET dosimeter (the use of which has not been so far reported in literature). Correspondingly, the structure of this thesis is as follows: The general properties of ruthenium-106 applicators and previous studies about theirs dosimetry were provided in chapter 1, the general principles of thermoluminescent dosimetry will be summarised in chapter 2, followed by the study of properties of $CaSO_4$:Dy TLD (sensitivity, dose linearity, reproducibility, etc) in chapter 3. Chapter 4 will deal with the experimental details and results of the application of small $CaSO_4$:Dy TLDs to dose investigation of Ru-106 ophthalmic applicators and chapter 5 will discuss the application of MOSFET dosimeter for determination of applicator relative depth dose curve. Finally, the results of the current work will be summarised in chapter 6.

The publications and presentations with which the author has been participated during the course of this research are:

Conference Presentations

Takam, R., Bezak, E. & Byas, K. (2002). Determination of Dose Distributions of Ruthenium-106 Ophthalmic Applicators. **15th National Congress of the Australian Institute of Physics, AIP, July 8 – 11, 2002, Sydney.**

Chapter 1

Ruthenium-106 Ophthalmic Applicators

1.1. Physical properties of ruthenium-106 ophthalmic applicators

Radioactive ophthalmic applicators, for example, Palladium-103, Strontium-90/Yttrium-90 and Iodine-125, have been widely used in radiotherapy for over 25 years for the treatment of tumours of the eyes such as retinoblastoma and choroid melanoma. Use of Ruthenium-106 applicators is relatively new as they have been used clinically for about a decade (Taccini *et al.*, 1997) and clinical papers have only more recently reported on their effectiveness in treatment of the above mentioned eye tumours (Lim & Petrovich, 2000, Gunduz *et al.*, 2000). Nowadays, Ruthenium-106 has become the preferred applicator due to its higher energy beta radiation with maximum energy of 3.54 MeV compared to 2.25 MeV for the Sr-90/Y-90 source (Binder *et al.*, 1990). It can therefore be used for treatments at larger depths in tissue.

Ruthenium-106 applicators are products of BEBIG Isotopen-und Medizintechnik GmbH, Germany. The plaques are hemispherically shaped with radius (R_c) of 12 mm to 14 mm (Figure 1.1) and are made of silver. A thin film of ruthenium-106 is electrolytically plated onto the concave side of the silver shell. The active surface is then covered with a 0.1 mm thick layer of silver, creating a leak-tight sealed beta source. The ruthenium-106 applicators are made available in various types as listed in the Table 1.1. The geometric shapes of the applicators are shown in Figure 1.2. The applicators are produced with initial activities between 12 and 37 MBq resulting in dose rates of approximately 5 to 12 Gy/h at the centre of the applicator (BEBIG Isotopen Germany, 1999, Binder *et al.*, 1990).

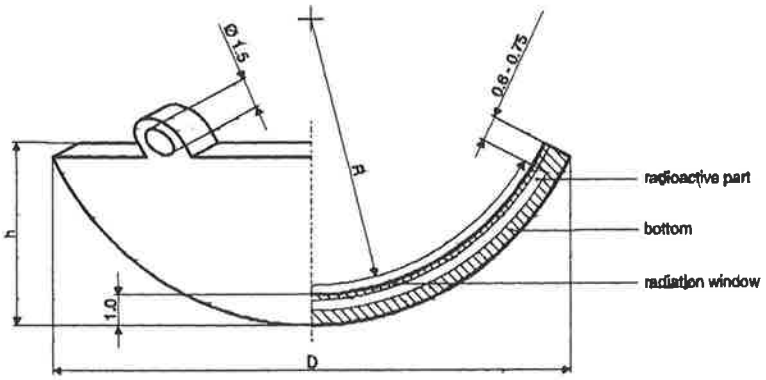

Figure 1.1 A schematic of the geometry of ruthenium-106 applicator.
(BEBIG Isotopen, Germany)

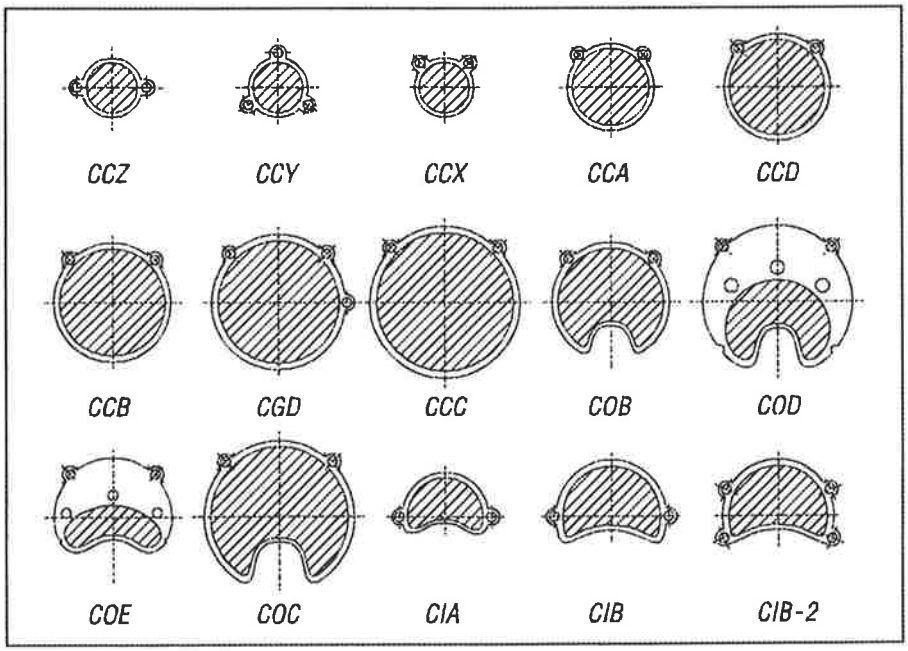

Figure 1.2 The geometric shapes of ruthenium-106 applicators. (BEBIG Isotopen, Germany)

Table 1.1 Commercially available types of ruthenium plaques (BEBIG Isotopen GmbH)

Type	Nominal Activity	Diameter (D)	Height (H)	Radius (R)
	MBq	mm	mm	mm
CCZ	7.8	11.5	2.3	12
CCY	7.8	11.5	2.3	12
CCX	7.8	11.5	2.3	12
CCA	11.1	15.5	3.3	12
CCD	13.3	17.8	4.3	12
CCB	16.7	20.0	5.5	12
CGD	21.5	22.5	7.5	13
CCC	22.2	25.0	8.3	13
COB	14.4	20.0	5.5	12
COD	18.5	24.8	7.0	14
COE	8.9	20.0	5.5	12
COC	21.5	24.8	7.0	14
CIA	9.6	15.5	3.3	12
CIB	15.5	20.0	5.5	12
CIB-2	15.5	20.0	5.5	12

1.2. Nuclear properties of ruthenium-106 applicators

Ruthenium-106 is a radioactive nucleus that disintegrates with half-life of 368.2 days via β^--decay into rhodium-106. The daughter product is again radioactive and almost immediately β^--decays (half-life of 29.9 s) into a stable nucleus of palladium-106. The nuclear decay schemes of both the isotopes are shown in Figures 1.3 and 1.4 together with average energies of β-particles emitted, E(i), and corresponding yields, y(i). The properties of radiation emitted following Rh-106 decay are summarized in Table 1.2.

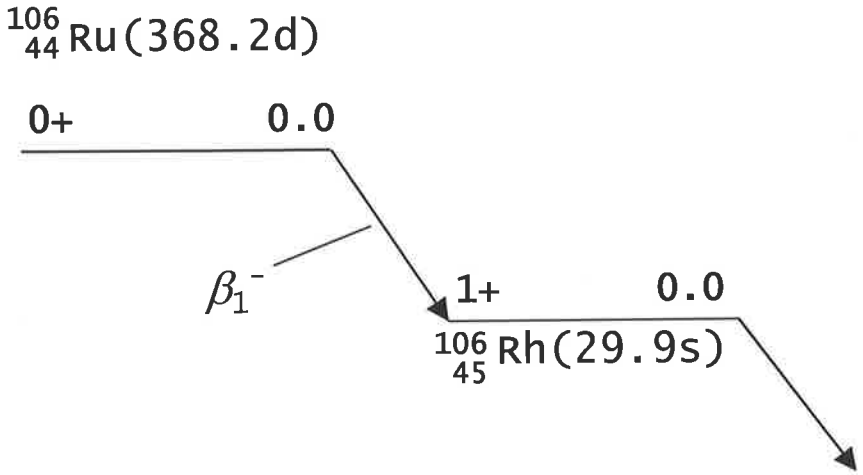

DECAY MODE: β^-

RADIATION EMITTED	YIELD: y(i) $(Bq\text{-}s)^{-1}$	AVERAGE ENERGY: E(i) (MeV)	Y(i) x E(i)
β_1^-	1.00E 00	1.003E-02	1.00E-02

THE RHODIUM-106 DAUGHTER IS RADIOACTIVE (see Figure 1.4)

Figure 1.3 A schematic diagram showing the decay scheme of ruthenium-106 and details of emitted decay radiation (average energy, E(i), and yield, y(i), of beta particles). (The International Commission on Radiological Protection, 1983)

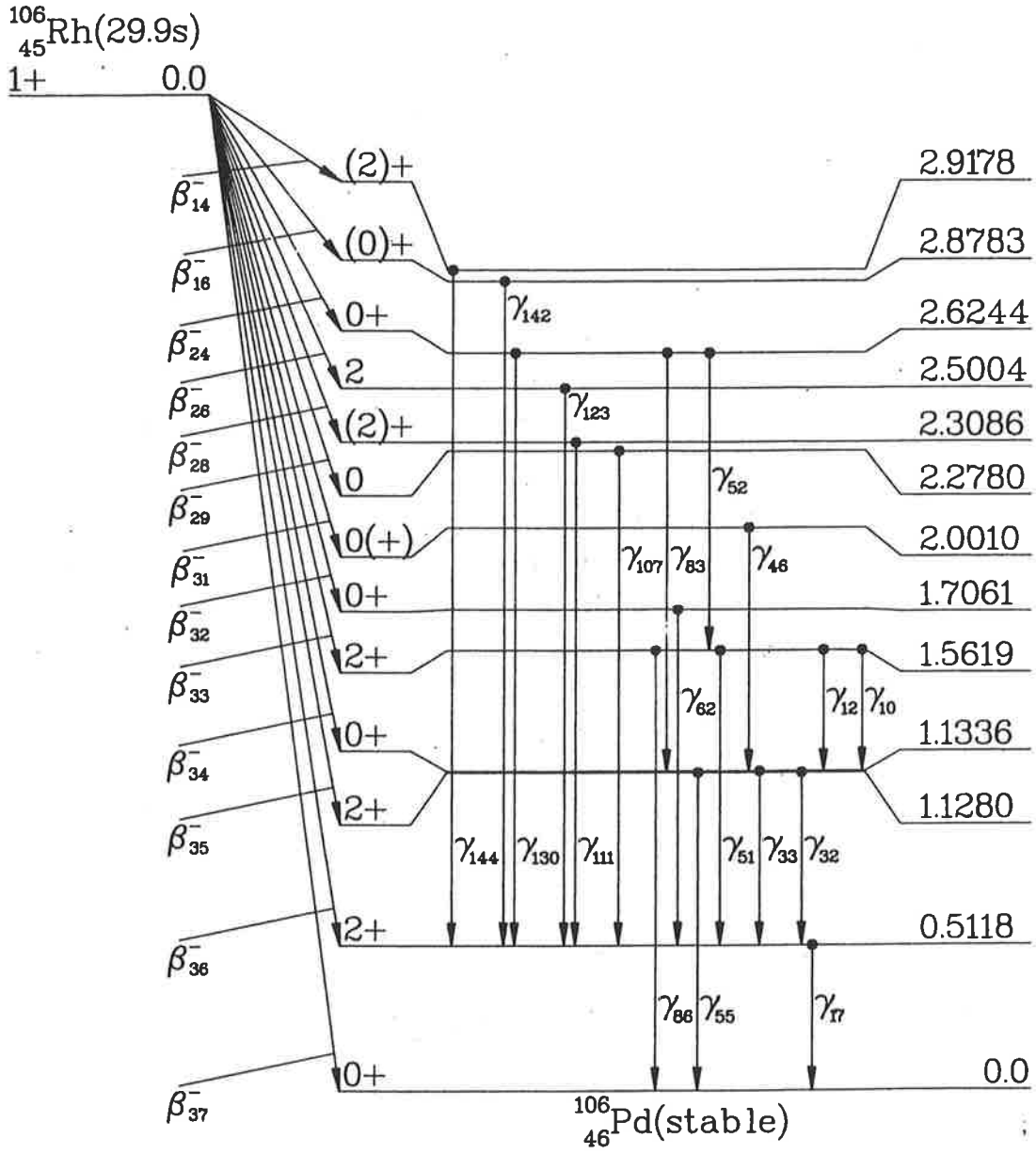

45-RHODIUM-106

HALFLIFE = 29.9 SECONDS

DECAY MODE(S): β^-

Figure 1.4 A schematic diagram showing the β and γ decay scheme of rhodium-106, a radioactive daughter of ruthenium-106.

(The International Commission on Radiological Protection, 1983)

Table 1.2 The average energies, E(i) and yields, y(i), of emitted β–particles and γ-rays emitted after rhodium-106 disintegration. (The International Commission on Radiological Protection, 1983)

RADIATION		y(i) $(Bq\text{-}s)^{-1}$	E(i) (MeV)	y(i) x E(i)
β^-	31	4.13E-03	5.817E-01*	2.40E-03
β^-	33	1.70E-02	7.792E-01*	1.32E-02
β^-	34	9.69E-02	9.761E-01*	9.46E-02
β^-	35	5.30E-03	9.787E-01*	5.18E-03
β^-	36	8.39E-02	1.267E 00*	1.06E-01
β^-	37	7.88E-01	1.508E 00*	1.19E 00
γ	10	9.27E-04	4.279E-01	3.97E-04
γ	12	4.74E-04	4.350E-01	2.06E-04
γ	17	2.06E-01	5.118E-01	1.05E-01
γ	32	7.00E-03	6.162E-01	4.32E-03
γ	33	9.81E-02	6.218E-01	6.10E-02
γ	46	4.16E-03	8.731E-01	3.63E-03
γ	51	1.46E-02	1.050E 00	1.54E-02
γ	52	2.47E-04	1.062E 00	2.63E-04
γ	55	3.85E-03	1.128E 00	4.35E-03
γ	62	5.27E-04	1.194E 00	6.30E-04
γ	83	2.57E-04	1.496E 00	3.85E-04
γ	86	1.46E-03	1.562E 00	2.28E-03
γ	107	2.33E-04	1.766E 00	4.11E-04
γ	111	2.53E-04	1.797E 00	4.55E-04
γ	123	2.20E-04	1.988E 00	4.38E-04
γ	130	3.21E-04	2.113E 00	6.79E-04
γ	142	2.14E-04	2.366E 00	5.07E-04
γ	144	1.24E-04	2.406E 00	2.97E-04
LISTED X, γ AND γ± RADIATION				2.01E-01
OMITTED X, γ AND γ± RADIATIONS**				3.86E-03
LISTED β, ce AND Auger RADIATIONS				1.41E 00
OMITTED β, ce AND Auger RADIATIONS**				2.32E-03
LISTED RADIATIONS				1.61E 00
OMITTED RADIATIONS**				6.19E-03

* AVERAGE ENERGY (MeV)
** EACH OMITTED TRANSITION CONTRIBUTES <0.100% TO $\sum y(i) \times E(i)$ IN ITS CATEGORY

THE PALLADIUM-106 DAUGHTER IS STABLE

As can be seen from Table 1.2, rhodium-106 is the main source of beta particles and gamma radiation. The electron spectrum of Ru-106 is very soft and has a maximum energy of 39 keV, whereas in the subsequent disintegration of Rh-106, the mean energies of the continuous beta spectra for the three transitions with the highest yields are 1.5 MeV (79%), 0.97 MeV (9.7%) and 1.27 MeV (8.4%). The maximum energy of β-particles is 3.5 MeV (Sanchez-Reyes *et al.*, 1998). Gamma rays are also radiated in the decay of Rh-106. Their energies range from 0.5 MeV up to 2.4 MeV, however their total yield is below 34% (with 0.5 MeV γ-ray accounting for 20%). The radiations released during the decay of ruthenium-106 to its stable daughter, Pd-106, make it suitable for the treatment of eye tumours. The energy range of emitted β- particles enables an absorbed dose to be delivered to tissue of the eye up to depths of 8 mm. In addition, most of the accompanying gamma rays have quite low energies (0.5 MeV) and much lower yields than beta particles, consequently giving rise to small radiation doses only within and beyond the eye tissue. Moreover, the relatively long half-life of Ru-106 reduces the necessity for frequent source replacements and therefore costs.

1.3 Dosimetry of ruthenium-106 applicators

The radiation dose delivery in brachytherapy must be carried out with accuracy (the effect of systematic errors) and precision (reproducibility) so that an adequate radiation dose is delivered to target (tumour) tissue while the healthy tissue is kept non-irradiated. Obviously, this requirement must also be fulfilled during Ru-106 applications. However, this objective cannot be achieved without the knowledge of the radiological characteristics of the ruthenium-106 applicators. The radiological properties that should be investigated are the dose distribution pattern in the eye tissue and the uniformity of the active layer (Ru-106) coated on to the plaque.

The plaque manufacturer, BEBIG, performed four measurements at various depths up to 5 mm in a water phantom and a planar measurement at 17 and 9 positions on the plaque surface for 20 mm and 15 mm plaques respectively, using a small scintillation detector. However, the relative deviations of the central axis values provided by the manufacturer are 30% - too high to provide an accurate radiotherapy treatment. As a result, over the last few years several reports have been published on this issue, using both experimental and theoretical (e.g. Monte Carlo) techniques to determine a more precise dose distribution. Comprehensive experimental data is difficult to obtain due to the rather short range of the beta radiations and existence of high dose gradients at small clinically relevant distances. The small size of the sources presents another challenge, as the measuring volume (or spatial resolution) of detectors used must be small enough to avoid significant averaging of the doses across the treatment plane at a particular depth as well as averaging over the treatment depths.

Binder *et al.* (1990) performed a central axis depth dose measurement for CCB-134 and CCB-144 Ru-106 applicators using small LiF Thermo-Luminescent Dosimeters (TLD). Planar dose distribution at 1 mm depth into the eye phantom was also measured. Other depths were not investigated. These authors found the dose variations of up to 40 % across the horizontal plane.

Davelaar *et al.* (1992) set up an experiment using an extrapolation ionisation chamber to measure depth dose in tissue-equivalent plastic disks. The differences in the percentage depth doses along the central axis in the phantom in comparison to those of the applicators' manufacturer were observed. These differences were about 15% to 20% lower for concave applicators and up to 15% lower for the flat applicators. In addition, the non-

uniformity of the dose distribution due to the inhomogeneity of the coated radioactive layer on the applicators was also observed. Due to limitations associated with the geometry of the extrapolation ionisation chamber, only the measurement of depth dose distribution along the central axis was carried out. Since the applicators used in the clinical treatment are of concave shape, a determination of the lateral dose distributions was also required.

Taccini *et al.* (1997) used radiochromic film detectors together with a TV-digitiser system in the measurement of the surface dose and dose distributions of a ruthenium-106 applicator in an eye-shaped PMMA phantom. Their experimental findings showed that there were differences between the depth dose profiles provided by the manufacturer and the measured ones. With the radiochromic film detectors, the standard deviations of dose distributions obtained from their measurements were lower than ±10% and ±4% for absolute dose rate and relative dose rate respectively. This improvement was attributed to the flexibility of the radiochromic film that can be made in size suitable for dosimetry of the ruthenium-106 plaques. Although the flexibility of the radiochromic film allowed them to measure both the central dose profile and the isodose distribution on the horizontal plane of the ruthenium-106 applicators, the latter measurement was carried out at the depth of 4.5 mm only. To achieve a more comprehensive dose distribution profile, the horizontal isodose distribution should be determined at several depths.

Sanchez-Reyes *et al.* (1997) determined the three dimensional dose distributions of small CCA and CCB concave ruthenium-106 applicators with the aid of the PENELOPE Monte Carlo simulation code. Statistical uncertainties of the dose calculations were in the order of ±2% at the close distances to the applicator. At further distances (~5 mm) the uncertainties were below ±6 %. However, the reliability of the simulation results of the Monte Carlo method depends upon the accuracy of the measured distribution pattern of the

radioactive material in the applicator. Therefore, the measurement of the dose distribution by another more reliable method is still required.

Recently, a three dimensional dose distribution of a CCA type ruthenium-106 applicator has been obtained from a measurement using magnetic resonance imaging of BANG polymer gels (Chan *et al.*, 2000). An eye phantom made of polymer gel was irradiated with a ruthenium source in two separate sessions in a glove bag filled with pure nitrogen, one for 1 hour and another for 0.3 hour. For calibration purposes, the gel vials were irradiated with 6 MV photon beam using a Varian Clinac 600C linear accelerator. To evaluate the dose distribution, magnetic resonance images were acquired with 1.5 T MR scanner and the proton relaxation rate (R_2) was calculated using custom-built software. The authors indicated that the dose response of polymer gels was linear for the doses up to 300 cGy with the standard deviation of less than 5% and up to 25% in the high dose region. However, this dosimetry method, as indicated by the authors, was not recommended for surface dose measurement since it would create the magnetic resonance (MR) artefacts due to the differences in chemical shifts and magnetic susceptibility. It was also concluded that the overall uncertainty in the calculated R_2 values was highly affected by the environmental temperature, light intensity and oxygen concentration during the experiment. As the technique is also somewhat expensive, the use of gel dosimetry was not recommended for evaluation of ruthenium-106 eye applicator dose profiles.

Soares *et al.*, 2001, published an extensive report on dosimetry of Sr-90/Y-90 and Rh-106 (namely CCB-570-planar and CCB-511-concave) applicators. A variety of measurement techniques were used that included radiochromic film, LiF TLD, alanine pellets, scintillator, diamond and diode detectors as well as small volume ion chambers. Relative percentage depth doses were measured up to depths of 10 mm in solid water eye

phantoms. Off-axis doses were also measured at various depths up to 10 mm using radiochromic film and a scintillator. While there was a reasonable agreement in the off-axis doses determined by film and scintillator for distances of up to 4 mm from the applicator centre, the doses measured beyond this distance varied considerably. The relative standard deviation of the reference absorbed dose rate at 1 mm depth in tissue for the concave Ru-106 applicator was reported to be around 14% and the authors emphasised the need for improved dosimetry for ophthalmic applicators.

1.4 Outline of the current project

Although improvements in the determination of the dose distributions of the ruthenium-106 ophthalmic applicators were achieved in previously published studies, evaluation of dose distribution characteristics of the ruthenium applicators needs be further investigated with the aim of obtaining more accurate dose distribution p atterns. A lso, a simple and fast technique is needed that will enable one to measure the radiation output of sources routinely, for example to confirm the doses reported by the manufacturer (during acceptance testing) or to check the integrity of the source after handling during treatments (quality assurance procedure). Some of the parameters to be investigated regularly may include the depth dose distribution (relative or absolute) along the central axis of the applicators, the horizontal dose distribution, and the non-uniformity of the radioactive material distribution (ruthenium-106) in the applicators.

Correspondingly, the specific aims of the present research project include:

1. Determination of dose distribution characteristics of COB-494 and CCA-610 concave type ruthenium-106 applicators used for eye radiation treatments at the Royal Adelaide Hospital. Dose distribution patterns values (central depth dose and off-axis dose) of these particular applicators have not been reported

previously and must be therefore determined with an uncertainty acceptable for clinical use.

2. Development of a standard dosimetry method that can be used for evaluation of the dose distributions of ruthenium-106 applicators for routine quality assurance purposes.

In order to achieve these aims, two dosimetry methods were employed in the current work: (i) small $CaSO_4$:Dy thermoluminescence dosimeters and (ii) a semiconductor MOSFET dosimeter (the use of which for this purpose has not been so far reported in literature). Correspondingly, the structure of this thesis is as follows: the general principles of thermoluminescent dosimetry will be summarised in chapter 2, followed by a study of the radiological properties of $CaSO_4$:Dy TLDs, such as sensitivity, linearity, reproducibility, etc, in chapter 3. Chapter 4 will deal with the experimental details and results of the application of small $CaSO_4$:Dy TLDs to dose investigation of Ru-106 ophthalmic applicators and chapter 5 will discuss the application of a MOSFET dosimeter for the determination of the applicator relative depth dose curve. Finally, the results of the current work will be summarised and discussed in chapter 6.

Chapter 2

General Properties of Thermoluminescent Dosimeters

2.1 Introduction

There are several types of dosimeters that have been used for determination of radiation dose from ruthenium eye plaques, for example, extrapolation ionisation chamber, radiochromic films, alanine detectors, scintillation detectors, diamond detectors and thermoluminescent (TL) dosimeters. Each of these dosimeters has its own advantages and disadvantages that the user must take into account when choosing the right dosimeter which is suitable for the radiological and physical properties of radioactive source. Among these dosimeters, in consideration to radiological and physical characteristics of the ruthenium ophthalmic applicator, thermoluminescent dosimeter is a versatile and appealing dosimeter for this purpose: It can be made small in size, it has a large useful dose range and a high radiation sensitivity and reproducibility. These are the key advantages that make the TL dosimeter suitable for use with a small radioactive source like a ruthenium eye plaque.

The theory of TLD dosimetry has been investigated for several decades and is by now well understood. This chapter will discuss only the basic principles of this technique and further details can be found in published textbooks, for example, McKeever *et al.*, (1995), Horowitz, (1983), Robertson, (1981), Attix, (1986).

2.2. Basic phenomenon of thermoluminescence

A TL dosimeter is a crystal that is in general non-conducting because there are no electrons in the conduction band. At room temperature, all electrons keep their place in the valence band. When a crystal is exposed to ionising radiation, electrons are released from the valence band into the conduction band. This leaves holes (positively charged sites) in the valence band. The electron and the hole may move through the crystal until they recombine or until they are trapped in metastable energy states, between the valence and conduction bands. These metastable states are thought to be associated with defects in the crystal such as impurity sites. At this point, there are two possible ways in which a thermoluminescence photon may be emitted. As the crystal is heated, sufficient energy may be given to the electron so as to raise it from its trapping site to the conduction band. The electron may then move around in the crystal until it recombines with a trapped hole and a thermoluminescence photon is emitted. Alternatively, the hole-trap may be less stable than the electron trap and, when the crystal is heated, the hole receives sufficient energy to move until it recombines with a trapped electron and a thermoluminescence photon is then emitted (see Figure 2.1).

The energy gap between the trap and conduction band determines the temperature required for releasing the electron and producing thermoluminescence, and is characteristic of the particular material employed. As the temperature of the crystal is increased, the probability of releasing an electron from a trap is increased. Hence, the emitted light will be weak at low temperatures, passing through one or more maxima at high temperature corresponding to thermal energies, and then decrease again to zero as no more filled traps remain.

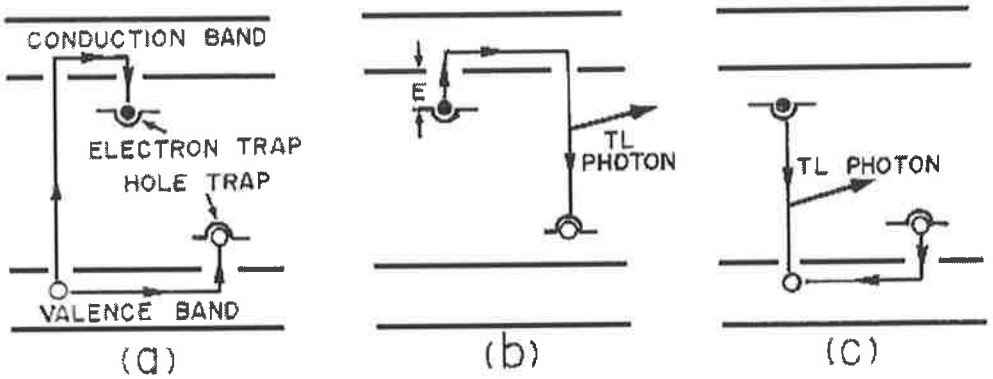

Figure 2.1. Schematic energy level diagram of a phosphor exhibiting thermoluminescence. (a) Exposure to ionizing radiation. (b) Electron trap is less stable during heating, and hole trap is the emitting centre. (c) Hole trap is less stable during heating, and electron trap is the emitting centre. (Weng *et al.*, 1989).

2.2.1 Characteristics of TLD phosphors

There are many materials which exhibit thermoluminescence. Selecting the most appropriate TL phosphor from many which are available is the most important consideration. Characteristics of some of the commonly used TL phosphors will be reviewed here.

2.2.2 Glow curves

The return of the trapped electrons or holes (stimulated by heating) to the stable state, is associated with a release of energy. This energy may be released as visible or UV light, i.e thermoluminescence. If several traps of different depths are involved in this process, the recording of the light emission as a function of heating time (or temperature) results in a glow curve consisting of several glow peaks.

The term "glow curve" refers to the graph of TL light as a function, either of temperature or of time. The glow curve of a phosphor characterises its dosimetric properties. For example, the appearance of glow peaks only at low temperatures implies that the phosphor loses its stored TL with time, and therefore would not be suitable for long-term measurements. A glow curve with peaks at very high temperatures indicates a phosphor that will produce infrared radiation at the temperature necessary to release the thermoluminescence. Ideally, a glow curve should reveal only a single thermoluminescent peak that occurs at a temperature high enough to ensure room temperature stability, but not so high as to present instrumental problems. Examples of glow curves of some commonly used TL phosphors are shown in Figures 2.2 – 2.5. There are several factors that may affect the shape of a glow curve. For instance, the heating rate and its uniformity, the size, shape and thermal conductivity of the sample, the recording instrument used the level of exposure, the type of radiation, the radiation and annealing history of the sample and possible spurious effects.

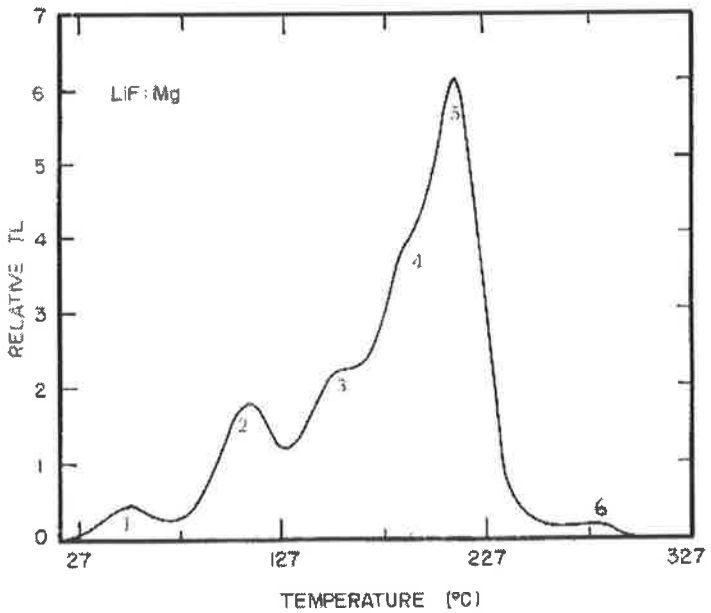

Figure 2.2 A Glow curve of LiF crystal doped with magnesium. (Weng *et al.*, 1989)

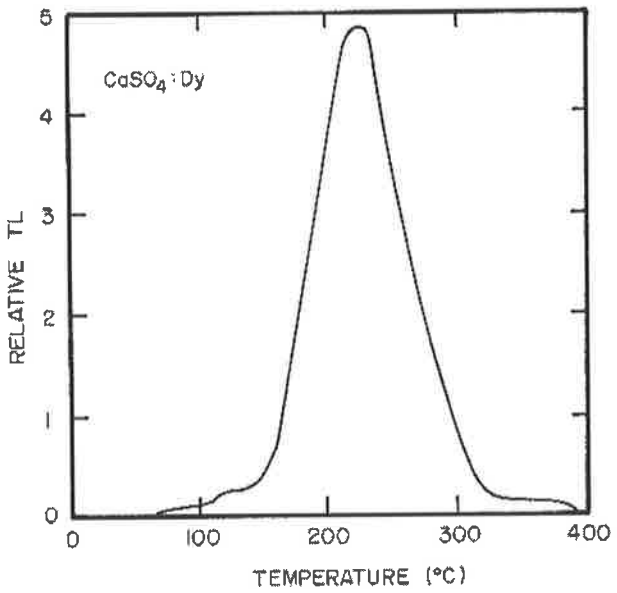

Figure 2.3 A typical glow curve of $CaSO_4$:Dy or $CaSO_4$:Tm. (Weng *et al.*, 1989)

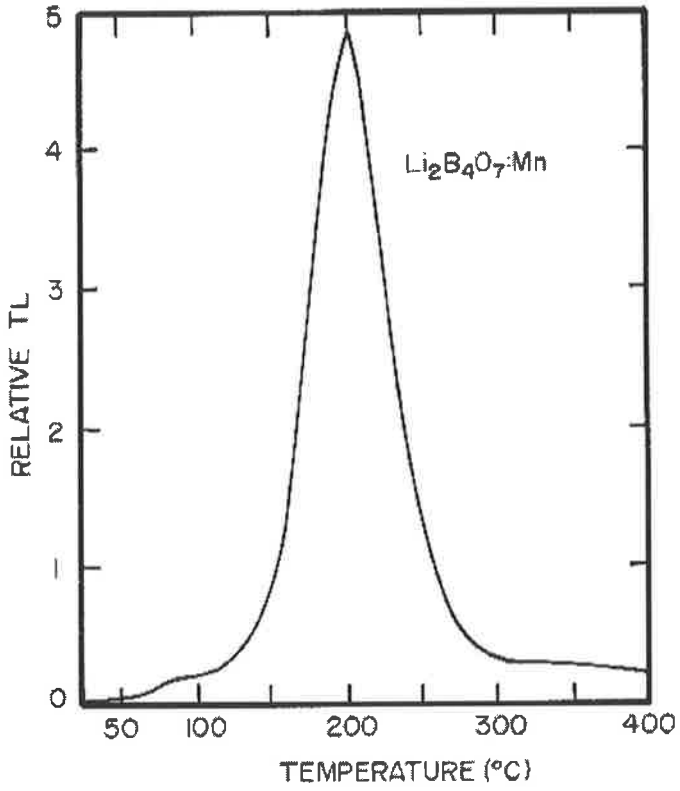

Figure 2.4 A typical glow curve of $Li_2B_4O_7$:Mn.
(Weng *et al.*, 1989)

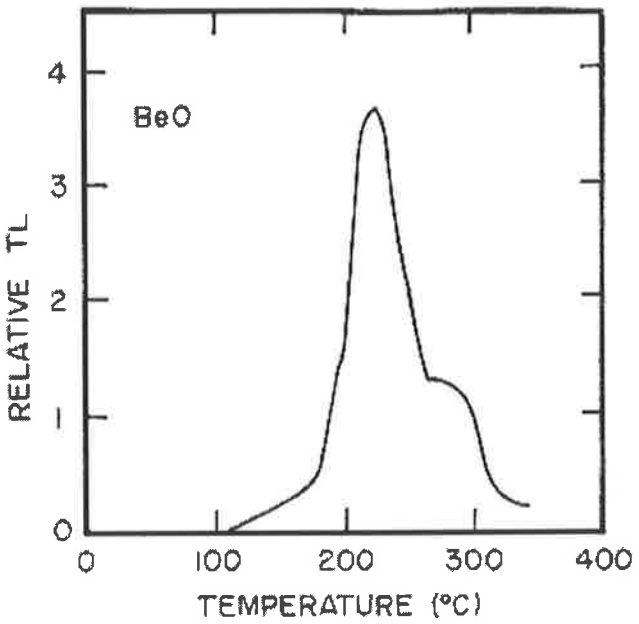

Figure 2.5 A typical glow curve of BeO.
(Weng *et al.*, 1989)

2.2.3 Sensitivity

Thermoluminescent sensitivity may be defined as the amount of light released by the phosphor per unit of radiation exposure. The lower limit of useful sensitivity depends on the characteristics of the phosphor and the TLD reader (the device that measures the light output from TL during the heating cycle). Most of the commercially available TLD readers can measure radiation doses of less than 1mGy. The upper limit of the useful range is generally limited by the phosphor alone. Normally, most of the commercial readers can be adjusted or modified to permit the reading of phosphors exposed to higher levels. Table 2.1 summarises the approximate useful exposure range for the currently available phosphors.

Table 2.1 General characteristics of some TL phosphors.

TLD phosphor	Relative gamma ray sensitivity	TL emission peak (A)	Dosimetric peak temp. (°C)	Useful dose range	TL fading
1. LiF:Mg, Ti	1	4000	195	50 μGy to 10^3 Gy	10%/month
2. MgB_4O_7:Dy	7	4800, 5700	210	-	10%/2 months
3. $Li_2B_4O_7$:Mn	0.4	6000	210	0.1 mGy to 10^3 Gy	10%/month
4. $Li_2B_4O_7$:Cu, Ag	1	3680	185	50μGy to 10^4 Gy	10%/month
5. $Li_2B_4O_7$:Cu	8	3680	205	-	9%/2 months
6. $CaSO_4$:Tm	3.2	4520	210	~μGy to 10^3 Gy	10%/month
7. $CaSO_4$:Dy	38	4800, 5700	210	~μGy to 10^3 Gy	3%/month
8. $CaSO_4$:Mn	70	5000	110	~μGy to 10^3 Gy	60%/day
9. CaF_2:Dy	16	4800, 5700	200	~μGy to 10^3 Gy	12%/month
10. CaF_2:Mn	5	5000	260	~μGy to 10^3 Gy	10%/month
11. CaF_2 (natural)	23	3800	260	10 μGy to 10^3 Gy	-
12. Mg_2SiO_4:Tb	53	5520	195	1 μGy to 10^3 Gy	3%/month
13. BeO	3.1	2400-4000	180-220	0.1 mGy to 10^3 Gy	5%/month
14. Al_2O_3	5	4250	250	10 μGy to 10^3 Gy	5%/two weeks

Source: Weng et al., (1989).

2.2.3. Dose response curves

The dose response is defined as the functional dependence of the intensity of measured TL signal upon the absorbed dose. The ideal dosimetric material would have a linear dose response over a wide dose range, however, most TL phosphors used in practical dosimetry display a variety of non-linear effects. In particular, the response of a TL phosphor is linear, then *supralinear* (appearance of the non-linear increasing in dose response/unit exposure), then *sublinear* (appearance of the non-linear decreasing in dose response/unit exposure) as the doses increased.

2.2.4. Energy response

The energy response is the variation of the TL output, for a fixed radiation dose, as a function of the energy of the absorbed radiation. This variation arises from the dependence of the material's absorption coefficient (μ) on beam energy. The effect of the photon energy response is aided by the definition of the Relative Energy Response (RER), defined with respect to 1.25 MeV photons from a ^{60}Co source and can be written as:

$$(RER)_E = \frac{S_E(E)}{S_E(1.25\ MeV\ Co\text{-}60)} \qquad (2.1)$$

where; $S_E(E)$ is the photon energy response for the TLD at the specified beam energy spectrum,

and S_E(1.25 MeV ^{60}Co) is the photon energy response of the TLD to reference 1.25 MeV photons from ^{60}Co source (McKeever, 1995).

2.2.5. Thermal fading

The rate at which the thermoluminescence energy is released is dependent upon the phosphor temperature and increases sharply at higher temperatures. If the TL signal from a TLD sample is unstable with time, specifically, if it decreases with time after irradiation, the signal is said to have faded. Fading can have several causes, but the most prevalent is thermal fading, i.e. the loss of TL signal induced by temperature. The thermal fading rate is influenced by two parameters: trap depth and a temperature-dependent frequency factor. The latter parameter is related to the local lattice vibration frequency and the entropy change associated with the charge release. The fading rate for commonly used TL phosphors is shown in Table 2.1.

2.2.6. Annealing conditions

The reliable re-use of TL phosphors requires the use of strict thermal annealing procedures. Thermal annealing normally implies a particular recipe of pre-irradiation annealing. Sometimes, a post-irradiation annealing recipe is also recommended. Generally, the purpose of pre-irradiation annealing is to empty the traps and re-establish the thermodynamic defect equilibrium that existed in the material before irradiation and readout. This is achieved by reversing the thermally driven diffusion reactions that sometimes occur during the TL process. To reset the occupancy of the stable trapping centres, the high temperature annealing is required. Exactly the right equilibrium-state must be achieved each time if the material is to be reliably re-used.

2.3. Characteristics of commonly used TL phosphors

2.3.1. LiF:Mg,Ti

LiF is a large family of thermoluminescent materials of often very dissimilar properties. The most common dopants in commercially available LiF-TLD are Mg and Ti (e.g TLD-100, TLD-600 and TLD-700 – Harshaw patent), however, the TL properties of even LiF:Mg,Ti are dependent, to a very significant extent on the details of the method of preparation. LiF:Mg,Ti dosimeter materials come in a variety of physical forms, including single crystal, extruded rods, hot pressed chips, powder or impregnated PTFE discs. TLD-100 (also TLD-600 and TLD-700) is produced by homogeneous melting of lithium fluoride, magnesium fluoride, lithium cryolite, and lithium titanium fluoride. A single crystal solidified from the melt is then pulverised and the powder grains are sieved and separated. The most sensitive LiF:Mg,Ti material is obtained with approximately 180 ppm Mg^{2+} and 10 ppm Ti^{4+}. Most samples contain several ppms of OH^- ions as an additional impurity. TLD-100 consists of Li in its natural form.

TL glow curves: LiF:Mg,Ti has a complex glow curve structure. A number of glow peaks have been identified, however, for most dosimetric applications, only the five peaks between room temperature and about 210 °C are taken into account. These peaks are identified as peaks 1 – 5 (figure 2.6). There are several factors that affect the glow curve structure of LiF:Mg,Ti, for example, variation in isothermal annealing or rate of cooling from the readout or annealing temperature.

Dose response: The dose response of LiF:Mg,Ti is linear up to 1 Gy, then it becomes supralinearity up to 10^3 Gy where sublinearity starts. The onset and degree of supralinearity in LiF:Mg,Ti is known to be dependent on a variety of materials and

experimental factors such as linear energy transfer (LET), glow peak temperature, batch of material, heating rate and the thermal treatment. The supralinearity dose response of LiF:Mg,Ti can be corrected by applying a supralinearity correction factor which can be obtained from experiment.

Sensitivity: LiF:Mg,Ti was reported to be sensitive to radiation dose as low as 100 μGy (McKeever, 1995). LiF:Mg,Ti (TLD-100) has been used as the standard reference with an assigned relative sensitivity of 1.00.

Photon energy dependence: LiF:Mg,Ti has effective atomic number of 8.2 which makes it to be a nearly tissue-equivalent TLD. However, LiF:Mg,Ti will respond to the radiation doses more than human tissue does, especially at the lower photon energies where the photoelectric interactions are dominant.

Thermal treatment: The TL response of LiF:Mg,Ti is extremely sensitive to the various thermal treatments, involved in the TL process. The main thermal treatment of LiF:Mg,Ti may include high temperature annealing and low temperature annealing.

The high temperature annealing before re-use (after irradiation and reading) of LiF:Mg,Ti has two purposes which are (1) to minimise the residual TL signal by emptying the high temperature traps and (2) to restore the original sensitivity and glow curve structure. The recommended high temperature annealing temperature is 1 h at 400 °C.

The purpose of low temperature annealing (before irradiation) is to reduce fading by minimising the contribution of the low temperature peaks (1-3). The standard low temperature pre-irradiation annealing for LiF:Mg,Ti is 24 h at 80 °C.

Fading: The rate of fading in LiF:Mg,Ti is affected by several experimental factors including storage temperature, method of annealing, radiation type and glow curve integration region. The amount of fading ranges between 10% in one month to 1% in one

year. However, the higher fading values are due to the inclusion of the low temperature peaks in the integrated TL signal.

2.3.2. LiF:Mg,Cu,P

Various forms of LiF:Mg,Cu,P are commercially available, for instance, powder, polycrystalline hot pressed chips, sintered circular chips and thin films on Kapton substrates. ^{6}Li and ^{7}Li enriched versions are also available. LiF:Mg,Cu,P powders is produced by mixing optical grade LiF powder with MgF_2, CuF_2 and $NH_4H_2PO_4$ powder in a platinum crucible at 1000-1050 °C under a N_2 or N_2/O_2 atmosphere. After 30 minutes in the molten stage the sample is fast-cooled to room temperature and the polycrystalline material is powdered, sieved and washed. LiF:Mg,Cu,P in the form of chips can be made from phosphor powders by either hot pressing or by sintering and then slicing.

TL glow curves: A typical glow curve of LiF:Mg,Cu,P is shown in Figure 2.2. The glow curve structure of LiF:Mg,Cu,P consists of an intense peak near 200 °C with lower intensity satellite peaks at lower temperature and higher temperatures.

Dose response: The dose response curve of LiF:Mg,Cu,P has a linear-sublinear pattern rather than linear-supralinear-sublinear for LiF:Mg,Ti. This pattern provides an advantage in radiotherapy applications where the dose levels are typically of the order of several Gy, well within the supralinearity region of LiF:Mg,Ti and $CaSO_4$:Dy. These are also frequently used for radiotherapy dosimetry. The linear part of the dose response curve of LiF:Mg,Cu,P covers the dose from 3 μGy up to 9 Gy where sublinearity starts.

Sensitivity: LiF:Mg,Cu,P phosphor has high sensitivity (23 times higher than TLD-100) which provides an advantage in personnel and environmental dosimetry applications. The sensitivity of this TL phosphor depends on the emission spectrum and on the spectral response characteristics of the light detector system. The sensitivity is also highly variable between samples from different manufacturers.

Photon energy dependence: TL efficiency of LiF:Mg,Cu,P decreases at the lower photon energies (below 80 keV) as a result of local saturation (decrease) of the TL efficiency in microscopic volumes along the tracks of secondary electrons. This phenomenon can be explained by the dependence of the TL efficiency on the ionisation density, an effect that is particularly noticeable for high LET particles.

Thermal treatment: The maximum readout temperature and the pre-irradiation annealing parameters have a strong effect on the sensitivity and glow curve shape of LiF:Mg,Cu,P. It has been widely accepted that it is necessary to pre-irradiation anneal this TL phosphor at 240 °C for 10 minutes (standard annealing) and to limit the readout temperature to a maximum of 240 °C (standard readout) to avoid the permanent loss of sensitivity of LiF:Mg,Cu,P.

Fading: There is no measurable fading in LiF:Mg,Cu,P for storage periods of up to two months at room temperature or in high humidity environments. However, the fading rate may increase in high temperature conditions. LiF:Mg,Cu,P material is also not light sensitive, however, some light induced fading (11%) was observed following 3 hours exposure to direct sunlight.

2.3.3. BeO

Beryllium oxide is a tissue-equivalent TLD material with an effective atomic number of 7.13. Since BeO has a TL sensitivity similar to TLD-100 and also is available in robust and easily handled ceramic disc form. As it has a good thermal conductivity and low cost, it is a very attractive TL for research activities. However, BeO in powder form is extremely toxic leading to a condition known as berylliosis. Hence, producing BeO TLD chips is only possible in commercial laboratories where stringent safety measures are employed. Other forms of the phosphor including hot pressed, powdered and sintered can be obtained from several manufacturers.

TL glow curves: Glow curves from BeO (Figure 2.5) are highly variable depending upon the origin of materials but normally consists of two broad peaks. In spite of this, the glow curve of BeO is actually quite complex as each peak consists of several overlapping components. Furthermore, spurious thermoluminescence (the production of a luminescence signal that is not radiation-induced) is also one potential problem in several forms of BeO. TL peaks of BeO are observed to be light sensitive and light-induced fading can be a problem for TLD applications if not prevented.

Dose response: The dose response curve of the main dosimetric peak of BeO has a linear-supralinear-sublinear in pattern with linear region extends from approximately 10 μGy up to 1 Gy where it becomes supralinear.

Sensitivity: The sensitivity of BeO is similar to that of LiF:Mg,Ti especially a BeO sintered disc, of which a sensitivity is almost equal to that of a ^{7}LiF Teflon disc in the exposure range of 2.5 mGy to 1 Gy, where the dose response of both materials is linear. The factor that significantly affects the sensitivity of BeO is the thickness of the detector as a result of self-absorption of the TL light in the detector itself.

Photon energy dependence: The effective atomic number of BeO is 7.1 that is approximately equivalent to human tissue. The photon energy dependence curve is almost flat in the energy range of 0.02 to 1.25 MeV.

Thermal treatment: The non-radiation-induced signal in association with a change in temperature in the TLD is one problem of BeO. This can be eliminated by a one-time annealing of new dosimeters at 1000 °C for 15 hours followed by 400 °C for 15 minutes pre-irradiation annealing with each use.

Fading: The average fading rate for BeO is approximately 4% per month when it is stored in the dark during the fading period. The light-induced fading is, however, more significant.

2.3.4. $CaSO_4$:Dy

Among the TL group of material based on $CaSO_4$, $CaSO_4$:Dy is the most stable detector. It is available in virtually every physical form. $CaSO_4$:Dy is an exceptionally sensitive TL material approximately 30 to 50 times more sensitive than TLD-100 and also less expensive than LiF on a gram-for-gram basis. One additional advantage is that the preparation technique is quite simple so that with proper attention to detail, any laboratory equipped with routine facilities can undertake its preparation. Preparation of $CaSO_4$:Dy uses analar grade $CaSO_4$ combined with rare earth oxides in concentrated sulphuric acid, resulting in a white polycrystalline material which can then be sieved to select a particular grain size. These grains are then fired at 600 °C for two hours.

TL glow curves: The glow curve from $CaSO_4$:Dy (Figure 2.3) consists of several overlapping peaks. The main glow peak occurs at approximately 220 °C at low doses. Increasing exposure causes the glow peak to move to higher temperature up to approximately 250 °C at 46 Gy. Initially, with increase in exposure, an additional peak is formed at about 260 °C, that reaches maximum intensity at approximately 10 Gy. With subsequent increase in exposure the additional peak saturates and the glow peak returns to its original shape. A further increase in dose beyond about 50 Gy will result in a shifting of the peak toward lower temperatures and reaches 190 °C at 10^4 Gy.

Dose response: The dose response curve of the main dosimetric peak (220 °C) of $CaSO_4$:Dy (TLD-900) is observed to be linear up to a dose level of 10 Gy where it becomes supralinear until 5 kGy. The response saturates at approximately 10^4 Gy and a dose-dependent sensitivity decrease due to radiation damage is observed at dose levels above 10^5 Gy.

Sensitivity: The sensitivity of the $CaSO_4$:Dy phosphor is observed to be as high as 30 – 50 times that of TLD-100. Its sensitivity can even be further increased to

approximately 57 times as compared to TLD-100 by using a photomultiplier tube with higher sensitivity to yellow light. The superb radiation sensitivity of $CaSO_4$:Dy makes it suitable for measurement of low doses, or as a small size TLD, it can be used to provide significant readouts.

Photon Energy dependence: The energy dependence of $CaSO_4$:Dy is characterised by a significant over-response for photon energies in the range 25 – 200 keV. However, using of response-flattening filters can modify the energy dependence. For instance, use a 2 mm Sn filter to remove the over-response to low energy photons below 200 keV. The response to photons with energy greater than 200 keV is quite flat. $CaSO_4$:Dy TLDs are not tissue-equivalent so they cannot be used directly for measurement of absolute doses. A calibration process with the appropriate photon energies is required to enable measurement of the absolute dose.

Thermal treatment: A pre-irradiation annealing cycle at 400 °C for one hour is recommended to be applied to $CaSO_4$:Dy. Some reports indicated that a higher annealing temperature (600 – 700 °C) could improve the sensitivity and reduce the residual signal. A post-irradiation annealing of 120 °C for 10 minutes or a preheating segment incorporated into the readout cycle may be applied for optimal fading characteristics. In the case of $CaSO_4$:Dy which is incorporated in a PTFE matrix, a lower annealing temperature is required to prevent the melting of the PTFE matrix, but this temperature must be high enough to eliminate the effects of previous irradiations. The thermal treatment parameters employed in this research were somewhat different from those indicated by several authors. The parameters used in this study were those found to be reliable from past experience in this department (Medical Physics Department, Royal Adelaide Hospital).

Fading: At room temperature, the fading of $CaSO_4$:Dy signals is observed to be approximately 5% over the storage period of 6 months. $CaSO_4$:Dy is also sensitive to light.

Three hours exposure to visible part of the sunlight spectrum may induce 50% loss of radiation exposures TL signals.

2.4. Thermoluminescence Readout Instrumentation

The thermoluminescent dosimeter reader (Figure 2.7) consists of three main parts: the TL material heating unit, the light collection unit and the light detection unit. There are two types of TLD reader: a manual reader that has the advantage of being cheaper in cost, and an automated system that usually gives more reproducibility in regard to the positioning of the TL dosimeter within the reader leading to an improvement in measurement precision.

2.4.1. Dosimeter heating system

In principle, the heating system in a TL readout instrument consists of two parts: a heat supplying medium or device and electronics for the control of temperature. A resistively heated metal planchet (by resistive heating) and a hot gas stream are two common methods of TLD heating. An optical heating by a remotely located laser and microwave heating are also employed in several modern TLD readers. The temperature control unit may simply consist of a transformer that supply an alternating current for resistive heating of a metal planchet. In more sophisticated instrument, a temperature measuring device may be connected to a feedback circuit with programmable reference ramps and plateaux that allow a wide variation of the heating cycle. In addition, the heating of a TLD can be carried out in three different ways: i.e. the TL material can be placed in thermal contact with a heating medium at high constant temperature, or with a heating medium whose temperature is gradually increased during readout, or by radiative heating using light pulses.

2.4.2. Light measuring systems

The light measuring equipment in a TLD reader consists of a photoelectric light detector and a photomultiplier tube in which light is converted into electric charge, amplifiers for this very small electric signal, and a signal registration unit that quantifies and stores the electric signal.

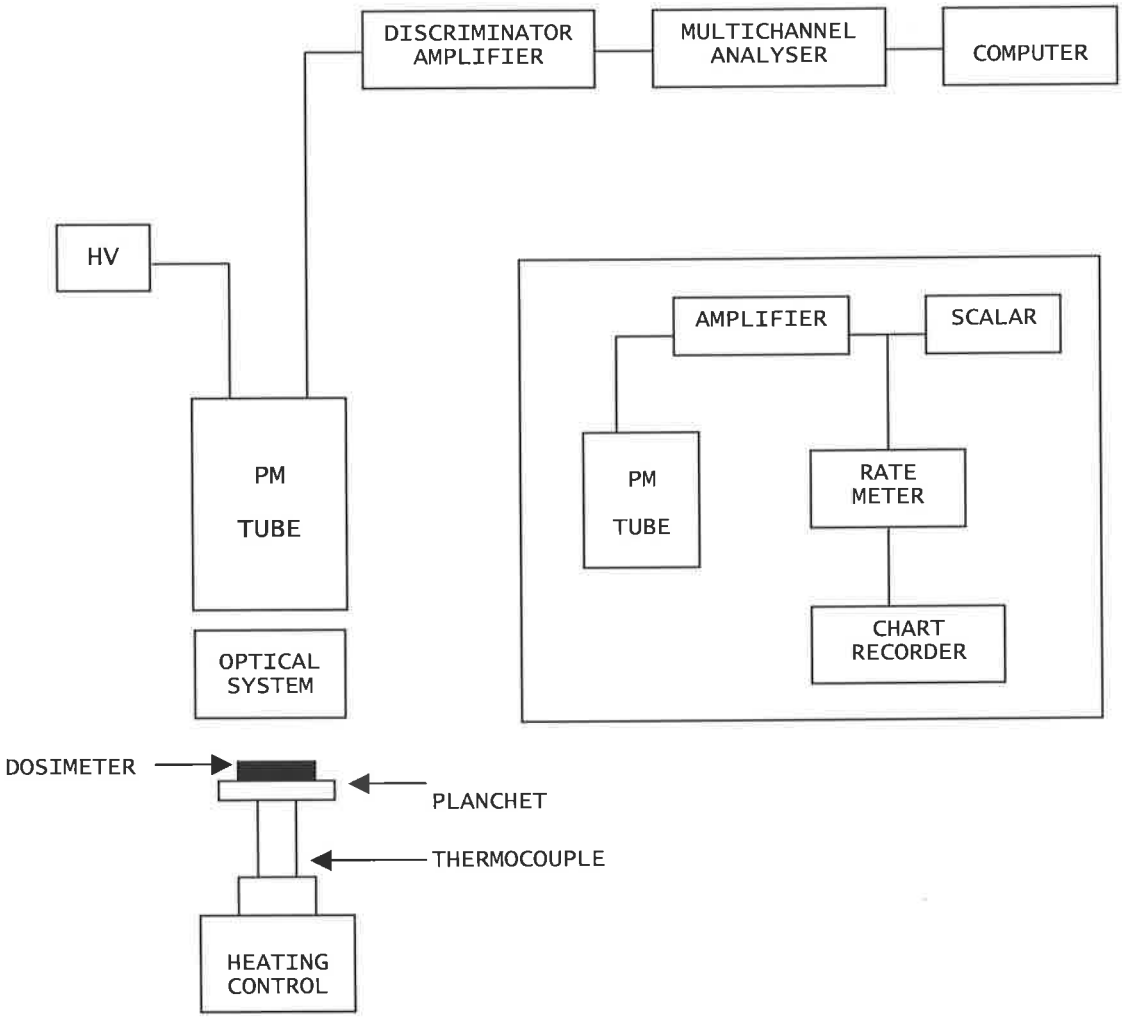

Figure 2.7 A schematic illustration of the TL photon counting method for glow curve readout and kinetic analysis. The insert shows the charge integration method. (Horowitz, 1984)

Photomultipliers that are employed in most commercially available TLD readers are well suited for the detection of the small quantities of light emitted by a TL material. There are some considerations that must be taken into account regarding photomultipliers. There are the optimisation of photomultiplier position in regard to the TLD and the light spectrum being detected. The PMT should also have a low infrared sensitivity to avoid increase of the background signal due to higher readout temperatures.

The signal recording system has the purposes of quantification and storage of the signal from the light detector. The signal from the PMT consists of charge pulses initiated by single photoelectron can be quantified by two methods: i.e. the charge can be integrated or the number of pulses counted.

The sensitivity of photomultiplier tube usually decreases with both age and usage. To account for this problem, many commercially available TLD readers have a built-in light source as a gain reference, usually a radioactive source such as ^{3}H or ^{14}C placed in a scintillator (NaI(Tl)) material. This built-in system will regularly check the changes of PMT sensitivity. A light emitting diode (LED) has also been installed as a reference light source in some modern TLD readers. The reference light source can be either placed manually in the reading position of TLD or the photomultiplier may be exposed to the light source each time a new TLD sample is loaded. In some readers, the in-built reference light signal is used automatically to correct the TL readings.

2.5 Beta radiation dosimeter

Dosimetry of beta radiation requires knowledge of the beta energy spectrum and to which the dosimeter is exposed in order to obtain an accurate result. This extra data is quitc

difficult to obtain either by measurement or from calculation. In addition, beta dosimetry is more difficult in the case of mixed beta-photon fields. Effective field determinations of beta dose rates can be performed by using an extrapolation chamber that is a cylindrical ionization chamber with a constant face or window area and a volume that can be varied by changing the depth of the chamber by means of the spacing between two electrodes (Kathren, 1987). However, beta dosimetry with an extrapolation chamber is also subject to error due to loss of beta energy in air as the distance between sources and detector varies.

Dosimetry of beta radiation with energies below a few MeV using a TLD is relatively simple. Several types of TLD provide high radiation sensitivity and low a coefficient of variation, that can be used for pure beta dosimetry or even for dosimetry of a mixed beta and gamma field. Applications of TL dosimeters for beta dosimetry have been proposed, for instance, the graphite mixed MgB_4O_7:Dy TL dosimeters were introduced for routine monitoring for the personnel who work in beta or beta-gamma radiation fields (Prokic, 1985). The equivalent dose assessment in mixed beta and gamma fields using pellets of $CaSO_4$:Dy has been proposed in the report of Daltro *et al.* (1999). Ultra-thin LiF:Mg,Cu,P has been used for beta dosimetry from Pm-147, Tl-204 and Sr-90/Y-90 sources (Bilski, *et al.*, 1995). These are some examples of applications of TLD in beta or mixed beta and gamma dosimetry.

2.6 Conclusion

There are several types of thermoluminescence dosimeter that may be used for determination of the dose distributions of ruthenium-106 applicators. However, $CaSO_4$:Dy TL dosimeters have been chosen for this research for several reasons. For instance, $CaSO_4$:Dy TL dosimeters available to be used in the laboratory were in the form of Teflon-based wafer that make them very easy to be cut into small pieces as required. The

$CaSO_4$:Dy TLD has a far higher dose response sensitivity than LiF:Mg,Ti TLD (30-50 times higher). This advantage makes the $CaSO_4$:Dy TL dosimeters an ideal dosimeter for measuring the dose distributions of ruthenium-106 applicators, as they are required to be cut into very small sizes and need to have high dose response sensitivity. Although they are not tissue equivalent, TLDs (with a proper calibration method) can be used for measurement of the absolute dose. $CaSO_4$:Dy TL dosimeters do not require extremely high temperatures for reading and annealing purposes, hence, special reading and annealing instruments are not needed. In addition, environmental conditions such as light intensity and humidity level have only a small influence on reproducibility, especially fading, of the $CaSO_4$:Dy TLDs.

Chapter 3

Study of Basic Characteristics of $CaSO_4$:Dy TLD

3.1. Introduction

Basic dosimetric characteristics of $CaSO_4$:Dy thermoluminescent dosimeters are investigated in this chapter, before they can be used for ^{106}Ru dose measurements. There were several reasons for choosing $CaSO_4$:Dy TLD as a radiation detector for this project. As mentioned in chapter 1, ^{106}Ru applicators produce very high dose gradients at small clinically relevant distances and are of small size. Consequently, measurement of the dose distribution in the eye phantom requires dosimeters that are small and thin enough to be placed in the eye phantom and to have reasonable spatial resolution to avoid significant averaging of the doses across the treatment plane at each depth as well as averaging over the treatment depths.

Second, as the measurement of relative doses for the ruthenium plaque was the objective of this project, $CaSO_4$:Dy TLD can be used for the measurement even though they are not tissue equivalent. Third, $CaSO_4$:Dy TLD has a very high sensitivity to radiation dose so it is able to measure the low energy photons from the plaques especially at the depth in the phantom where the dose rate was very low.

A number of measurements were performed in order to observe basic dosimetric properties of $CaSO_4$:Dy TLD, namely, reading reproducibility, dose response linearity, sensitivity, irradiation-orientation dependence and reading-orientation dependence. In the next chapter, a number of small $CaSO_4$:Dy TLD chips will be made from selected TLD discs and used for the measurements of dose distributions for ruthenium-106 applicators.

3.2. General properties of $CaSO_4$:Dy TLDs

3.2.1. Reading reproducibility

Reading reproducibility is a measure of the precision of the TLD in the measurement of radiation dose. Different TLDs, from the same batch may produce a large reading difference. However, accuracy can be obtained from individual calibration and averaging of several TLDs in a batch (Attix, 1986).

3.2.2. Dose response linearity

The linearity of the dose response for any TLD will define a useful range for radiation measurements for that TLD. This radiological property must be investigated with a specific TLD reader and a specific type of TLD before it can be used for radiation dosimetry.

3.2.3. Sensitivity

The sensitivity of a particular TLD is the TL signal strength per unit absorbed dose (McKeever *et al.*, 1995). Determination of this parameter is necessary since it not only depends on the TLD itself but also upon the TLD readout system parameters, for example, the heating rate, method of TL signal measurement and type of optical filters. A sensitivity factor for each TLD against an average readout of the whole batch must be determined.

3.2.4. Orientation dependence for irradiation and readout

These two parameters are also important when using the TLD as a radiation dosimeter. Since a TLD disc has two sides, the reading output results depend on which side has been irradiated and alternating between the two faces throughout the experiments may lead to a poor reproducibility. Further variation may be introduced if the TLD positioning is varied (irradiated face up or down) during the reading cycle in the TLD reader. Hence, investigation of such differences between the two orientations during irradiation and reading processes is necessary in order to obtain correct readout results.

3.3. Experimental instruments and procedures

3.3.1. Experimental instruments

3.3.1.1. $CaSO_4$:Dy TLDs

The $CaSO_4$:Dy TLDs used in this project were obtained in the form of teflon-impregnated discs. They have a density of 2.61 gm/cm^3 and effective atomic number of 15.3. However, information about their manufacturer and chemical contents is not available.

3.3.1.2. Radiation sources

There were two sources of radiation used in this research project. Firstly, a 4 MV photon beam from a medical linear accelerator located at the Royal Adelaide Hospital was used for calibration and reference purposes. The linac model used was Clinac 4/100 produced by Varian Medical System Inc., USA. This machine generates photons with the mean energy of ~ 1.3 MV. The electron spectrum produced in tissue by the 4 MV beam will range from 0.6 to 2.5 MeV, close to the mean energies of the beta particles of ruthenium-106 applicators. The second radiation source used was the ruthenium-106 ophthalmic applicator itself. The details of this applicator were provided in Chapter 1 of this thesis.

3.3.1.3. TLD Reader

The TLD reader used was a TOLEDO Universal TLD Reader, Model 654D (figure 3.1), product of Vinten Instruments Limited, England. The reading parameters used in this research were set as following:

Pre-reading annealing:

Temperature: 120 °C Time: 30 seconds

Readout:

Temperature: 280 °C Time: 30 seconds

Reading environment:

Pure nitrogen was used with flow rate at 400 mL/min.

Figure 3.1 The front panel of the Toledo universal TLD reader (Vinten Instruments Limited, England) used in the research project.

3.3.1.4. Annealing Oven

For TLD annealing purposes, a Victoreen annealing oven, Model Number 2600-62-5 was used. The annealing temperature and time parameters were 270° C and 120 minutes, respectively. The TLD samples were placed between a pair of copper block for shock-cooling after retrieval from the oven.

3.3.1.5. Effective Point of Measurement

The radiation is generally absorbed at some depth into the detector, known as an effective point of measurement. The exact position of the effective point of measurement has not been investigated in the current work, but usually it is assumed to be in the middle of the TLD disc (0.2 mm in our case) (Soares *et al.*, 2001).

However, all experiments presented are only relative measurements calibrated against 4 MV photon linac beam. In this calibration, the TLD surface was positioned at d_{max} (depth of maximum dose) and the effective point of measurement was 0.2 mm below the surface. However, the TLD reading was matched with the expected dose at d_{max} (i.e. 100 cGy in tissue per 100 monitor units) and therefore the readout obtained from the TLD represents the dose at its surface after the linac calibration is applied. Consequently, the position of the effective point of measurement does not have to be taken into account and the depth in tissue of later measurement is taken to be at the TLD surface.

3.3.2. Experimental procedures

3.3.2.1. Irradiation and reading of TLD samples

During the investigation of $CaSO_4$:Dy characteristics, TLD samples were irradiated with a 4 MV photon linac beam. TLDs were placed on a perspex phantom and, then, covered with 1 cm build-up plate; i.e. TLDs were at the depth of maximum dose, d_{max}. A Source to phantom Surface Distance (SSD) of 100 cm and a field size of 10 x 10 cm^2 were used and a 2 Gy radiation dose was delivered. The linac radiation output has been routinely calibrated with an ion chamber. After irradiation, the TLD samples were placed in a holder and left overnight at room temperature in order to allow for the decay of unstable lower energy traps. Afterwards, TLD samples were read with a TLD reader using the reading parameters given in section 3.3.1.3. Finally, TLD samples were annealed, shock-cooled and re-used. These irradiation and reading procedures and settings were maintained throughout all measurements.

Three annealed $CaSO_4$:Dy TLDs were selected and kept non-irradiated as control during each irradiation cycle, in order to check for the presence of TLD previous radiation history due to incomplete annealing as well as due to any increase in reading as a result of

background radiation received during the performance of the experiment. Therefore, the quality of the annealing procedure and the contribution of the background radiation toward reading of TLD samples can be determined. Any radiation information that has not been completely removed by the annealing process would contribute towards the background reading of the samples and needs to be subtracted. However, readouts obtained from measurements of those non-irradiated TLDs were low in comparison to irradiated ones (in range of up to a few hundreds compared to readings of $\sim 10^5$). Therefore, these reading values, though subtracted from to the main readings, were insignificant.

3.3.2.2. Measurement of dose response sensitivity and reproducibility of $CaSO_4$:Dy TLDs

In order to measure the sensitivity, i.e. dose response for each $CaSO_4$:Dy TLD sample, three consecutive irradiations of 2 Gy were delivered to the TLD samples. To obtain a sensitivity correction factor of a TLD disc, an average readout was calculated from readings, corrected for background, of all TLDs after every irradiation. A mean readout was obtained from three average readouts (after three irradiation cycles of all TLDs). Finally, a normalised readout for a TLD for each irradiation was obtained using the average readout for a given TLD after three irradiations and the mean readout determined from all irradiations and all TLDs (see Table 3.1 and equation 3.1, 3.2 and 3.3 below for clarification).

Table 3.1 Example of TLD irradiation readouts for determination of TLD sensitivity

TLD No.	1ST Irradiation Readout	Norm. Readout	2ND Irradiation Readout	Norm. Readout	3RD Irradiation Readout	Norm. Readout	Mean of Norm. Readout
TLD1	TLD1(R1)	TLD1(NR1)	TLD1(R2)	TLD1(NR2)	TLD1(R3)	TLD1(NR3)	MNR1
TLD2	TLD2(R1)	TLD2(NR2)	TLD2(R2)	TLD2(NR2)	TLD2(R3)	TLD2(NR3)	MNR2
TLD3	TLD3(R1)	TLD3(NR3)	TLD3(R2)	TLD3(NR2)	TLD3(R3)	TLD3(NR3)	MNR3
...	...	...	...	...	...	...	...
TLDn	TLDn(R1)	TLDn(NR3)	TLDn(R2)	TLDn(NR2)	TLDn(R3)	TLDn(NR3)	MNRn
	AVR1		AVR2		AVR3		

Average readout (per irradiation of all TLD), e.g. AVR1 (after first irradiation) =

$$[TLD1(R1) + TLD2(R1) + TLD3(R1) + \ldots + TLDn(R1)]/n \quad (3.1)$$

Mean readout (from all TLDs after 3 irradiations) =

$$(AVR1 + AVR2 + AVR3)/3 \quad (3.2)$$

For one TLD, n, and irradiation, i,

Normalised readout =

$$(TLDn(Ri)/AVRi) \times Mean\ readout \quad (3.3)$$

An average normalised readout, MNRn, is calculated from normalised readouts for three irradiations and for each TLD, n:

$$\mathbf{MNR_n} = (TLD_n(NR1) + TLD_n(NR2) + TLD_n(NR3))/3 \quad (3.4)$$

Finally a sensitivity correction factor can be determined as:

Sensitivity correction factor (e.g for TLD1) = $(Mean\ readout/MNR1)$ (3.5)

All readouts and the corresponding sensitivity correction factors obtained are shown in the Table 3.2.

Using the readout results from the three irradiations, a simple statistical calculation was carried out in order to obtain the reproducibility for each TLD sample. For each TLD, its three irradiation readouts were combined and a mean, deviation, standard deviation (SD), standard deviation of mean (SDOM), fractional uncertainty (FU) and relative deviation (RD) were calculated and the reproducibility of that TLD was assessed. The statistical values obtained and the reproducibility of measured TLD samples are shown in Table 3.3.

3.3.2.3. Measurement of dose response linearity of $CaSO_4$:Dy TLDs

Investigation of the dose response linearity of $CaSO_4$:Dy TLD samples was carried out by irradiating the TLD samples with various doses. The gross readout of each TLD was corrected for individual sensitivity of a TLD and by a batch variation correction (variations affecting the whole batch of TLDs – see explanation below) to provide corrected readouts. For each dose several irradiations were performed and mean values of corrected readouts were calculated. Finally, a dependence of the TLD readout on delivered dose was plotted.

For each TLD irradiation, three TLDs were selected to act as control TLDs. These three control TLDs provide the third type of correction factor. They were given a radiation dose of 2 Gy from the 4 MV linac irradiation. Their gross readouts were corrected for their individual sensitivities. The mean readout obtained for the three controls was calculated and compared with an expected readout, i.e. a mean of their normalized readouts from the measurement of dose response sensitivity carried out previously. A ratio of these two numbers defines a batch correction factor that represents a deviation of reading results due to unexpected irradiation condition, reading or previous annealing environmental conditions. Consequently, for all measurements, the corrected readout for a given TLD can be expressed as:

$$\text{Corrected readout} = [GR \times SCF] \times BCF \qquad (3.6);$$

where: GR = gross readout,

BCF = batch correction factor,

SCF = sensitivity correction factor.

3.3.2.4. Observation of orientation and reading dependences of the $CaSO_4$:Dy TLD

Two experiments aimed to observe the irradiation-orientation dependence and reading-orientation dependence of TLDs were also explored. In the first experiment, TLDs were irradiated with their marked side facing the radiation beam (face-down). The reading results obtained from these TLDs were corrected with the individual sensitivity correction factor and compared with control TLDs which were placed in the normal manner (face-up, i.e. unmarked side facing the radiation beam) (Figure 3.2).

The experiment to measure the reading-orientation dependence was performed by placing the exposed TLD in the reading tray with the marked side facing the photomultiplier tube window, opposite to the normal readout position, (Figure 3.3). The corrected readout results from those TLDs were compared with other TLDs placed in the normal manner while they were being read. The observation results are shown in the Table 3.5 and Table 3.6.

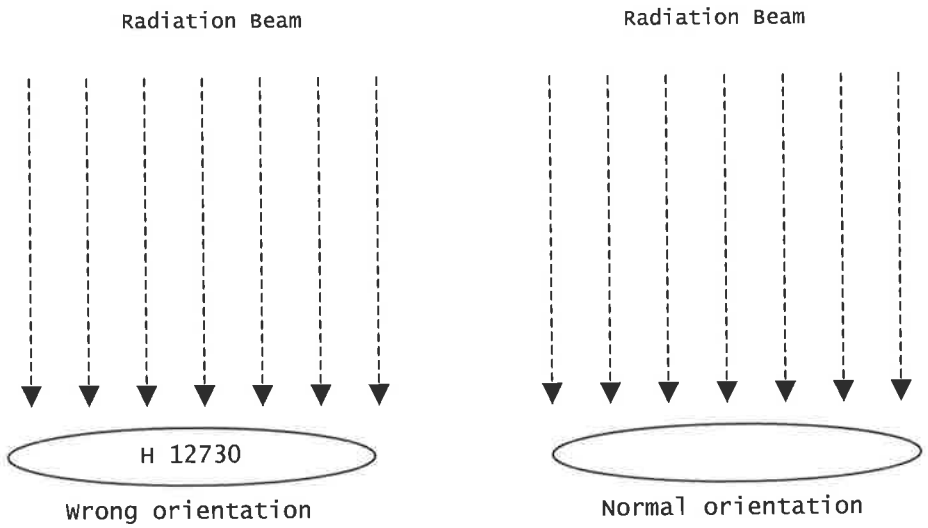

Figure 3.2 Diagram shows two different TLD samples orientation during irradiation process for observation of irradiation-orientation dependence of $CaSO_4$:Dy TLD.

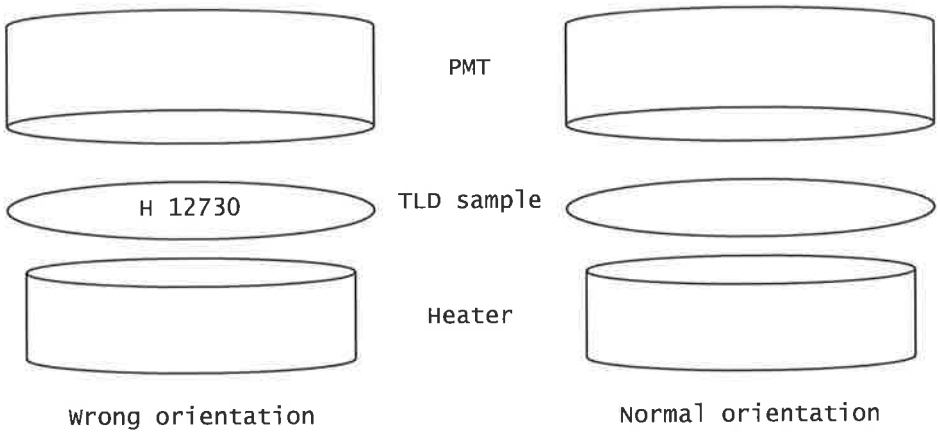

Figure 3.3 Diagram shows two different placement orientations of TLD sample on heating tray during reading process.

3.4. Experimental results

3.4.1. $CaSO_4$:Dy TLD dose response sensitivity

Readout results of TLD samples after irradiation with a 2 Gy dose, as shown in Table 3.2, indicate differences in dose response sensitivity for each TLD, although they were from the same batch. Relative dose response sensitivity for $CaSO_4$:Dy TLD samples ranged from approximately 2% below the mean and up to 30% above. Most of the TLDs (nine) were slightly less sensitive to radiation than the rest. One TLD (H 12730) had a slightly higher sensitivity in dose response whereas TLD discs numbered H 11199, H 16813 and H 19517 had a very high sensitivity to radiation dose compared to the rest of the TLD discs. The measured sensitivity factors were applied to the gross readouts in a further set of measurements in order to obtain the corrected readout for each TLD (as described in section 3.3.23).

Table 3.2 Reading results and calculated statistical values of $CaSO_4$:Dy TLDs given a radiation dose of 2 Gy.

TLD No.	1ST Readout	2ND Readout	3RD Readout
H 01179	185348	177898	206668
H 02487	190590	181003	206774
H 9314	201791	195100	223155
H 8373	191124	177796	204749
H 8020	181922	166512	183870
H 03031	205657	193938	203711
H 05581	202297	188864	209379
H 8598	208703	199580	211692
H 8025	203254	187542	207779
H 12730	213263	218003	224048
H 11199	273308	261287	-
H 16813	244944	-	314554
H 19517	245238	232164	270644
Average	211341.46	198307.25	222251.92

Mean of average readouts = [(211341.46 + 198307.25 + 222251.92)/3] = 210633.54

TLD No.	1ST Normalized Readout	2ND Normalized Readout	3RD Normalized Readout	Mean of Normalized Readout (MNR)	Sensitivity Correction Factor (SCF)
H 01179	184727.15	188955.70	195864.29	189849.05	1.1095
H 02487	189951.59	192253.70	195964.74	192723.35	1.0929
H 9314	201115.07	207226.94	211489.42	206610.48	1.0195
H 8373	190483.80	188847.36	194045.60	191125.59	1.1021
H 8020	181312.63	176861.98	174258.07	177477.56	1.1868
H 03031	204968.12	205992.71	193061.87	201340.90	1.0462
H 05581	201619.38	200603.32	198433.57	200218.76	1.0520
H 8598	208003.92	211985.40	200625.65	206871.66	1.0182
H 8025	202573.17	199199.15	196917.21	199563.18	1.0555
H 12730	212548.64	231553.53	212335.73	218812.64	0.9626
H 11199	272392.52	277527.96	-	274960.24	0.7661
H 16813	244123.52	-	298110.47	271117.00	0.7769
H 19517	244416.54	246594.75	256495.90	249169.06	0.8453

3.4.2. $CaSO_4$:Dy TLD dose response reproducibility results

Readout results and the corresponding reproducibility of each TLD are shown in Table 3.3. From these results, it was observed that, with the irradiation, reading and annealing conditions employed in this experiment, the experimental results were obtained with a range of reproducibility from approximately 4.5% to as good as 1.4% with some TLD discs. Two TLDs, numbered H 11190 and H 16813, were unselected as they have only two irradiation results which were statistically unacceptable. In addition, the TLD numbered H 19517 was unselected because it had the largest standard deviation.

Table 3.3 $CaSO_4$:Dy TLD irradiation readouts and statistical calculation for their reproducibility.

TLD No.	1ST Irradiation Readout	2ND Irradiation Readout	3RD Irradiation Readout	Mean Readout	Standard Deviation	Standard Deviation Of Mean (SDOM)
H 01179	185348	177898	206668	189971.33	14931.83	8620.90
H 02487	190590	181003	206774	192789.00	13025.47	7520.26
H 9314	201791	195100	223155	206682.00	14653.06	8459.95
H 8373	191124	177796	204749	191223.00	13476.77	7780.82
H 8020	181922	166512	183870	177434.67	9509.32	5490.21
H 03031	205657	193938	203711	201102.00	6280.04	3625.78
H 05581	202297	188864	209379	200180.00	10420.06	6016.02
H 8598	208703	199580	211692	206658.33	6309.57	3642.83
H 8025	203254	187542	207779	199525.00	10621.35	6132.24
H 12730	213263	218003	224048	218438.00	5405.64	3120.95

TLD No.	Fractional Uncertainty	Relative Deviation (Reproducibility) (%)
H 01179	0.045	4.54
H 02487	0.039	3.90
H 9314	0.041	4.09
H 8373	0.041	4.07
H 8020	0.031	3.09
H 03031	0.018	1.80
H 05581	0.030	3.01
H 8598	0.018	1.76
H 8025	0.031	3.07
H 12730	0.014	1.43

3.4.3. $CaSO_4$:Dy TLD dose response linearity results

Various radiation doses up to 12 Gy were given to TLD samples and readout numbers were obtained. The batch correction factor and individual sensitivity correction factor were applied to the gross readouts with procedures as described previously. Corrected readouts for each irradiation sequence are shown in the Table 3.4. For each given dose, corrected readouts and their standard deviations are displayed in the Table 3.5. A plot showing the dependence of the mean corrected readouts and given radiation doses is presented in Figure 3.4.

Table 3.4 Linearity measurement results.

TLD No.	Dose (Gy)	Gross Readout	Corrected Readout
H 8373	1	103348	109570.28
H 03031	2	223316	236358.91
H 8020	3	303285	321319.93
H 9314	4	481938	510851.93
H 01179	5	563754	597755.71
H 02487	6	642801	681365.92

TLD No.	Dose (Gy)	Gross Readout	Corrected Readout
H 01179	6	707068	755565.51
H 02487	7	837075	894221.45
H 9314	8	1035203	1105875.49
H 03031	9	1076893	1148686.54
H 8373	10	1115089	1191453.42
H 8020	11	1125850	1202109.72

TLD No.	Dose (Gy)	Gross Readout	Corrected Readout
H 05581	1	95535	91701.69
H 12730	2	206777	198182.36
H 8025	3	304232	292024.79
H 8598	4	410462	393677.09
H 03031	5	503728	483032.47
H 8020	6	600727	576623.03
H 8373	8	785492	754502.28
H 01179	10	1046844	1005643.76
H 9314	12	1372670	1318250.99

TLD No.	Dose (Gy)	Gross Readout	Corrected Readout
H 8020	1	114246	150125.78
H 9314	2	297003	390474.11
H 03031	3	370433	486283.28
H 02487	4	556639	731821.29
H 8373	5	663208	872103.42
H 11199	6	970250	1239640.43
H 01179	8	1192721	1568557.71
H 16813	10	1801386	2442887.38
H 19517	12	2156756	2836651.96

TLD No.	Dose (Gy)	Gross Readout	Corrected Readout
H 8020	1	114246	146519.95
H 11199	2	296368	369559.94
H 8373	3	297003	381171.62
H 02487	4	370433	475316.15
H 03031	5	556639	713172.85

Table 3.5 Corrected readouts and their statistical values.

Dose (Gy)	1ST Irradiation Readout	2ND Irradiation Readout	3RD Irradiation Readout	4TH Irradiation Readout	Mean Readout
1	109570.28	91701.69	150125.78	146519.95	124479.43
2	236358.91	198182.36	390474.11	369559.94	298643.83
3	321319.93	292024.79	486283.28	381171.62	370199.91
4	510851.93	393677.09	731821.29	475316.15	527916.62
5	597755.71	483032.47	872103.42	713172.85	666516.11
6	681365.92	755565.51	576623.03	1239640.43	813298.72
8	1105875.49	754502.28	1568557.71	-	1142978.49
10	1191453.42	1005643.76	2442887.38	-	1546661.52
12	1318250.99	2836651.96	-	-	2077451.48

Table 3.5 Corrected readouts and their statistical values (continued).

Dose (Gy)	Standard Deviation	Standard Deviation Of Mean	Relative deviation (%)
1	28520.07	14260.03	11.46
2	95627.42	47813.71	16.01
3	85822.16	42911.08	11.59
4	144516.87	72258.44	13.69
5	166169.82	83084.91	12.47
6	293554.10	146777.05	18.05
8	408294.06	235728.68	20.62
10	781694.89	451311.76	29.18
12	1073671.62	759200.49	36.54

3.4.4. Measured results of irradiation-orientation and reading-orientation dependence of $CaSO_4$:Dy TLD

3.4.4.1. Results of irradiation-orientation experiment

Table 3.6 presents the corrected readouts obtained from measurement investigating the readout dependence on the TLD position (face-up and face-down) on the irradiation phantom during exposure to radiation.

Table 3.6 Readout results of experiment in TLD orientation dependence.

	Corrected Readout	
TLD No.	Unmarked-side facing radiation beam	Marked-side facing radiation beam
H 8598	217549.66	-
H 05581	212538.13	-
H 8025	225986.90	-
H 9314	-	238823.03
H 03031	-	221220.78
H 8373	-	222240.30
H 8020	-	205754.47
H 02487	-	236513.73
H 11199	-	181489.95
H 19517	-	189677.99
H 16813	-	134285.10
H 12730	-	209567.55
Average	218691.56	204396.99

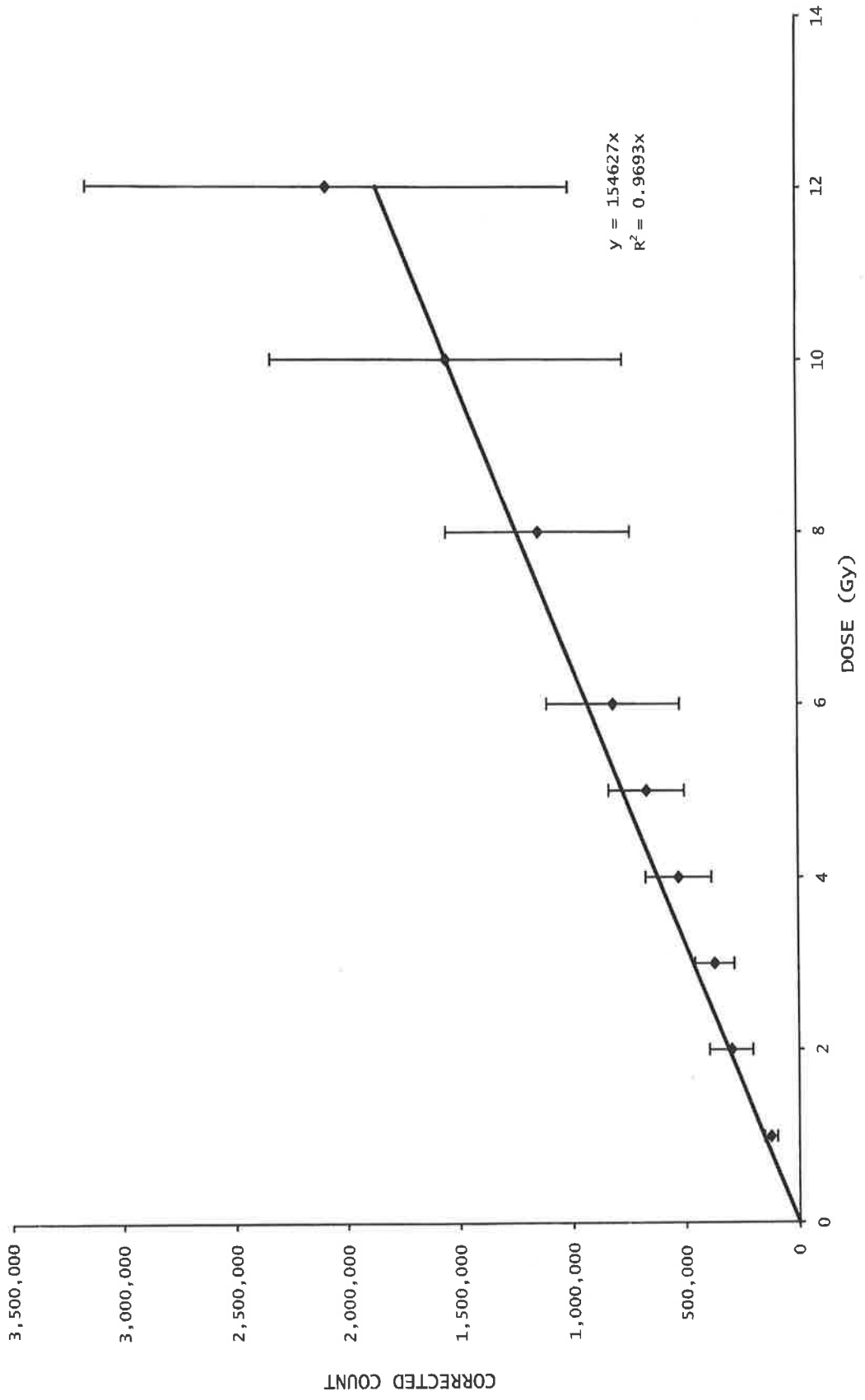

Figure 3.4 Dose response curve of $CaSO_4$:Dy TLD for radiation doses of up to 12 Gy.

From corrected readouts shown in Table 3.6 above, the difference between the two alternative ways of placing the TLD is approximately 6% in the mean corrected readout. TLD samples placed with their marked-side facing toward the radiation beam resulted in lower reading results than that of those TLD samples which were placed in the usual manner (unmarked-side facing to radiation beam).

3.4.4.2 Results of reading-orientation experiment

Table 3.7 presents two groups of corrected readouts obtained from an experiment investigating the dependence of the TLD readout values on the two ways of placing the TLD samples on the reading tray during the readout.

Table 3.7 Readout results of experiment in TLD reading-orientation dependence.

	Corrected Readout	
TLD No.	Unmarked-side facing PMT window	Marked-side facing PMT window
H 8598	271772.17	-
H 05581	266028.15	-
H 8025	288762.92	-
H 9314	-	321328.34
H 03031	-	310168.70
H 8373	-	306231.74
H 8020	-	296853.42
H 02487	-	321972.67
H 01179	-	215361.42
H 19517	-	221116.15
H 16813	-	224214.09
H 12730	-	259669.14
Average	275521.08	275212.85

From above results, it was observed that there is a very small difference between two readings obtained from the two different TLD placements manners on the reading tray.

3.5. Discussion of experimental results

3.5.1. Dose response sensitivity of $CaSO_4$:Dy

Although the TLD samples used in this experiment were taken from the same batch the measurement results showed that they had different dose response, reflected by their sensitivities. The TLDs that have a high sensitivity (e.g H 11199, H 16813 and H 19517) tend to give higher reading results than those which have low sensitivity. The sensitivity correction factors obtained from the calculations were shown to be reasonable as they were applied to gross readouts in later measurements. There are two sources of sensitivity variation: intrinsic variables which are the result of the manufacturing process, and extrinsic variables associated with the treatment of the TLDs such as the irradiation method and reading conditions (Robertson, 1981).

3.5.2. Measurement of reproducibility of $CaSO_4$:Dy TLD

The factors that affect the degree of sensitivity of $CaSO_4$:Dy TLD samples are also considered to be influential factors on the reproducibility of TLD samples. However, the treatment conditions of TLD (extrinsic variation) including irradiation method and reading parameters appear to have a greater impact on the reproducibility of TLDs than the intrinsic factors. Variations due to the irradiation method were kept to a minimum as the output of the linac was checked before the irradiation with an ionization chamber (error ±0.3%). In addition, the irradiation setting parameters were not complicated and could be exactly reproduced. On the other hand, reading parameters appear to result in greater variations of TLD readout values. Changes in the gain of the reading system due to temperature changes, humidity and blockage of light transmission through the window of the photomultiplier tube from dust will affect the readout. These changes can be monitored with an aid of built-in internal and external light sources as the reading results obtained

from measuring these two light sources were compared with the previous results and any unusual differences were observed. As a result of the above measures, the measurements of the $CaSO_4$:Dy TLD samples employed in this research provided acceptable reproducibility of less than 5% for all TLD samples. For some TLDs, reproducibility nearly as good as 1%, was obtained. The systematic error due to accelerator output measurement of 0.3% is negligible compared to statistical errors.

3.5.3. Measurement of $CaSO_4$:Dy TLD dose response linearity

Dose response of $CaSO_4$:Dy TL dosimeters (TLD-900) are normally linear up to a dose of 10 Gy where supralinearity starts to appear (McKeever, 1995). Results obtained from the experimental measurements are consistent with the reported values. Linearity and the onset of supralinearity of TL dosimeters are normally influenced by a variety of factors, both intrinsic and extrinsic. For instance, concentration of impurity composition, ionization density grain size, heating rate and annealing conditions are all influential factors for dose response linearity and onset of supralinearity of TLDs. Observation of the dose response linearity of TLD samples is important as that will define the useful measurement range of the TLD samples. As observed from the measurements, the dose response of the $CaSO_4$:Dy TLD samples was linear for the dose levels up to 8 Gy. In the subsequent irradiation of TLD with Ru-106 source (Chapter 4), doses between 3 - 5 Gy were applied that are well within the linear TLD region.

3.5.4. Measurement of irradiation-orientation dependence and reading-orientation dependence of $CaSO_4$:Dy TLD

These measurements simulated the situations when TLD samples were accidentally placed in a different manner as they should be during irradiation and reading processes in which any difference in reading results might be observed. It was observed that the reading

results obtained from TLD samples which were placed as their unmarked-side facing radiation beam were 6% higher than that obtained from TLD samples with their marked-side facing the radiation beam during irradiation process. Normally, both ways of placing the TLD samples should provide similar reading results as the TLD samples have a very small thickness and the photons originated from the linear accelerator are able to penetrate through the TLD disc and deposited radiation dose to both sides of the TLD sample. The small difference of 6% in reading results observed in the experiment could have other causes, for example, the variation due to the intrinsic properties of the TLD sample itself. As result of the observed irradiation-orientation dependence, in all the measurements the TLD samples were always positioned in the same orientation, i.e. with their unmarked side face towards the radiation beam.

Variations due to incorrect placing of TLD samples on the reading tray during the reading process are negligible and differences are within the error of the measurement. This phenomenon may be explained by the fact that during the reading process, a TLD will be heated by the heating plate. The transmitted heat was high enough to release almost of all of the storage energy in the form of luminescence that can be detected by a photomultiplier tube located inside the reader. The reading process was also performed under nitrogen gas-filled environment that diminishes light absorption before reaching PMT window. Hence, placing of TLD sample on reading tray with its non-irradiated side facing PMT window would not affect the reading results of the sample.

3.6. Conclusion

Before each TLD can be used for dosimetric measurements, it must be properly examined to obtain its response pattern to the radiations being studied and it is also required to be accurately calibrated against a standard radiation source. In this research, a

number of $CaSO_4$:Dy thermoluminescent dosimeters were investigated to obtain their response to radiation from a 4 MV medical linear accelerator. The reproducibility, linearity, irradiation-orientation dependence and reading-orientation dependence of a batch of $CaSO_4$:Dy TLDs were observed. As a result, a sensitivity correction factor for each TLD disc and a batch correction factor were obtained and applied to correct the gross readout in order to obtain a corrected readout in each experiment.

Chapter 4

Measurements of COB and CCA Type Ruthenium-106 Ophthalmic Applicator Dose Distributions

4.1 Introduction

In the previous chapter, $CaSO_4$:Dy TLD discs were examined for their basic dosimetric properties such as dose response sensitivity, dose response linearity, irradiation-orientation and reading-orientation dependencies, and dose measurement reproducibility. In this chapter, three $CaSO_4$:Dy TLD discs were selected and cut into small pieces, studied for their dosimetry characteristics, and, used for measurement of absolute dose rate distributions of ruthenium-106 applicators. The three TLDs with reproducible results were selected and cut into small pieces with dimensions of approximately 2 x 3 x 0.4 mm^3. They were calibrated against radiation from the 4 MV linear accelerator as before. Then a number of measurements were carried out to evaluate the absolute dose rate and percentage depth dose rate distributions of ruthenium-106 applicators.

4.2. Preparation and calibration of small $CaSO_4$:Dy TLDs

Three selected TLD discs numbered H 12730, H 8025 and H 05581 were cut with a scalpel into small dosimeters with dimensions of 2 x 3 x 0.4 mm^3. In total, 40 small TLDs were obtained and numbered from 1 to 40. These three TLDs were selected as they provided a dose response very close to the mean expected value (measured in chapter 3) and, therefore, had very small correction factors.

Calibration of small $CaSO_4$:Dy TLDs was carried out with the 4 MV linear accelerator. The calibration procedures consisted of an irradiation of TLD with radiation dose of 2 Gy, with the TLD surface at d_{max} in a Perspex phantom. The irradiation, reading and annealing parameters used were the same as those that used in previous calibration of large $CaSO_4$:Dy TLDs. Reading results obtained from three consecutive irradiations were averaged and individual sensitivity correction factors were calculated using the same statistical calculation procedure described previously in the Chapter 3 (see Table 3.1 and equations 3.1, 3.2, 3.3 and 3.4). All reading results and individual sensitivity correction factors are shown in the Table 4.1. Individual sensitivity correction factors, together with a batch correction and background subtraction, were applied to gross reading results to obtain the corrected readouts.

4.3. Measurement of ruthenium-106 ophthalmic applicator dose distributions with small $CaSO_4$:Dy TLDs

4.3.1. Measurement instrumentation

This consisted of:

1. Calibrated small $CaSO_4$:Dy TLDs

2. Eye phantoms: the solid acrylic $(C_5H_8O_2)_n$ eye phantoms (Figure 4.1) that were used in these measurements consist of:

i. Five phantom bases that have a disc-like shape for placement of the TLDs. They have diameter of 15 mm and 20 mm for each type of ruthenium applicators.

ii. Phantom tops: there are five pieces of phantom top that have various heights from 1 mm to 5 mm. They are concave in shape to simulate the curved surface of the eye. TLDs were positioned on the base and covered with a corresponding phantom top. The thickness of the phantom top represents the depth into the eye tissue at which the doses were measured.

iii. Additional discs of phantom materials: the depth into the eye phantom can be increased from 6 mm up to 10 mm by adding one or more discs of phantom material which have a thickness of 1 mm each between the top and the base.

iv. Phantom holder: is used for holding the eye phantom in place during the irradiation with the ruthenium-106 applicator. It has two slits on the side in which the notches of the ruthenium-106 applicator slide into. This ensures a reproducible positioning of the ophthalmic applicator on the eye phantom for the measurements (see Figure 4.2).

Table 4.1 Readouts of 40 small $CaSO_4$:Dy TLD chips and their individual sensitivity correction factor.

TLD No.	First readout	Norm. readout	Second readout	Norm. readout	Third readout	Norm. readout	Average Norm. Readout	Sensitivity Correction Factor
1	20738	21526.09	22030	22210.22	22814	21837.32	21857.88	1.0886
2	23182	24062.96	25319	25526.13	25609	24512.67	24700.59	0.9633
3	24301	25224.49	26131	26344.77	27424	26249.97	25939.74	0.9173
4	22493	23347.78	24003	24199.36	25322	24237.95	23928.37	0.9944
5	20544	21324.72	22889	23076.25	24426	23380.31	22593.76	1.0531
6	24239	25160.13	26232	26446.60	26928	25775.20	25793.98	0.9225
7	22344	23193.12	23674	23867.67	24882	23816.79	23625.86	1.0071
8	21123	21925.72	22649	22834.29	24074	23043.38	22601.13	1.0528
9	22824	23691.36	23975	24171.13	25570	24475.34	24112.61	0.9868
10	21916	22748.85	22716	22901.83	24512	23462.63	23037.77	1.0328
11	21781	22608.72	22861	23048.02	24354	23311.39	22989.38	1.0350
12	21381	22193.52	22310	22492.51	24493	23444.44	22710.16	1.0477
13	22610	23469.23	23143	23332.33	25314	24230.30	23677.28	1.0049
14	21848	22678.27	22032	22212.24	23657	22644.23	22511.58	1.0570
15	21288	22096.99	21640	21817.03	23250	22254.66	22056.23	1.0788
16	20757	21545.81	21318	21492.40	22541	21576.01	21538.07	1.1048
17	19711	20460.06	20375	20541.68	21891	20953.84	20651.86	1.1522
18	23557	24452.22	23965	24161.05	25664	24565.31	24392.86	0.9755
19	21296	22105.29	21775	21953.14	22968	21984.73	22014.39	1.0808
20	22148	22989.67	23234	23424.07	24523	23473.16	23295.63	1.0214
21	18294	18989.21	19381	19539.55	19119	18300.51	18943.09	1.2561
22	18594	19300.61	19325	19483.09	18999	18185.64	18989.78	1.2530
23	24951	25899.19	26157	26370.98	26526	25390.41	25886.86	0.9192
24	21263	22071.04	21480	21655.72	23237	22242.21	21989.66	1.0821
25	20928	21723.31	22318	22500.58	23410	22407.81	22210.56	1.0713
26	20657	21442.01	21395	21570.03	22872	21892.84	21634.96	1.0998
27	24653	25589.87	25437	25645.09	26992	25836.46	25690.47	0.9262
28	26399	27402.22	27544	27769.33	28021	26821.41	27330.99	0.8706
29	25762	26741.01	26125	26338.72	26648	25507.19	26195.64	0.9083
30	26646	27658.60	26338	26553.46	29357	28100.21	27437.43	0.8672
31	23658	24557.05	23861	24056.20	26067	24951.06	24521.44	0.9703
32	26417	27420.90	26115	26328.64	27565	26384.93	26711.49	0.8908
33	23043	23918.68	22751	22937.12	23814	22794.51	23216.77	1.0249
34	22099	22938.81	21209	21382.51	22381	21422.86	21914.72	1.0858
35	24655	25591.94	24530	24730.67	25989	24876.40	25066.34	0.9492
36	23409	24298.59	23919	24114.68	24370	23326.71	23913.33	0.9950
37	26056	27046.18	26427	26643.19	26593	25454.54	26381.31	0.9019
38	25200	26157.65	25065	25270.05	26426	25294.69	25574.13	0.9304
39	27998	29061.98	27191	27413.44	28748	27517.28	27997.57	0.8499
40	26160	27154.13	25206	25412.20	26986	25830.72	26132.35	0.9105
Avg.	22923.08		23601.13		24858.40			
Mean of average readouts = (22923.08 + 23601.13 + 24858.40) ÷ 3 = 23794.20								

1.3 Ruthenium-106 ophthalmic applicators: there are two types of applicators that were used in measurement, CCA and COB types which have diameter (D) of 15-mm and 20- mm respectively (the properties of ruthenium-106 applicator were described in Chapter 1).

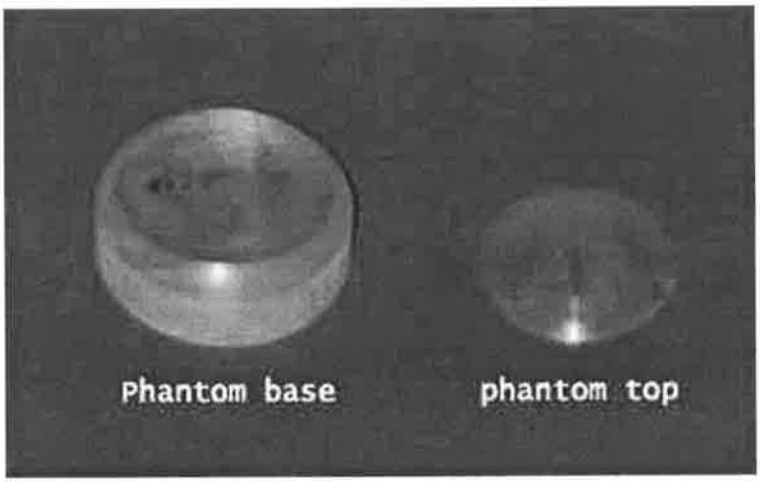

Figure 4.1 The eye phantom used in the measurement. A phantom base and a top are shown in this picture.

4.3.2. Measurement procedures

Measurement of the ruthenium-106 applicator dose distribution at a particular depth in the eye phantom started with placement of small $CaSO_4$:Dy TLDs on the phantom base at the positions marked by vertical and horizontal grid lines (Figure 4.3).

Five or nine dosimeters can be placed on the phantom base for each measurement, depending on surface area of the phantom base that is covered by a phantom top. Five TLDs were used for 1-mm and 2-mm eye phantom tops that have smaller surface area than other tops. Each position, in relation to the centre position, is named for further reference (Figure 4.4).

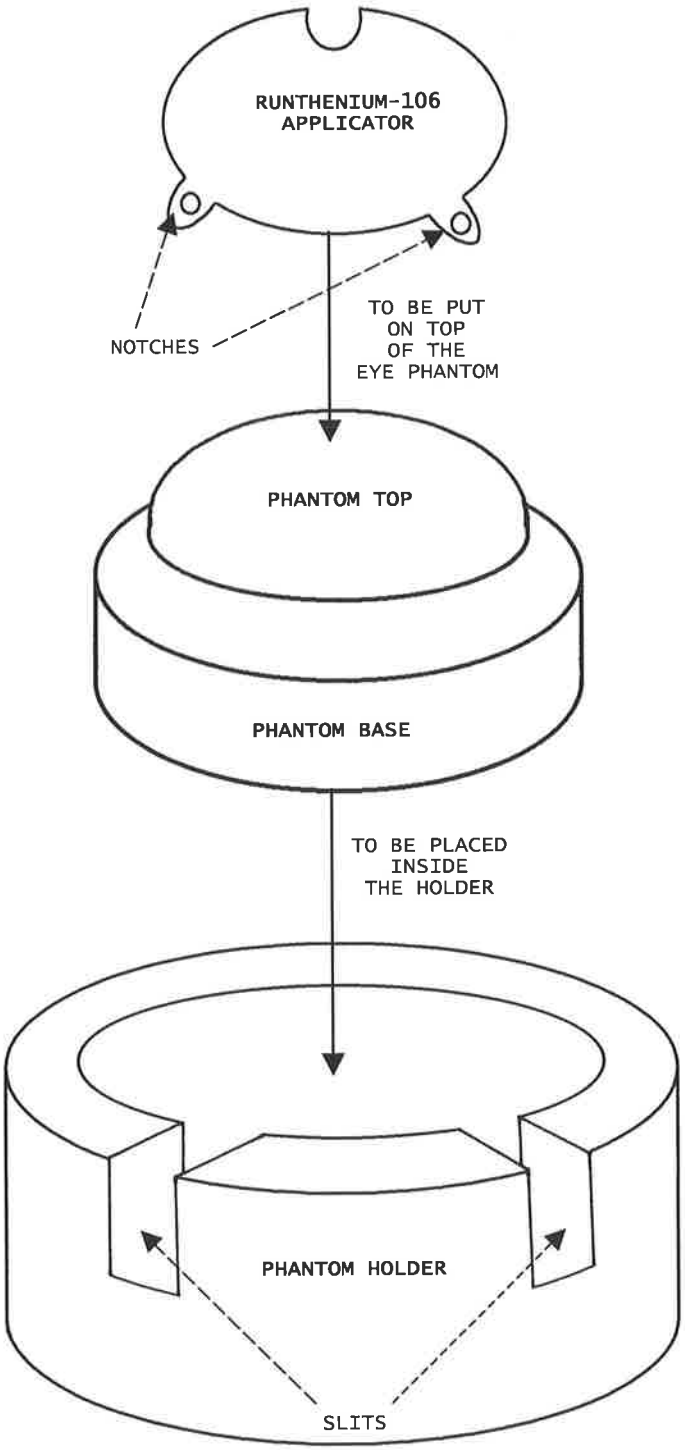

Figure 4.2 Diagram shows arrangement of ruthenium-106 applicator, eye phantom and phantom holder for measurements of dose distribution of ruthenium-106 applicator.

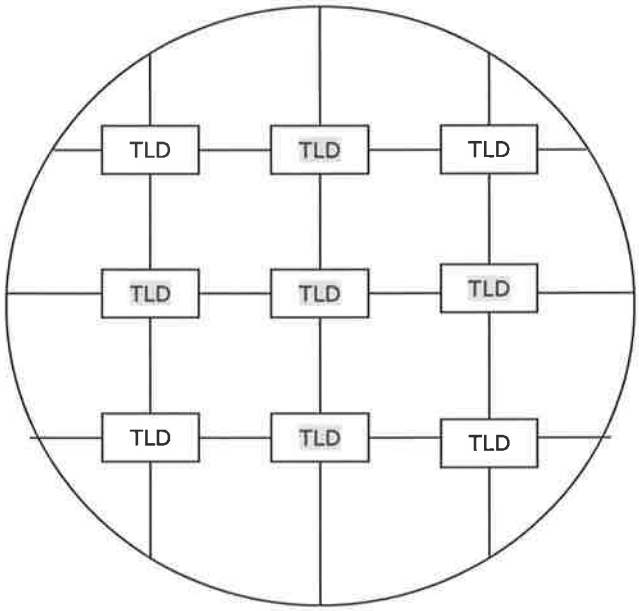

Figure 4.3 The picture shows the surface of the eye phantom base. Vertical and horizontal lines made up reference positions for placing small $CaSO_4$:Dy TLDs. Positions colored gray indicate TLD placing for thinner phantom tops (1, 2 mm).

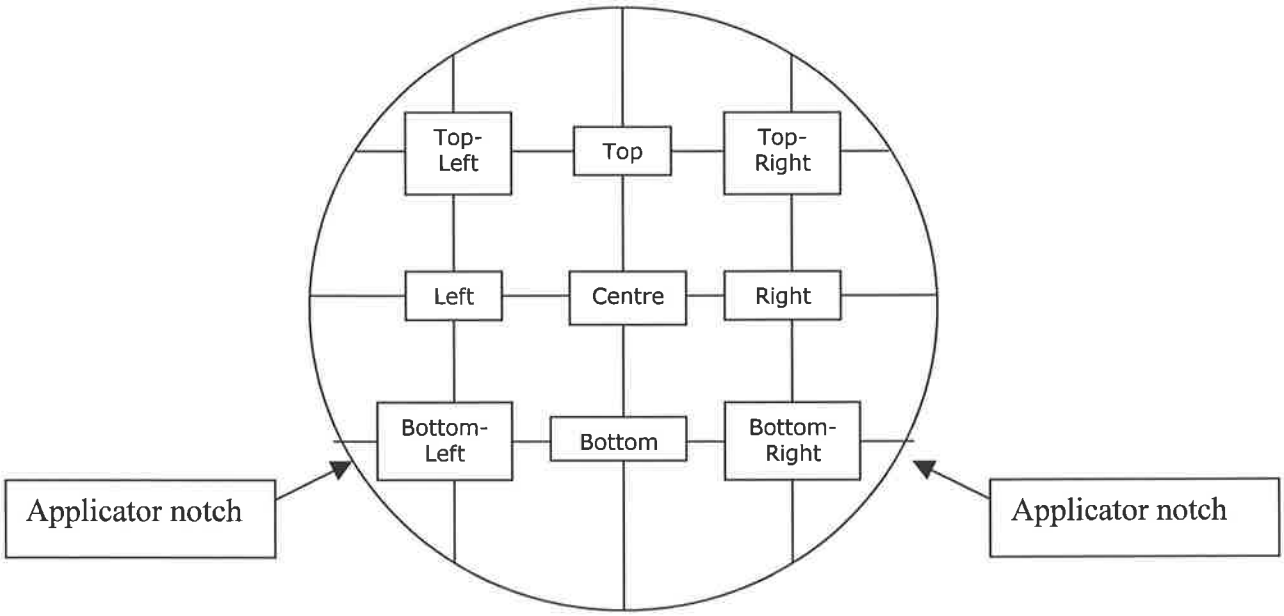

Figure 4.4 The picture shows the naming used for TLD positions.

After the required numbers of TLDs were placed on the phantom base, a corresponding phantom top was put over the top of the TLDs. Similarly, a pair of vertical and horizontal lines was drawn on the phantom top to be used as markers for placing on the base in a reproducible manner. To hold the whole assembly firmly in their position, thin tape was used in order to prevent TLDs and phantom top from moving during the measurement.

The TLDs and the phantom were then placed inside the phantom holder. Markings were also drawn on the phantom holder in order to obtain reproducibility in placement of the eye phantom for each measurement. Finally, the ruthenium-106 eye applicator was put on the phantom using plastic forceps. There were two slits on the phantom holder that fitted the notches of the applicator (Figure 4.5). This resulted in a firm positioning of the applicator on the phantom.

Figure 4.5 Position of the ruthenium-106 applicator on the eye phantom. As shown in the picture, both of the phantom slits firmly hold the applicator notches resulting in a firm positioning of the applicator.

The applicator was left on the phantom for a period of time, estimated to correspond to the radiation dose of 4 Gy delivered to the depth of the TLDs (varying from 1 to 24 hours depending on the measured depth). The time required was calculated using the dose rate values provided by the manufacturer, corrected for decay. After irradiation, the exposed TLDs were left standing at room temperature overnight before proceeding with the reading process.

As well as the irradiation of the TLDs, six TLDs were irradiated with a radiation dose of 4 Gy from the 4-MV linear accelerator. These TLDs were used as control TLDs in order to monitor any shifts in reading results due to changes in the reading and annealing conditions. The results (number of counts) of these control TLDs were corrected by the sensitivity correction factors. An average readout was calculated and compared to the expected normalized readout, i.e. the average of the reading results for these TLDs obtained from the calibration measurement of Table 4.1. A number, called the "batch correction factor", was calculated as:

$$\text{Batch correction factor (BCF)} = \frac{\text{Expected readout}}{\text{Average corrected readout}} \qquad (4.1)$$

This process of obtaining the batch correction factor was carried out each time all TLDs were used and annealed.

To obtain the corrected readout (in numbers of counts) for each reading result for individual TL dosimeter, the equation (3.5) as described previously in chapter 3 was used.

When all 34 TLDs were used for plaque measurements, they were annealed with the annealing oven with an annealing temperature of 270 °C for 2 hours. Finally, they were shock cooled by placing them between two steel blocks to make them available for further measurement. Measurements of depth dose distribution of ruthenium-106 applicator for the depths from 1 mm to 10 mm were performed. However, for measurement of dose rate at zero depth (contact dose), a TLD was placed on top of the phantom top and put on the phantom base.

4.3.3. Calculation of depth dose from reading results

A corrected readout for each TLD was compared with the expected normalized readout obtained from calibration measurements and corresponding to a dose of 4 Gy from linac irradiation to obtain the radiation dose given to the TLD in Gy. The absolute dose, then, was divided by the irradiation time (in hours) to obtain an absolute dose rate (Gy/hr). The absolute dose rate (Gy/hr) was calculated for the unit in mGy/min and corrected with the corresponding decay correction factor to obtain a final corrected absolute dose rate (mGy/min) (Equation 4.2, 4.3). The decay correction applied in this calculation was relative to an activity measured on a calibration date that was provided by the manufacturer (May 2000).

Final corrected dose rate (mGy/min) =

$$\left[\left(\frac{\text{corrected readout}}{\text{expected readout}} * 4\right)/\text{irradiation time (hour)}\right] \times \frac{1000}{60}\frac{(mGy)}{(\text{min})} \times \begin{pmatrix}\text{Decay}\\ \text{correction}\\ \text{factor}*\end{pmatrix} \quad \textbf{(4.2)}$$

$$* \text{ Decay correction factor } = \frac{\text{Halflife}}{\text{Decay}-\text{time}}\frac{(Days)}{(Days)} \quad \textbf{(4.3)}$$

4.4. Measurement results

4.4.1. Calibration results of small $CaSO_4$:Dy TLDs

As shown in the Table 4.1, it was observed that each small $CaSO_4$:Dy TLDs, although cut from the same TLD disc, responded to radiation dose with different degree of sensitivity. For small TLDs numbered 1 – 12 (cut from TLD disc numbered H 12730) and small TLDs numbered 13 – 26 (cut from TLD disc numbered H 05581), most responded to radiation doses with a lower sensitivity than average as their individual sensitivity correction factors had positive values rather than negative ones. In contrast, most of those small TLDs (numbered 27 – 40) that were cut from the third TLD disc responded to radiation dose with a higher sensitivity than average as their sensitivity correction factors had negative values. The sensitivity factors of such small TLDs (even those obtained from the same TLD disc) vary mainly due to differences in their size (as they were cut into small pieces by hand) and due to inhomogeneity of the TLD material.

4.4.2. Results from the measurements for dose distribution of a 20-mm (COB type) ruthenium-106 ophthalmic applicator

The measurement procedures described previously were preformed for measurements of the dose distribution of a 20-mm (COB type) ruthenium-106 applicator. The average absolute depth dose rate distribution along the central axis and off-axis absolute depth dose rate distributions obtained from measurements were shown in the Table 4.2. Several measurements (4-6 times) were carried out for each depth to ensure good statistical significance of the data. The complete measurement results are shown separately in Appendix I. The measurement results show a decrease in the absolute dose rate (mGy/min) as the depth of the eye-phantom increases.

On the central axis, the Percentage Depth Dose (rate), PDD, decreased from 100% (177.36 mGy/min) at the contact vicinity of the ruthenium-106 plaque to 1.12% (1.99 mGy/min) at a depth of 10 mm. Differences of the off-axis dose distributions at any depth were also observed from the measurements. Generally, the absolute dose rates of the areas located near the notch of the applicator were lower than for other areas. In addition, the dose rate in the areas around the bottom part of the applicator appeared to be higher than that for other areas (Figure 4.5).

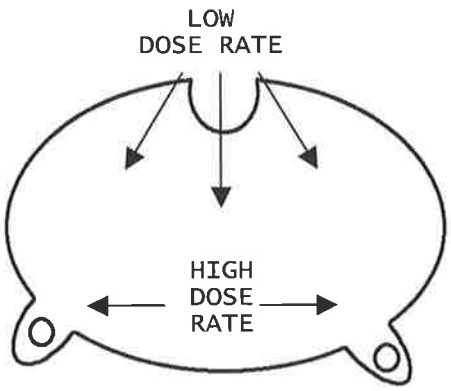

Figure 4.5 This drawing of a 20-mm ruthenium-106 applicator shows the areas where the measured dose rate (mGy/min) is lower or higher than other areas.

Table 4.2 Dose rate and statistical values for the dose distribution at various depths of 20-mm (COB) ruthenium-106 applicator. Percentage dose rate is normalized to surface dose.

Position	Depth (mm)	Average Corrected Dose Rate (mGy/min)	Standard Deviation (mGy/min)	Relative Error (%)	Percentage Depth Dose Rate
Centre	0	177.36	6.10	3.55	100.00 (±3.55)
	1	138.23	3.75	2.72	77.94 (±3.41)
	2	109.00	4.85	4.45	61.46 (±3.46)
	3	82.70	2.14	2.59	46.63 (±2.01)
	4	57.87	1.31	2.97	32.63 (±1.34)
	5	31.73	1.61	5.07	17.89 (±1.10)
	6	20.47	0.34	1.67	11.54 (±0.44)
	7	12.17	0.28	2.33	6.86 (±0.28)
	8	7.33	0.18	2.39	4.13 (±0.17)
	9	3.84	0.08	2.12	2.17 (±0.09)
	10	1.99	0.11	5.35	1.12 (±0.07)
Top	1	151.95	6.08	4.00	85.67 (±4.52)
	2	115.72	8.89	7.68	65.25 (±5.49)
	3	69.24	2.06	2.97	39.04 (±1.78)
	4	46.44	1.19	2.55	26.18 (±1.12)
	5	22.64	1.00	4.40	12.76 (±0.71)
	6	13.59	0.49	3.58	7.66 (±0.38)
	7	8.71	0.43	4.93	4.91 (±0.30)
	8	4.89	0.22	4.52	2.76 (±0.16)
	9	2.63	0.09	3.30	1.48 (±0.07)
	10	1.27	0.13	10.37	0.72 (±0.08)
Right	1	162.39	5.70	3.51	91.56 (±4.50)
	2	139.38	4.31	3.09	78.59 (±3.63)
	3	109.44	5.32	4.86	61.71 (±3.67)
	4	77.51	5.06	6.52	44.84 (±3.22)
	5	38.58	1.59	4.13	23.69 (±1.17)
	6	24.53	1.98	8.06	16.37 (±1.21)
	7	14.60	0.44	3.03	9.61 (±0.38)
	8	8.97	0.28	3.13	5.97 (±0.23)
	9	4.05	0.17	4.11	3.03 (±0.12)
	10	2.26	0.15	6.72	1.86 (±0.10)
Bottom	1	151.87	6.27	4.13	85.63 (±4.60)
	2	119.94	8.02	6.68	67.63 (±5.08)
	3	108.57	4.06	3.74	61.21 (±3.11)
	4	79.52	4.01	5.04	44.84 (±2.74)
	5	42.02	1.96	4.66	23.69 (±1.37)
	6	29.03	0.59	2.04	16.37 (±0.65)
	7	17.05	0.45	2.63	9.61 (±0.42)
	8	10.59	0.36	3.37	5.97 (±0.29)
	9	5.38	0.16	3.00	3.03 (±0.14)
	10	3.30	0.22	6.74	1.86 (±0.14)

Table 4.2 Dose rate and statistical values for the dose distribution at various depths of 20-mm (COB) ruthenium-106 applicator. Percentage dose rate is normalized to surface dose (continued).

Position	Depth (mm)	Mean Corrected Dose Rate (mGy/min)	Standard Deviation (mGy/min)	Relative Error (%)	Percentage Depth Dose Rate
Left	1	161.96	4.26	2.63	91.32 (±3.95)
	2	137.03	4.60	3.36	77.26 (±3.71)
	3	107.63	1.94	1.80	60.68 (±2.36)
	4	77.43	3.46	4.46	43.66 (±2.46)
	5	47.14	1.75	3.72	26.58 (⊥1.35)
	6	29.91	1.07	3.57	16.86 (±0.84)
	7	16.81	0.78	4.66	9.48 (±0.55)
	8	9.89	0.25	2.56	5.58 (±0.24)
	9	5.53	0.21	3.76	3.12 (±0.16)
	10	2.85	0.10	3.43	1.61 (±0.08)
Top-Right	3	108.58	4.11	3.79	61.22 (±3.13)
	4	70.17	3.93	5.60	39.56 (±2.60)
	5	29.76	1.17	3.92	16.78 (±0.88)
	6	16.55	1.33	8.04	9.33 (±0.82)
	7	9.95	0.34	3.44	5.61 (±0.27)
	8	6.06	0.06	0.95	3.42 (±0.12)
	9	2.84	0.17	5.92	1.60 (±0.11)
	10	1.39	0.17	12.44	0.78 (±0.10)
Bottom-Right	3	126.89	4.83	3.81	71.54 (±3.67)
	4	85.43	6.03	7.05	48.17 (±3.78)
	5	45.62	1.89	4.14	25.72 (±1.38)
	6	28.71	1.54	5.36	16.19 (±1.0.3)
	7	15.97	0.84	5.29	9.00 (±0.57)
	8	10.13	0.50	4.95	5.71 (±0.34)
	9	4.47	0.28	6.28	2.52 (±0.18)
	10	3.04	0.34	11.28	1.71 (±0.20)
Bottom-Left	3	123.58	6.26	5.07	69.68 (±4.27)
	4	101.27	2.82	2.78	57.10 (±2.53)
	5	56.26	2.19	3.89	31.72 (±1.65)
	6	36.94	1.04	2.83	20.83 (±0.93)
	7	18.99	1.03	5.41	10.71 (±0.69)
	8	11.86	0.83	6.97	6.69 (±0.52)
	9	6.02	0.25	4.18	3.39 (±0.18)
	10	3.47	0.17	4.86	1.96 (±0.12)
Top-Left	3	116.32	4.48	3.85	65.58 (±3.39)
	4	85.91	3.39	3.95	48.44 (±2.54)
	5	42.48	1.36	3.21	23.95 (±1.13)
	6	23.57	0.86	3.65	13.29 (±0.67)
	7	13.20	0.86	6.54	7.44 (±0.55)
	8	6.99	0.07	0.97	3.94 (±0.14)
	9	3.82	0.15	3.88	2.15 (±0.11)
	10	1.81	0.20	11.14	1.02 (±0.12)

Table 4.3 Variation of depth dose rate and percentage depth dose rate for a 20-mm (COB) ruthenium-106 applicator along the central axis. The depth dose rates provided by the manufacturer are also presented.

TLD Measurement values			Applicator's manufacturer data		
Depth (mm)	Average dose rate (mGy/min)	Percentage Depth Dose Rate	Depth (mm)	Dose rate (mGy/min)	Percentage Depth Dose Rate
0	177.36 (±6.10)	100.00 (±3.55)	0	183 (±54.9)	100.00 (±30.00)
1	138.23 (±3.75)	77.94 (±3.41)	1	140 (±42.0)	76.50 (±22.95)
2	109.00 (±4.85)	61.46 (±3.46)	2	102 (±30.6)	55.74 (±16.72)
3	82.70 (±2.14)	46.63 (±2.01)	3	71 (±21.3)	38.80 (±11.64)
4	57.87 (±1.31)	32.63 (±1.34)	3.5	61 (±18.3)	33.33 (±10.00)
5	31.73 (±1.61)	17.89 (±1.10)	4	50 (±15.0)	27.32 (±8.20)
6	20.47 (±0.34)	11.54 (±0.44)	5	34 (±10.2)	18.58 (±5.57)
7	12.17 (±0.28)	6.86 (±0.28)	6	23 (±6.9)	12.57 (±3.77)
8	7.33 (±0.18)	4.13 (±0.17)	7	16 (±4.8)	8.74 (±2.62)
9	3.84 (±0.08)	2.17 (±0.09)			
10	1.99 (±0.11)	1.12 (±0.07)			

4.4.3. Results from the measurements for dose distribution of a 15-mm (CCA) ruthenium-106 ophthalmic applicator

The same measurement procedure was applied to the 15-mm ruthenium-106 applicator. However, only the dose distribution along the central axis up a depth of 5 mm was measured. Results obtained for this CCA type applicator are similar to that obtained from COB type applicator. The dose rate in the close vicinity to the applicator was 131 mGy/min (PDD 100%) and decreased to 28.8 mGy/min (PDD 21.9%) at the depth of 5 mm (Table 4.4 and Table 4.5). The variation of depth dose rate and percentage depth dose rate of the 15-mm applicator in comparison with the manufacturer values are presented in the Table 4.6. Figures 4.8 and 4.9 show plots of depth dose rate and percentage depth dose rate of 15-mm ruthenium-106 applicator also in comparison with the data provided by applicator's manufacturer.

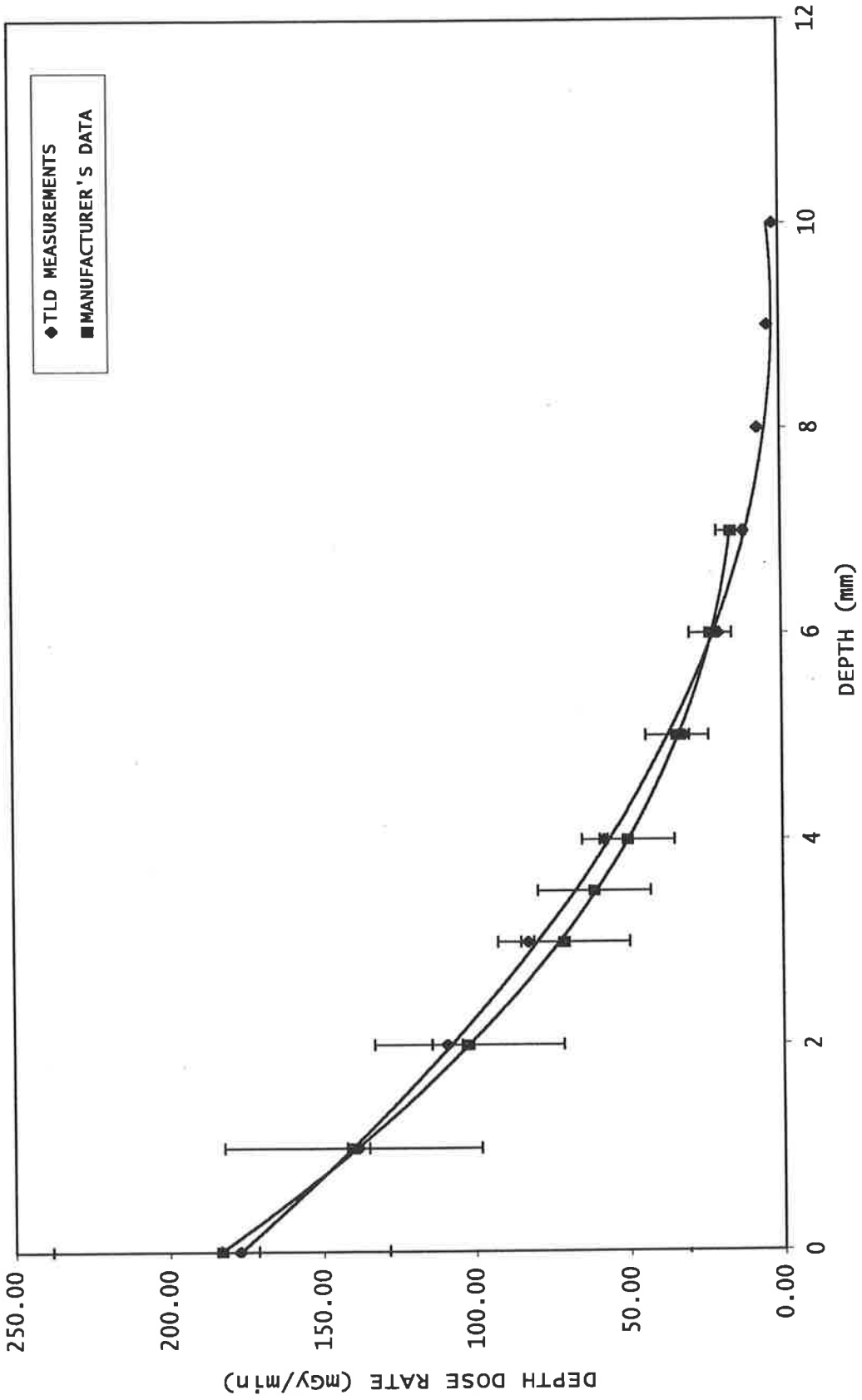

Figure 4.6 The absolute depth dose rate for a 20-mm (COB) Ru-106 ophthalmic applicator measured with small $CaSO_4$:Dy TLD chips along the central axis. The depth dose rate curve provided by the manufacturer is also presented.

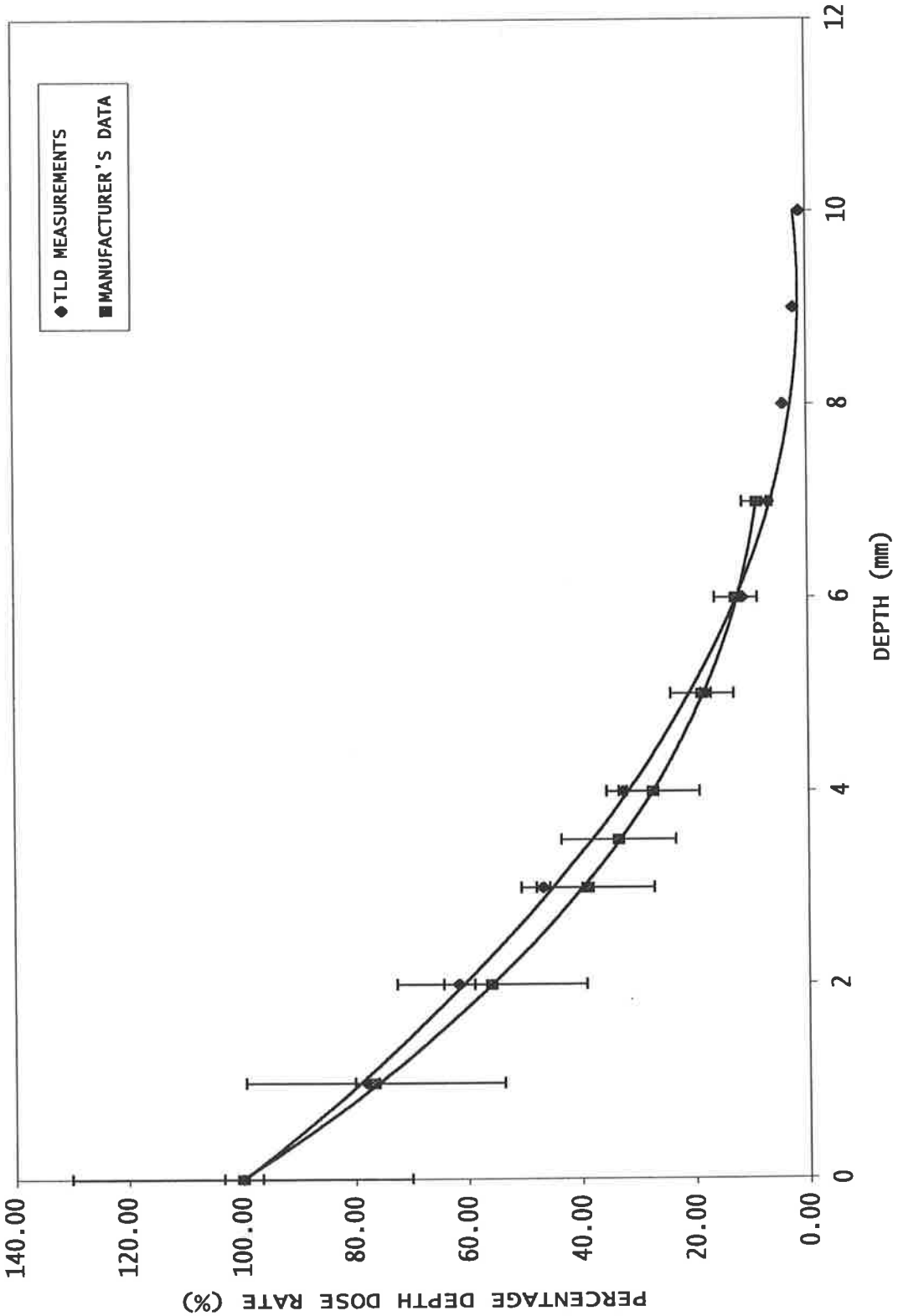

Figure 4.7 The percentage depth dose rate for a 20-mm (COB) Ru-106 ophthalmic applicator measured with small $CaSO_4$:Dy TLD chips along the central axis. The relative depth dose rate curve provided by the manufacturer is also presented.

Table 4.4 - Absolute depth dose rate along the central axis for the 15-mm ruthenium-106 ophthalmic applicator.

Depth (mm)	Corrected absolute dose rate (mGy/min)					Average Dose Rate (mGy/min)
	1ST Measure-ment	2ND Measure-ment	3RD Measure-ment	4TH Measure-ment	5TH Measure-ment	
0	128.69	136.59	126.38	126.85	138.34	131.37
1	103.80	106.86	110.94	-	-	107.20
2	72.99	84.30	77.79	-	-	78.36
3	50.68	52.18	54.25	-	-	52.37
4	36.06	39.18	43.80	-	-	39.68
5	30.17	30.66	25.56	-	-	28.80

Table 4.5 - Dose rate and statistical values for the dose distribution at various depths along the central axis for the 15-mm applicator.

Depth (mm)	Average Corrected Dose Rate (mGy/min)	Standard Deviation (mGy/min)	Relative error (%)	Percentage Depth Dose Rate (%)
0	131.37	6.46	4.91	100.00 (±5.15)
1	107.20	2.07	1.93	81.60 (±3.19)
2	78.36	3.28	4.18	59.65 (±2.85)
3	52.37	1.03	1.97	39.86 (±1.56)
4	39.68	2.25	5.67	30.20 (±1.68)
5	28.80	1.62	5.64	21.92 (±1.21)

Table 4.6 Variation of the depth dose rate and percentage depth dose rate for a 15-mm (CCA) Ru-106 ophthalmic applicator measured with small $CaSO_4$:Dy TLD chips along the central axis. The depth dose rate curve provided by the manufacturer is also presented.

TLD Measurement results			Applicator's manufacturer data		
Depth (mm)	Depth dose rate (mGy/min)	Percentage Depth dose Rate (%)	Depth (mm)	Depth dose rate (mGy/min)	Percentage Depth dose Distribution (%)
0	131.37 (±6.46)	100.00 (±5.15)	0	119 (±35.7)	100.00 (±30.0)
1	107.20 (±2.07)	81.60 (±3.19)	1	100 (±30.0)	84.03 (±25.2)
2	78.36 (±3.28)	59.65 (±2.85)	2	82 (±24.6)	68.91 (±20.7)
3	52.37 (±1.03)	39.86 (±1.56)	3	58 (±17.4)	48.74 (±14.6)
4	39.68 (±2.25)	30.20 (±1.68)	3.5	51 (±15.3)	42.86 (±12.9)
5	28.80 (±1.62)	21.92 (±1.21)	4	41 (±12.3)	34.45 (±10.3)
-	-	-	5	28 (±8.4)	23.53 (±7.1)
-	-	-	6	20 (±6.0)	16.81 (±5.0)
-	-	-	7	14 (±4.2)	11.76 (±3.5)

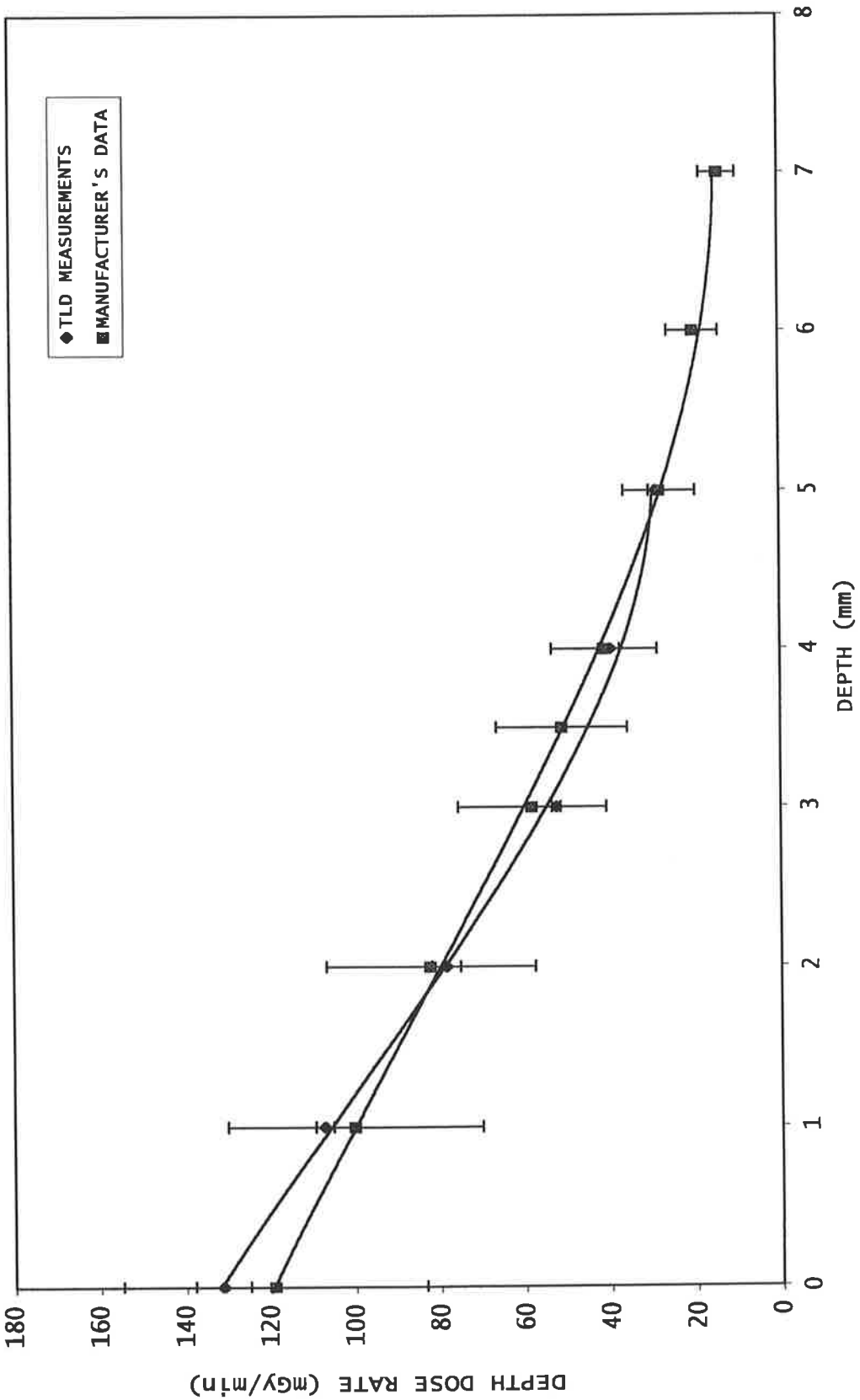

Figure 4.8 The absolute depth dose rate for a 15-mm (CCA) Ru-106 ophthalmic applicator measured with small $CaSO_4$:Dy TLD chips along the central axis. The depth dose rate curve provided by the manufacturer is also presented.

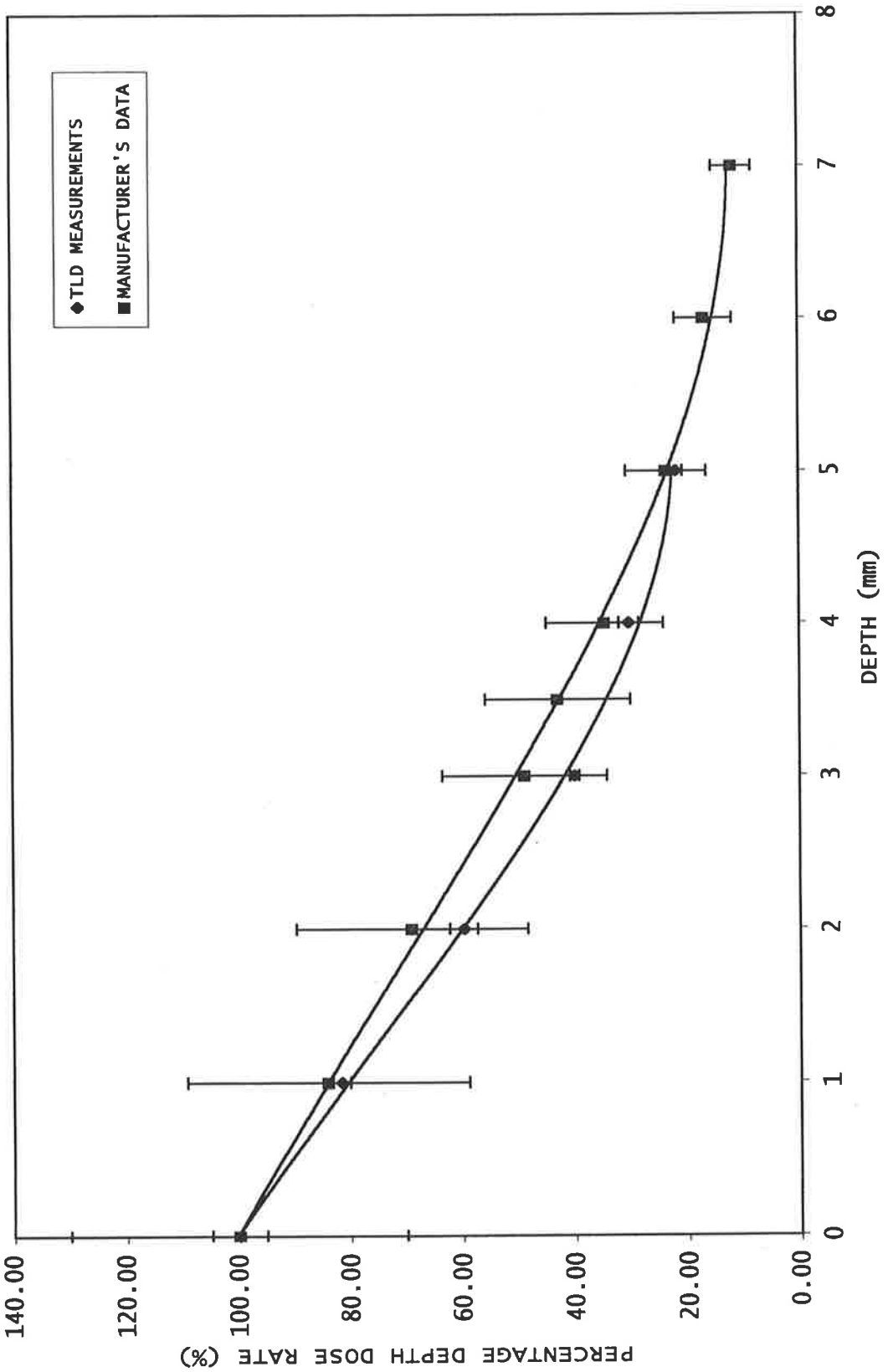

Figure 4.9 The percentage depth dose rate for a 15-mm (CCA) Ru-106 ophthalmic applicator measured with small $CaSO_4$:Dy TLD chips along the central axis. The relative depth dose rate curve provided by the manufacturer is also presented.

4.5. Discussion of the experimental results

4.5.1. Calibration of small $CaSO_4$:Dy TLDs

It was observed from the calibration measurements that, on average, the readouts of small $CaSO_4$:Dy TLDs obtained after irradiation of a radiation dose of 2 Gy were lower than those obtained from large $CaSO_4$:Dy TLD discs. This was simply the result of decreasing in disc area from approximately 49 mm^2 to 6 mm^2. It was also observed that small TLDs that were cut from the same $CaSO_4$:Dy TLD disc had different radiation dose sensitivity. This variation is due to non-uniformity in distribution of active substances on a disc and due to size variation (making of small TLDs was carried out by hand). However, these effects were taken into account by calibrating each small TLD individually. Furthermore, a batch correction factor (BCF) was also introduced, in cooperation with ISCF, to account for other influential factors due to irradiation, reading and annealing conditions. Reproducible readouts were obtained throughout the measurements when these two correction factors were applied.

4.5.2. Measurements of dose rate distribution of the 20-mm and 15-mm ruthenium-106 ophthalmic applicators

The use of small TLDs provided several advantages for the measurement of the dose rate distribution of the applicator. The high sensitivity of $CaSO_4$:Dy TLD also enabled to measure radiation dose (dose rate) at depth where dose rate was low. The curvature and small size of the ruthenium-106 plaque make it difficult to measure the dose distribution in a phantom with a larger detector requiring connection with cables such as ionization chamber. These small TLDs have an advantage in dose measurements for this applicator.

In general, the results showed a good reproducibility for both low and high dose rate distributions of the applicator (corresponding to different depths). The maximum uncertainty obtained from the measurements, for instance, at the depth of 5 mm was approximately 5% (compare to 30% of that as provided by applicator's manufacturer). Generally, the relative errors for all depths and positions ranged between 2% to 6%. In addition, the central axis percentage depth dose distribution obtained from small $CaSO_4$:Dy TLD chips measurements was comparable to that provided by the applicator manufacturer but with better precision and reproducibility. However, there were some discrepancies in depth dose distribution patterns between both profiles. At depths between 1 mm to 4 mm, the percentage depth dose values obtained from TLD measurement were relatively higher than that of the applicator's manufacturer. In contrast, to the depths above 5 mm, the percentage depth dose values obtained with TLD measurements were relatively lower than that of the applicator's manufacturer (Table 4.4). This appeared to be the results of build up effect in both radiation detectors.

The measurement results of dose distribution of the 20-mm ruthenium-106 applicator also indicated that the coating of active layer of radioactive ruthenium-106 on the surface of the applicator was equally distributed except for the area around the notch of the applicator. The dose distributions of the two opposite areas around the central axis, for example, right and left, top-right and top-left, bottom-right and bottom-left, were almost equal. However, the dose distribution values for those areas located around the notch of the 20-mm ruthenium-106 applicator were relatively lower than other areas. This notch was made to be located around the optic nerve of the eye in order to deliver as low a radiation dose as possible to the optic nerve during treatment.

Measurement of the depth dose rate of a 15-mm ruthenium-106 applicator was less complicated than that of a 20-mm ruthenium-106 applicator because it has a plain concave shape without an indentation like 20-mm applicator. The variation of depth dose rate of the 15-mm applicator was measured along the central axis to a depth of 5 mm. As shown in Figure 4.9, it is observed that there is a significant difference between the measured and the manufacturer's curves, especially between 2 and 4 mm depth. There were approximately 4% - 10% differences between the values obtained from experimental TLD measurements and values that were provided by the applicator manufacturer for the depth of 0 mm – 4 mm.

In conclusion, the variations and uncertainties occurring in measurements of the dose rate distributions of both 20-mm and 15-mm applicators were due to several factors. Firstly, the positioning of the TLDs in the eye phantom was difficult to maintain accurately especially for the depths of 1 mm and 2 mm. This was because each phantom top is quite small and its curved shape may result in changes of the thickness of absorption material (phantom top) over the TLD chips. And, consequently, the changes in absorbed dose of TLDs. Secondly, the most important cause of differences between the percentage depth dose rate values of experimental TLD measurements and the applicator manufacturer's values was 0-mm depth dose rate value obtained with TLD measurements. These values obtained from TLD measurements were quite different from ones that provided by the applicator manufacturer. These variations were partly the result of a build-up effect of the TLDs and a shift in placement or positioning of ruthenium-106 applicators during the measurements. Thirdly, a measurement result obtained from each small TLD chip could be an average value of dose rates over the whole area that covered the TLD chip in the eye phantom. Finally, radiation dosimetry using $CaSO_4$:Dy TLD chip that has very high

sensitivity may result in providing the measurement results with high degree of variation due to various influential factors. For example, the environmental conditions such as light intensity, room temperature level, and humidity level during the measurement. Furthermore, reading parameters, thermal treatment conditions during the annealing process and instability of TLD reader that can vary over long time periods also affected the accuracy and precision of reading results. However, although some variations and uncertainties were observed in the dose rates of 20-mm and 15-mm ruthenium-106 applicators, apparently the measurement results obtained with these small $CaSO_4$:Dy TLD chips nevertheless provided a greater accuracy and precision than those of the applicator manufacturer. In addition, good reproducibility was observed in dose rate determinations using the small $CaSO_4$:Dy TLD chips.

4.6 Conclusion

There are three main experiments included in this chapter: first, preparation and calibration of small $CaSO_4$:Dy thermoluminescent dosimeters, second, measurement of the dose distribution of a 20-mm ruthenium-106 ophthalmic applicator and, finally, a measurement of the on-axis dose distribution of a 15-mm ruthenium-106 applicator. It was observed that small $CaSO_4$:Dy TLD chips, which were calibrated with a 4 MV medical linear accelerator, can be used for measurement of the dose rate distributions of COB and CCA type ruthenium-106 applicators. Their small dimensions ($2 \times 3 \times 0.4$ mm^3) allows them to be placed at the position in the eye phantom where a measurement of the depth dose rate was required. Their high radiation sensitivity also enables them to measure a dose distribution at a depth where the dose rate is very low. Despite their high radiation sensitivity, low-uncertainty measurement results were obtained at most depths. These advantages make small $CaSO_4$:Dy TLD chips ideal dosimeters for the measurement of dose distributions of ruthenium-106 applicators.

Chapter 5

Determination of the dose rate distribution using a MOSFET detector

5.1 Introduction

In the previous chapter, small $CaSO_4$:Dy TLD chips were used as dosimeters in measurements of dose rate distributions of 20-mm and 15-mm ruthenium-106 ophthalmic applicators. There were several advantages observed in using those TLDs for that purpose: for example, high radiations dose sensitivity, a wide-range of dose response linearity, and feasibility for measurement in situation where there is complexity in the shape and dimensions of the applicators. However, against these advantages, there are also some disadvantages in using TLDs for radiation dose measurements, for instance, they show an environmental sensitivity to light, temperature, and humidity, require long irradiation times, have delayed reading results, and there are some handling and processing procedures difficulties. Hence, another type of dosimeter that is able to provide real-time measurement readout, more resistance to environmental conditions and is easier to handle

and operate was trialed. A metal oxide-silicon semiconductor field effect transistor (MOSFET) detector was used for determination of depth dose distribution of a 20-mm ruthenium-106 applicator, and the measurement results were compared with those of the small chip $CaSO_4$:Dy TLDs. In this chapter, a few experiments are described in order to investigate the general dosimetric characteristics of MOSFET detectors to radiation doses from a 20-mm ruthenium-106 ophthalmic applicator. It also aims to find an alternative dosimeter to TLD to provide a simple measurement procedure and immediate readout. As a result, it can be used for routine checks of plaque integrity after handling during treatment procedures.

Applications of a MOSFET dosimeter are well recognised in many fields from space applications, nuclear power plants monitoring, military and emergency dosimetry and medical applications. A MOSFET dosimeter is well adapted for use in radiation dosimetry in the space shuttle as it has similar structure to basic components of electrical circuits on the space shuttle. Its ability to measure radiation dose in continuously real-time mode makes it very suitable for environmental monitoring around the area of nuclear power plants. A personnel dosimeter for military use is another application of MOSFETs due to the wide dose rate response with acceptable accuracy when used in the unbiased mode. Also, many medical applications use MOSFETs as radiation dosimeters. Simple calibration procedures, instant readout, good dose accuracy and fair reproducibility (only marginally different from TLD measurements) make a MOSFET a suitable dosimeter for clinical dosimetry (Ramani *et al.*, 1997). Although a cable that is connected to the detector may restrict its use, it is quite small and flexible enough to allow it to be accepted by patients if it has to be inserted into a body cavity.

Applications of MOSFET dosimeters in medical fields include *in vivo* dosimetry e.g. entrance and exit dose measurements, total body irradiation dosimetry with unbiased MOSFET dosimeters, and intracavity or interstitial dosimetry for several radiotherapy procedures. In addition, a MOSFET dosimeter is also used in medical applications such as the stereotactic radiosurgery, brachytherapy (for radiation sources such as ceasium-137, iridium-192, and ruthenium-106). Furthermore, a miniature MOSFET dosimeter probe is occasionally employed in unsealed source therapy (radioimmunotherapy) for measurement of absorbed dose after injection of a radioactive-labelled antibody (Gladstone *et al.*, 1993 and Gladstone & Chin, 1995).

5.2. Basic structure and principle of operation of MOSFET

First fabricated in 1960 (Dimitrijev, 2000), the MOSFET or metal-oxide-semiconductor field-effect transistor became one of the most widely used electronic devices, particularly in digital integrated circuits. The MOSFET is developed from the MOS capacitor and one type of MOSFET, called an N-channel MOSFET, is illustrated in Figure 5.1.

As shown in Figure 5.1, the MOSFET consists of four terminals, the silicon substrate (bulk, B), the gate (G), the source (S), and the drain (D). The voltage applied to the gate (G) of the MOS capacitor controls the state of the silicon surface (B). If negative voltages are applied to the gate, they will attract the holes from the P-type silicon to the surface (accumulation), while positive voltages larger than the threshold voltage create a layer of electrons at the surface (inversion) (Dimitrijev, 2000). The threshold voltage (V_T) represents the value of the gate voltage (V_G) needed to set the silicon surface at the onset of strong inversion.

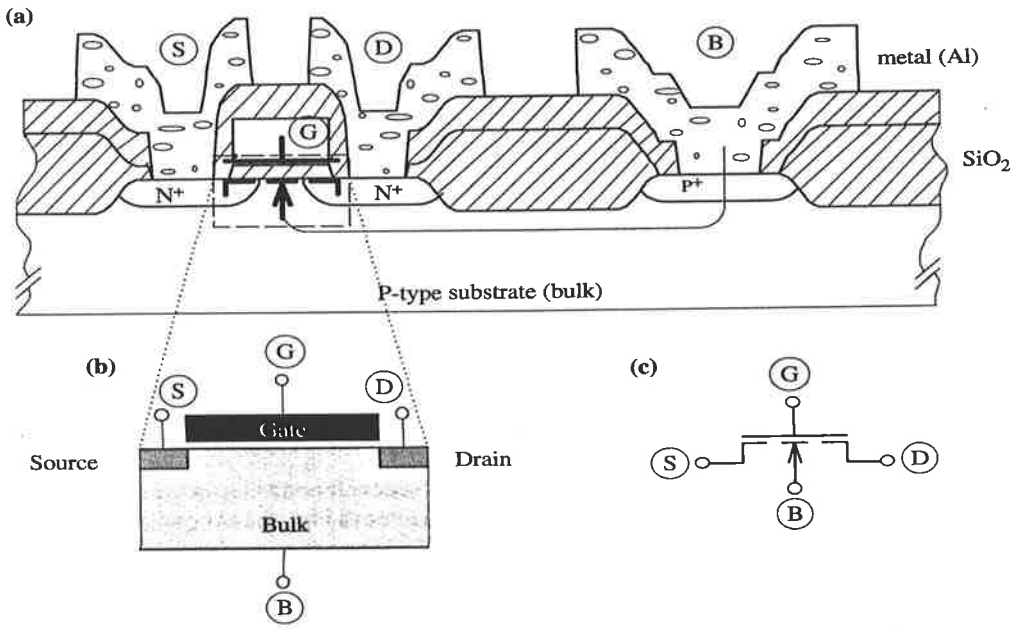

Figure 5.1 A diagram shows structure of a typical N-channel MOSFET detector (Dimitrijev, 2000).

In this N-channel MOSFET, the conduction between the source and the drain is provided by the N-type carriers (electrons). In a complementary transistor type called P-channel MOSFET, N-type substrate and P^+ source and drain are used. In order to create a surface channel of holes, the negative gate voltage is needed. In measurement of radiation dose, irradiation creates electron-hole pairs throughout the whole volume, in particular, in the insulator region. Electrons are rapidly swept out of the insulator and holes move slowly towards the gate (substrate), some are trapped in a narrow region near the cathode on previously existing hole traps generated during insulator processing. The net result is the creation of a permanent positive charge in the gate that shifts the threshold voltage (V_T) of the transistor by an amount ΔV_T. The degree of shifting depends upon the amount of absorbed dose (D) deposited, the gate bias during irradiation, the type and the energy of the radiation and the thickness of insulator.

ΔV_T is the measured dosimetric parameter and can be obtained by measuring the output voltage V_T before and after a fixed irradiation period and can be written as equation following below:

$$\Delta V_T = V_T^{after} - V_T^{before} \quad \textbf{(5.1)}$$

The dose response of a MOSFET to different levels of radiation depends on two modes of operation, a biased mode and an unbiased mode. In the biased mode, the dose response was found to be linear in the low dose region and departs from linearity at the higher dose (Sarrabayrouse & Siskos, 1998). It was also observed that, in the biased mode, using a 1.5 μm-thick insulator with a bias of about 40V, radiation doses as low as 500 μGy could be measured with ease. In addition, in order to measure radiation in high-dose range (MGy), MOSFET sensitivity may be reduced by reducing the thickness of insulator. The unbiased mode may be used for high dose measurements, such as in medical applications where complex circuitry and a power supply are not needed. The dose response, in the unbiased mode, is approximately linear over a smaller range of doses (below 500 cGy) due to the thick insulator.

Although there are some advantages in using MOSFET as a radiation dosimeter over other types of detector but some limitations that reduce its measurement accuracy and the lowest measurable dose have been identified. These limitations include read-time instability, instability of the threshold voltage due to temperature changes, and signal-to-noise ratio. The read-time instability occurs as a result of slow interface states produced during irradiation and are manifested by an increase of the magnitude of the threshold voltage (drift up) during read-out (Sarrabayrouse & Siskos, 1998).

It was reported that the read-time instabilities were found to be less than 1% of the total ΔV_T for silicon oxides (SiO_2). Temperature sensitivity of threshold voltage (V_T) due to thickness of the oxide is also a limitation of the MOSFET detector. For thick oxide layers, the threshold voltage shift in the range from 4 to 20 mV/°C was reported (Sarrabayrouse & Siskos, 1998).

In order to reduce the effect of temperature changes two measurement procedures were proposed. Firstly, a measurement, using a value of a constant-current source where the temperature sensitivity is minimal, was recommended to reduce the sensitivity of the output voltage in the range 0.1 to 1 mV/°C. On the other hand, a dual-bias dual-transistor dosimeter system was designed, consisting of a pair of identical MOS transistors so the temperature response of each transistor is the same when biased with the same current (Sarrabayrouse & Siskos, 1998). In addition, the dose response sensitivity of the two transistors was set to be different by applying different gate-to-substrate biases to them during irradiation. As a result, a temperature coefficient as low as 0.015 mV/°C was reported. The third limiting factor that affects the minimum measurable dose of MOSFET dosimeter is the signal-to-noise ratio that is associated with a high-sensitivity of MOSFET dosimeter. It has been reported that the minimum measurable dose was limited to 100-μGy range by 1/f noise (Sarrabayrouse & Siskos, 1998).

5.3. Experimental instrumentation

5.3.1. MOSFET semiconductor dosimeter

The MOSFET semiconductor dosimeter used in this experiment was produced by the Centre for Medical Radiation Physics, University of Wollongong, Australia (Dr

Anatoly Rosenfeld). There are three main parts contained in this dosimeter system: dosimetry probes, the dosimetry electronic system and auxiliary components.

A. Dosimetry probes

There are two types of MOSFET sensors contained in each dosimeter system (Figure 5.2), a low dose radiation detector for low dose dosimetry and a high dose radiation detector for high dose dosimetry. The low dose detector (R-type MOSFET) operates with the bias voltage between 9 V and 24 V. All measurements carried out in this experiment were with this detector since no radiation dose greater than 15 cGy was given. Radiation dose response of this low dose detector is claimed to be linear but is not completely over the whole range of operating voltage. The high dose radiation detector (K-type MOSFET) has an operating voltage between 3 V and 16 V so it provides a wide range of radiation dose response linearity. The effective point of measurement is 0.3 mm below the probe surface for both detectors.

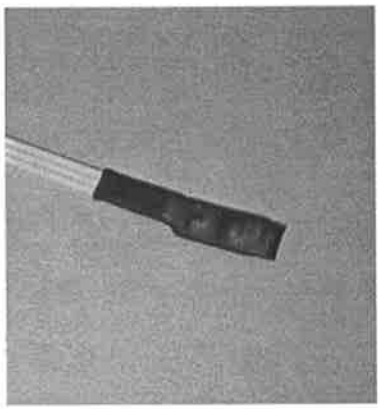

Figure 5.2 A picture of MOSFET radiation dosimetry probe.

B. Dosimetry system operation unit

The dosimetry system operation unit (Figure 5.3) contains several switches for controlling the dosimetry operation and five input ports for connecting up to five radiation dosimetry probes. On the rear panel (not shown in the picture) there is a RS232 computer

serial connection port and battery access. An auxiliary input is a connection port for the active bias unit or the interface unit. The computer ON/OFF switch is in the ON position when a computer is connected and on-line measurement mode is used. Otherwise, it must be in the OFF position. The probe readout selection thumb-switch is used for the selection of a number of dosimetry probes to give a reading result when the manual read push-button is pushed. This can allow up to five readouts to be obtained at a time when all five probe inputs are connected.

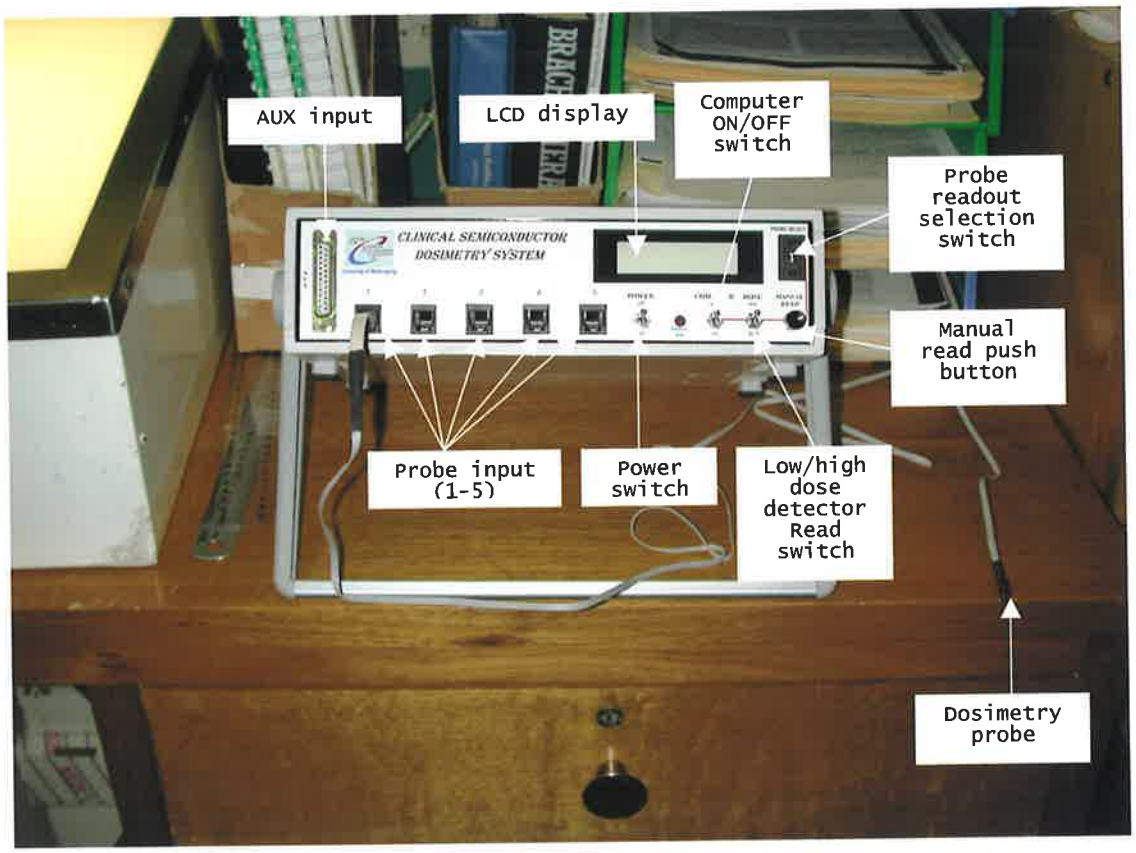

Figure 5.3 This picture shows the front panel of the dosimetry system operation unit. The name and location of control switches is indicated. One dosimetry probe connecting to probe input No. 1 is also presented.

The dosimetry system operation unit operates with the power source consisting of 4 x 1.5 V alkaline D-cell batteries. The low-battery indicator is located at the front panel between the power switch and computer ON/OFF switch.

C. Auxiliary components

Auxiliary components included in this MOSFET dosimetry system are:

1. Active bias unit – can be used when a measurement in the biased mode is required by connecting it with the MOSFET detector. The sensor is irradiated with a radiation dose as required. The detector is inserted back to the reader at the same probe input number as used in the active bias unit and the threshold voltage shift is measured.

2. Interface unit – this unit allows an irradiation of the MOSFET detector to be carried out at a safe distance away from the reader to avoid radiation exposure personnel who perform the measurement. In addition, on-line and *in vivo* measurements can be done with the aid of this interface unit.

3. Auxiliary cable – the auxiliary cable (15 m) is used for connection of the dosimetry system with the interface unit. There are 25-pin connectors attached at each end of the cable.

5.3.2. Eye phantom modification

Eye phantoms employed in this experiment were the same as phantoms were used in previous experiments. However, they were slightly modified to make them suitable for the shape and dimension of the MOSFET detector. The phantom base was drilled to make a groove having a depth and width sufficient to hold the MOSFET sensor in place and its effective point of measurement located at the centre of the eye phantom base on the central axis (Figure 5.4). In addition, a piece of wax was placed on top of the detector during the

irradiation to help hold the detector in place, to prevent any movement, and also to fill any air gaps around the sensor in the groove.

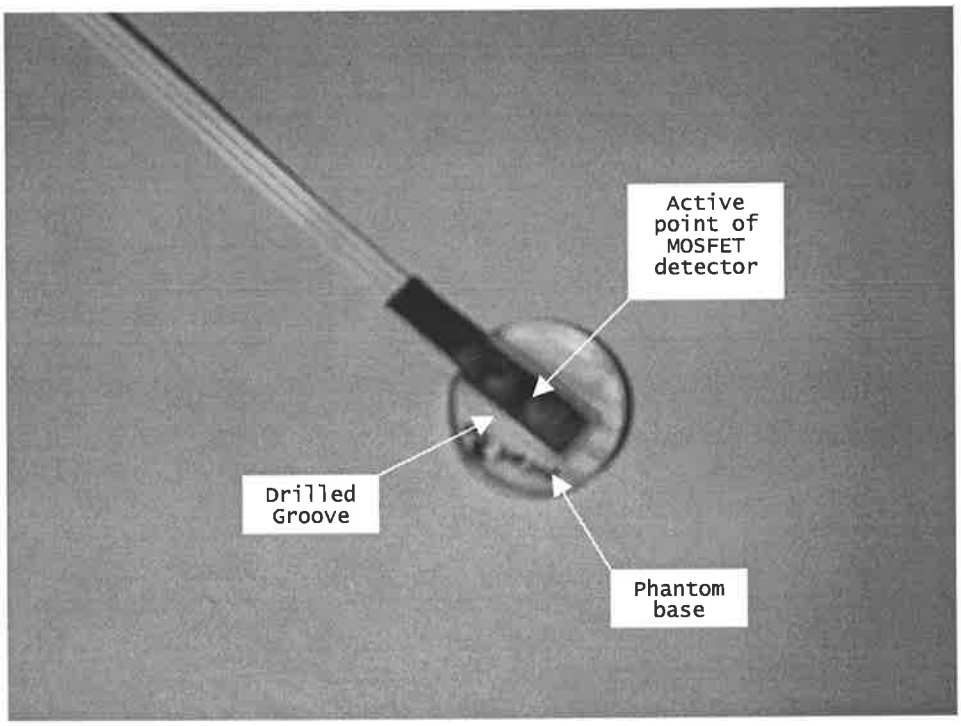

Figure 5.4 A picture shows a modified eye phantom base and placing of the MOSFET detector.

5.3.3. Ruthenium-106 ophthalmic applicator

Only the COB-494 type (20-mm) ruthenium-106 ophthalmic applicator was used in the measurements of distribution of rate of depth dose.

5.4. Experimental procedures

Prior to the depth dose-rate measurements being made, the dose response linearity of the MOSFET was investigated. Various doses from 1 cGy up to 20 cGy were given to the MOSFET dosimeter, positioned in an eye phantom at the depth of 5 mm. The voltage changes after each irradiation were calculated and recorded. Subsequently, the depth dose

rate in acrylic eye phantom from 20-mm ruthenium-106 applicator was measured. In order to measure the dose response for depth from 1 mm up to 9 mm, an eye phantom base with corresponding cap was used. The phantom base was put inside a phantom holder and the MOSFET radiation detector was put in the groove of the phantom base with a piece of wax put on top to assist holding the MOSFET detector in place.

Several pieces of adhesive tape were also used to help placement of the MOSFET detector and its cable and to prevent any movement during irradiation. The MOSFET detector was, then, connected through the interface unit to the reader. The dose detector read switch was pushed to LOW position, the computer switch was in OFF position and, then, the power switch was pushed to ON position. Inside the irradiation room, the ruthenium-106 applicator was put on top of the phantom with plastic forceps.

Before a measurement was started, the reader was left in ON position for about 10 – 15 minutes in order to warm up and stabilise the dosimetry system. To start the measurement, the manual read button was pushed and the gate voltage appearing on the LCD display was read and recorded. At the same time that the manual read button was pushed a stopwatch was started to give a time long enough for a radiation dose of 15 cGy at the depth of measurement. When the irradiation time was reached, the manual read button was pushed to display the voltage that was, then, read and recorded. The shift in voltage (mV) is the difference between the voltage reading at the start of irradiation time and the voltage reading at the end of irradiation time. Several measurements were carried out at each depth. The same procedure as described above was employed at every depth but with different irradiation times (to correspond to 15 cGy dose).

5.5. Measurement results

5.5.1. Measurement of dose response linearity

The voltage shift readouts obtained from the measurements were corrected by the corresponding decay-correction factor of the ruthenium-106 applicator relative to the calibration date provided by the manufacturer and decay-corrected voltage shift were obtained as a result. The decay-corrected voltage shift values are shown in Table 5.1 and a plot between dose given (cGy) and average shifting voltage (mV) is shown in Figure 5.5.

Table 5.1 A table shows decay-corrected shifting voltage (mV) obtained from measurement of dose response linearity of a MOSFET detector.

Dose Given (cGy)	Decay Corrected Voltage Shift (mV)			Average Shifting Voltage (mV)	Standard Deviation of Mean (mV)	Relative Error (%)
	1ST Measure-ment	2ND Measure-ment	3RD Measure-ment			
2	1.65	2.31	1.98	1.98	0.1901	9.62
4	4.28	4.61	4.28	4.39	0.1098	2.50
6	6.59	6.92	7.24	6.92	0.1901	2.75
8	9.88	9.55	10.54	9.99	0.2904	2.91
10	11.53	12.84	12.51	12.29	0.3958	3.22
12	14.49	14.82	-	14.65	0.1646	1.12
15	18.11	18.44	-	18.28	0.1646	0.90
20	24.37	25.03	-	24.70	0.3293	1.33

5.5.2. Measurement of depth dose rate of ruthenium-106 applicator with MOSFET detector

A number of ΔV_T results were obtained from several measurements for each depth. Each ΔV_T (mV) result was divided by irradiation time Δt in minute to give voltage shifting per minute $\Delta V_T / \Delta t$ (mV/min). Then each $\Delta V_T / \Delta t$ was corrected for radioactive decay back to the calibration date of the applicator.

All decay-corrected $\Delta V_T / \Delta t$ (mV/min) values is shown in the Table 5.2. Figure 5.6 shows the dependence between dose response of the MOSFET detector and the on-axis depth into the eye phantom.

Table 5.2 Experimental values of decay-corrected voltage shift per minute obtained from MOSFET detector measurements.

	Decay-corrected voltage shift per minute (mV/min)									
Measure-ment No.	0 mm	1 mm	2 mm	3 mm	4 mm	5 mm	6 mm	7 mm	8 mm	9 mm
1	7.07	5.12	3.81	2.79	1.73	1.25	0.51	0.36	0.19	0.08
2	6.95	5.22	3.75	2.69	1.83	1.18	0.67	0.36	0.18	0.07
3	6.95	5.50	3.78	2.69	1.83	1.09	0.68	0.36	0.18	0.08
4	7.07	5.22	4.29	2.84	1.99	1.19	0.59	0.37	-	-
5	7.07	4.94	3.81	2.60	1.83	1.00	0.62	0.36	-	-
6	7.20	4.84	3.68	2.74	1.83	1.03	0.64	0.34	-	-
7	6.95	4.94	-	-	-	1.18	0.72	-	-	-
8	6.95	-	-	-	-	1.07	0.59	-	-	-
9	-	-	-	-	-	-	0.59	-	-	-
Mean	7.03	5.11	3.85	2.73	1.84	1.12	0.62	0.36	0.19	0.08

	Decay-corrected voltage shift per minute		
Depth (mm)	Mean	Standard Deviation of Mean (mV/min)	Percentage Depth Dose Response (%)
0	7.03	0.03	100 (±0.60)
1	5.11	0.08	72.7 (±1.18)
2	3.85	0.09	54.7 (±1.30)
3	2.73	0.03	38.8 (±0.46)
4	1.84	0.03	26.2 (±0.44)
5	1.12	0.03	16.0 (±0.43)
6	0.62	0.02	8.89 (±0.29)
7	0.36	0.001	5.08 (±0.03)
8	0.19	0.002	2.64 (±0.03)
9	0.08	0.003	1.11 (±0.04)

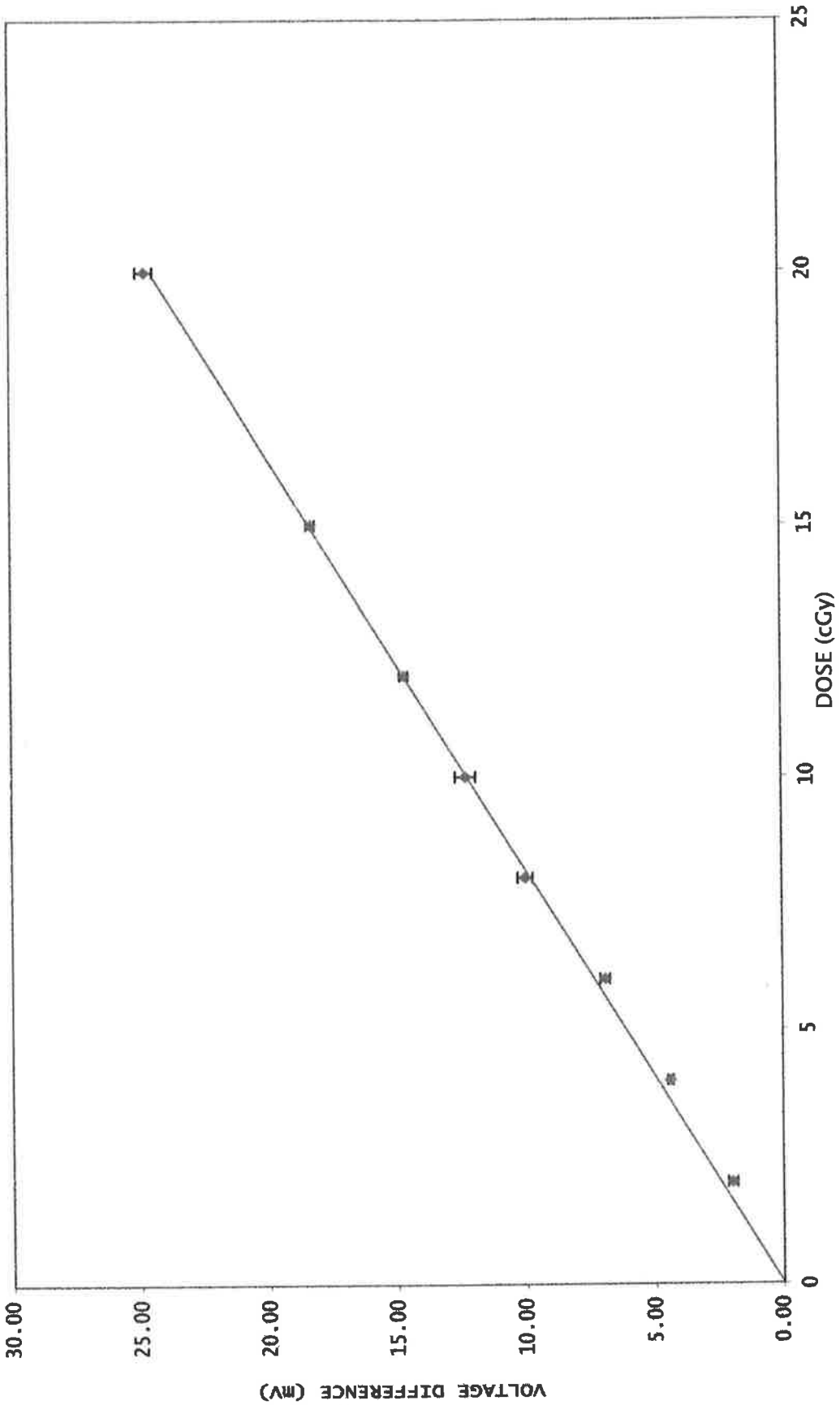

Figure 5.5 A curve shows dependence of the measured shifting voltage (mV) and radiation dose (cGy) given to the MOSFET detector.

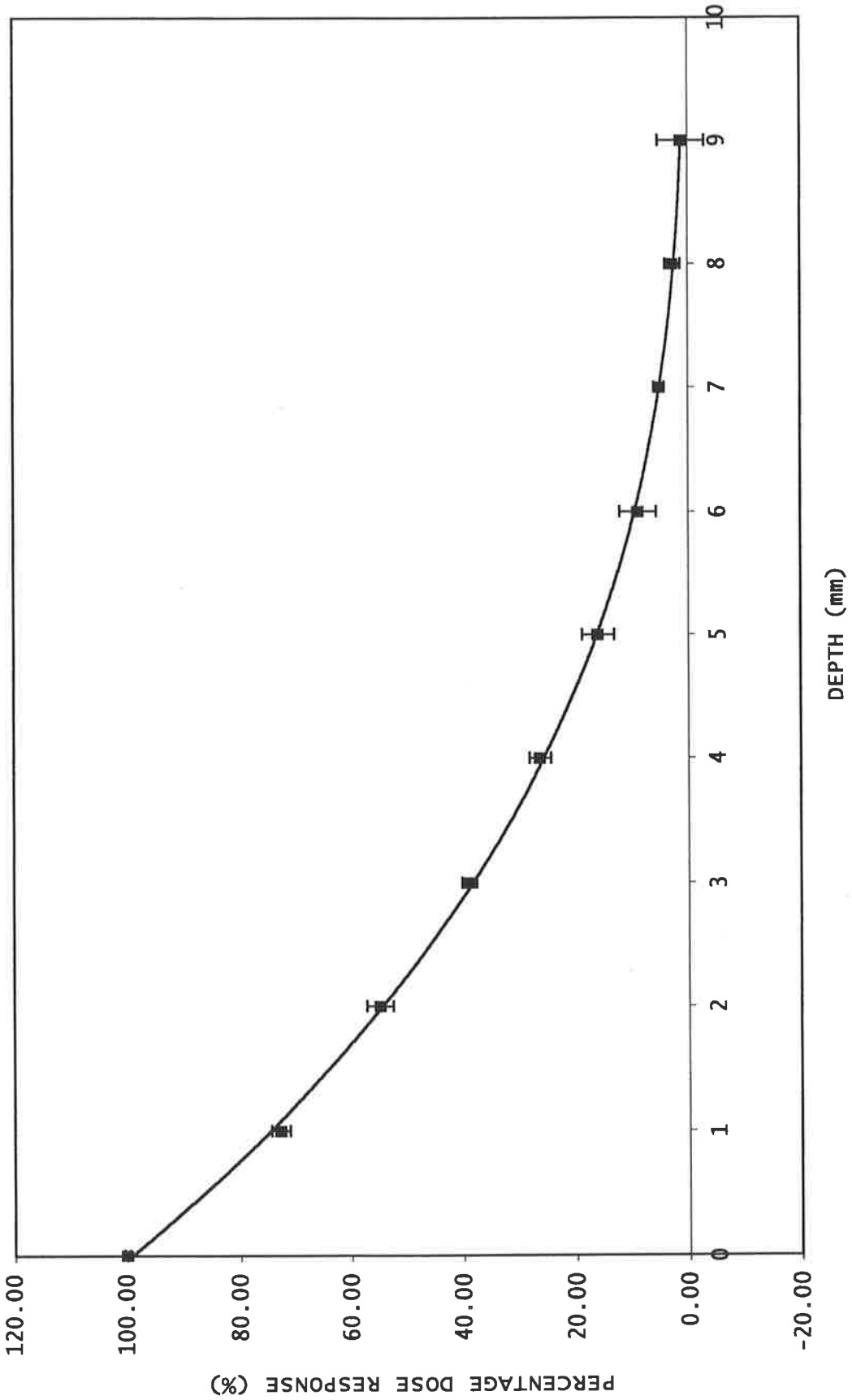

Figure 5.6 Percentage depth dose response of the MOSFET dosimeter to radiation doses from 20-mm (COB-494) ruthenium-106 applicator.

5.6. Discussion

Only relative measurements of on-axis percentage depth dose rate in the acrylic eye phantom for the COB-494 ruthenium-106 applicator using the MOSFET dosimeter was investigated in this research. The results of the measurements of dose response linearity and depth dose rate indicated that the MOSFET detector could be an excellent device for rapid measurement of the central axis relative dose rate distribution of ruthenium-106 applicator. In the measurement of dose response linearity, in which radiation doses up to 20 cGy were given to the MOSFET's low-dose detector, it was observed that its dose response was linear over the range of given doses to within ±4%. In an unbiased mode, the MOSFET dosimeter using 1.6-μm insulator could provide dose response linearity for radiation doses up to 500 cGy (Sarrabayrouse & Siskos, 1998). However, the observed linearity over that dose range was sufficient to allow the use of the MOSFET dosimeter for depth dose determination of ruthenium-106 applicator using doses of about 15 cGy.

Table 5.3 The percentage depth dose rate distributions of COB-494 ruthenium-106 applicator obtained from measurement with small CaSO4:Dy TLD chips, MOSFET dosimeter and the applicator manufacturer data.

Depth (mm)	Percentage depth dose rate distribution/ Percentage depth dose response		
	Small $CaSO_4$:Dy TLD (%)	Applicator's manufacturer (%)	MOSFET Dosimeter (%)
0	100.00 (±3.55)	100.00 (±30.00)	100 (±0.60)
1	77.94 (±3.41)	76.90 (±22.95)	72.7 (±1.18)
2	61.46 (±3.46)	55.74 (±16.72)	54.7 (±1.30)
3	46.63 (±2.01)	38.80 (±11.64)	38.8 (±0.46)
4	32.63 (±1.34)	27.32 (±10.00)	26.2 (±0.44)
5	17.89 (±1.10)	18.58 (±8.20)	16.0 (±0.43)
6	11.54 (±0.44)	12.57 (±5.57)	8.89 (±0.29)
7	6.86 (±0.28)	8.74 (±3.77)	5.08 (±0.03)
8	4.13 (±0.17)	-	2.64 (±0.03)
9	2.16 (±0.09)	-	1.11 (±0.04)
10	1.09 (±0.07)	-	

Table 5.3 shows the percentage depth dose rate distributions measured with small $CaSO_4$:Dy TLD chips, the applicator manufacturer data and the percentage depth dose rate obtained from the MOSFET measurement. The MOSFET measurement of the percentage depth dose rate of ruthenium-106 applicator yielded impressive results which were also comparable to those obtained from the experiments using small $CaSO_4$:Dy TLD chips. They were, in addition, also comparable to those provided by the applicator manufacturer.

The dose response of MOSFET dosimeter appeared to be similar to that of an ionization chamber that was used by the applicator manufacturer, rather than to the small $CaSO_4$:Dy TLD chips. However, for the depths greater than 5 mm, differences between both values (MOSFET and manufacturer data) appeared to be more significant. However, the manufacturer did not measure any doses beyond 5 mm and the listed ones were obtained from extrapolation of the manufacturer's data. As indicated early in this section, the measurement results indicated that the MOSFET dosimeter can be used in dosimetry of the ruthenium-106 applicator. In addition, its dose response linearity was observed to be excellent. It was also considered that the MOSFET detector is an excellent dosimetry system for evaluation of the dose rate distribution of ruthenium-106 applicator.

5.7. Conclusion

Very low doses can be measured with high precision (approximately 3% relative error for 15 cGy dose) and, therefore, the whole measurement time is short, providing effectively instantaneous results. This, together with the simple measurement set-up, means that MOSFET can be used as a fast and effective technique to measure the applicator radiation output routinely: to confirm the doses reported by the manufacturer

(acceptance testing) or to check the integrity of the source after handling (quality assurance procedure). With its several advantages such as high radiation dose sensitivity, excellent dose response linearity and capability of giving an instant readout, the MOSFET dosimetry system can be used for measurement of the on-axis relative dose-rate distribution of ruthenium-106 applicators. The lower stability at the early stage of making measurement can be improved allowing 10 – 15 minutes warm-up before starting the measurement. On the other hand, the MOSFET dosimeter has large size in comparison to the size and dimension of the eye phantoms and ruthenium-106 applicators. This limits the application of MOSFET dosimeter to measurement of the depth dose rate distribution along the central axis only. In addition, temperature dependence is another disadvantage that was reported by several authors (Gladstone *et al.*, 1994, Soubra, 1994, and Sarrabayrouse & Siskos, 1998). However, this factor was not studied in this research.

Chapter 6

Summary and Conclusion

Ruthenium-106 ophthalmic applicators are used in brachytherapy for treatment of eye tumours, for example, retinoblastoma and choroide melanoma. Accuracy of radiation dose prescription depends upon the accuracy and precision of depth dose distribution values. Several methods for determination of the depth dose distributions of both 20 mm and 15 mm ruthenium-106 ophthalmic applicators have been proposed. For instance, Davelaar *et al.* (1990) used an extrapolation ionisation chamber and Monte Carlo simulation for measurement of the absolute dose and percentage depth dose of a ruthenium-106 applicator in a tissue-equivalent plastic phantom. A radiochromic film detector with a TV-digitiser system was employed in the measurement of the surface dose and dose distributions of a ruthenium plaque by Taccini *et al.* in 1996. In 1997, Sanchez-Reyes et al. proposed a method of using the PENELOPE Monte Carlo simulation code for determination of the dose distributions of CCA and CCB concave ruthenium-106 applicators.

Recently, Chan *et al.* (2001) proposed a method using magnetic resonance imaging of BANG polymer gels to measurement the three dimensional dose distribution of a CCA type ruthenium-106 applicator. Those methods proposed by above authors have some limitations that might lead to high level of uncertainty of the dose distribution values.

Although the extrapolation ionization chamber does not require a calibration for the measurement of the absolute dose, there is a major limitation that can affect the absolute accuracy of the measurement. That is the determination of the geometrical properties of the chamber, in particular, the effective area of the collecting electrode (Soares *et al.*, 2001). In addition, it also has a large size and is bulky in dimensions so it is suitable for measurement only of a planar source and may be used for measurement of the depth dose rate along the central axis. The radiochromic film method also has some major limitations that limit the reproducibility of the measurement, i.e. variations in the thickness of the sensitive emulsion coating and backing material (Soares *et al.*, 2001). BANG Polymer-gels are quite expensive and the overall uncertainty of the calculated values is affected by the environmental conditions such as temperature level, light intensity and oxygen concentration during the measurement (Chan *et al.*, 2001). Calculation of the dose distributions of the ophthalmic applicators (Ru-106 and Sr-90/Y-90) using Monte Carlo simulation provides good results for measurements of the bare sources in an infinite, homogeneous medium but is more difficult to use for encapsulated applicators. And the results become worse if measured at larger depths (Cross *et al.*, 2001).

In this research project, small $CaSO_4$:Dy TLDs and a semiconductor MOSFET dosimeter were used for the determination of on-axis depth dose-rate distributions of 15-mm and 20-mm ruthenium-106 ophthalmic applicators in acrylic eye phantoms. The TLDs

were also used to determine off-axis dose distribution. Before being cut into small chips, $CaSO_4$:Dy TLD discs were calibrated against a 4 MV medical linear accelerator to observed their radiation dose response characteristics. From this calibration, these $CaSO_4$:Dy TLD discs were observe to have a linear dose response for radiation doses up to 10 Gy. Above this supralinearity existed. Differences in dose response sensitivity were also observed from the calibration. A sensitivity correction factor as high as 30% was found in one $CaSO_4$:Dy TLD disc whereas the sensitivity correction factor for most of the TLD discs appeared to be in the range between 5% – 15%. In the measurement of the dose reproducibility, it was observed that, with the irradiation, reading and annealing conditions employed in this experiment, the measurement results were obtained with a reproducibility of up to 4.5%. In addition, a reproducibility as good as 2% was also obtained with some $CaSO_4$:Dy TLD discs. Measurements of the irradiation-orientation and reading-orientation dependencies of $CaSO_4$:Dy TLD discs were also carried out in this thesis. An approximately 6% difference in readouts obtained from two groups of TLD disks that were placed in two different manners (face-up and facedown) during an irradiation was found. In an experiment where two groups of irradiated TLD discs were placed in two different ways (face-up and face-down) during the reading process, the readouts obtained by measurement indicated no significant difference between the two groups. In addition, it was also observed from calibration measurements that there was no significant radiation history left in the TLD discs after the annealing procedure using the thermal treatment parameters as described previously in the section 3.3.1.3 in Chapter 3.

Forty small $CaSO_4$:Dy TLD chips were made from three selected $CaSO_4$:Dy TLD discs that had been previously calibrated. These forty small $CaSO_4$:Dy TLD were also calibrated against a 4 MV linear accelerator in which their dose response sensitivity was investigated. Each small $CaSO_4$:Dy TLD chip had its own dose response sensitivity

characteristic. The individual sensitivity correction factor ranged from approximately ±1% to around ±20% in some cases. These variations were influenced by several factors. For example, there were variations in dimension of each TLD chip as they were cut manually with a scalpel. The sensitivity variation may also be affected by many intrinsic factors, including the non-homogeneity of the TLD phosphor in each disc, its previous thermal history, and optical transmission. This individual sensitivity correction factor, in cooperation with a batch correction factor and background subtraction, was applied to the gross readouts obtained from dose distribution measurements in order to obtain the corrected readouts. Background corrections were not required because small readouts, in comparison to irradiated TLDs, were obtained from non-irradiated TLDs. These calibrated small $CaSO_4$:Dy TLD chips, then, were used in measurement of the dose rate distributions of 15-mm and 20-mm ruthenium-106 applicators. A number of small TLD chips were placed in the eye phantom made of acrylic material (muscle substitute, $\rho = 1.170$ gm/cm^3). The applicator, then, was placed on top of the phantom in order to irradiate the TLD chips put in the phantom at a certain depth. The absolute on-axis depth dose distribution and percentage depth dose distribution curves were plotted using corrected readouts obtained from the measurements. It was observed that the depth dose distribution patterns of both 20-mm and 15-mm ruthenium-106 from small $CaSO_4$:Dy TLD chips agree closely to those provided by the applicator manufacturer (within 8%). Moreover, the measurements of the depth dose rate with the proposed method of using small $CaSO_4$:Dy TLD chips had better accuracy than that of applicator manufacturer. The highest relative error obtained from these measurements at a depth of 5 mm was approximately 5% whereas the depth dose rate values provided the manufacturer came with uncertainties as high as 30%. In addition, for the depths between 1 – 5 mm (the clinical depths) the relative errors obtained from $CaSO_4$:Dy TLD measurements mostly ranged between 3% - 5% and the highest relative error was approximately 8%. From the measurements, it was also observed that, at the

same depth, there was non-uniformity of the dose distribution throughout the plane at that depth. There were cold spots near the notch of the applicator where the dose rate was lower than that of surrounding areas. This was intentional on the part of the plaque's manufacturer in order to prevent an unnecessary irradiation of the optic nerve of the eye during the treatment.

Although there were several advantages of using such small $CaSO_4$:Dy TLD chips for measurements of the dose distributions of ruthenium-106 applicators there were also some technical difficulties that needed to be taken into account. For instance, movement of the small $CaSO_4$:Dy TLD chips during the set up of the measurement may lead to the occurrence of unexpectedly high deviations, particularly in measurements of a few mm depth. In addition to the radiation response properties investigated in this thesis, it may also be necessary to define an effective depth of small $CaSO_4$:Dy TLD chips in order to obtain greater accuracy and precision in the measurement results.

In contrast to dose distribution measurements using small $CaSO_4$:Dy TLD chips which were obviously time-consuming procedures, dosimetry using MOSFET dosimeters spent less processing time. A MOSFET dosimeter was also used in the measurements of the on-axis depth dose distribution of a 20-mm ruthenium-106 ophthalmic applicator. Response sensitivity to high radiation doses, instant readout and the simple measurement setup were some of the MOSFET advantages. Some modifications were made to the eye phantoms in which the phantom base was drilled to make a groove where the MOSFET dosimeter was placed during measurement. This dosimeter was used for relative measurements of the on-axis percentage depth dose rate of the 20-mm ruthenium-106 applicator. MOSFET dosimeter showed excellent dose response to radiations from the ruthenium-106 applicator. Its dose response was found to be linear through the range of

radiation doses (up to 20 cGy). From measurements, the MOSFET dosimeter percentage depth dose response characteristic to the ruthenium-106 applicator was quite similar to that of the applicator manufacturer's ionisation chamber. However, a measurement uncertainty of less than ±5% was obtained. Figure 6.1 shows the on-axis percentage depth dose rate distributions obtained using the TLDs, and the MOSFET dosimeter, with that supplied by the manufacturer.

From all the measurements of the depth dose distributions of ruthenium-106 applicators that were carried out by the two methods used in this thesis it, may be concluded that:

1. Depth dose distributions of ruthenium-106 applicators measurements with the small $CaSO_4$:Dy TLD chips are recommended in the case that the detailed depth dose distributions in both horizontal and vertical planes are required. The excellent dosimetric properties, for example, high radiation dose sensitivity, wide-range of dose response linearity, and good reading reproducibility make TLD discs ideal dosimeters for this purpose. Furthermore, they are also ideal dosimeters for measurements with small radiation sources and small radiation fields as they can be cut into small discs and still have high radiation sensitivity;

2. If a quick on-axis depth dose distribution measurement is required, as in a quality control testing, a MOSFET dosimeter is an alternative dosimeter because of its instant reading, simple set up procedures, high dose response sensitivity and linearity. It can be used for routine quality assurance and for verification of calibration data provided by the manufacturer when an applicator is purchased. However, because of its size, which is larger in comparison to the dimensions of the ruthenium-106 applicators, MOSFET

detector is not suitable for measuring the dose distribution at points other than on the central axis.

In order to improve the precision and accuracy of the two measurement methods the following suggestions are made:

(i) uncertainties of the measurement results in relation to inaccuracy of placement of small $CaSO_4$:Dy TLD chips on the phantom base could be reduced with the aid of transparent self-adhesive tape and well-established gridlines on the phantom base;

(ii) the effective depth of measurement of TLD may be taken into account in order to improve the accuracy of the measurement results obtained from using small $CaSO_4$:Dy TLD chips;

(iii) an appropriate calibration method should be made with the MOSFET dosimeters in order to enable them to be used for measurement of the absolute dose distributions of the ruthenium-106 applicators; and

(iv) in order to improve the accuracy of the measurement results obtained with the MOSFET dosimeter, a correction factor due to temperature dependence of the MOSFET dosimeter should be investigated and applied to the readouts.

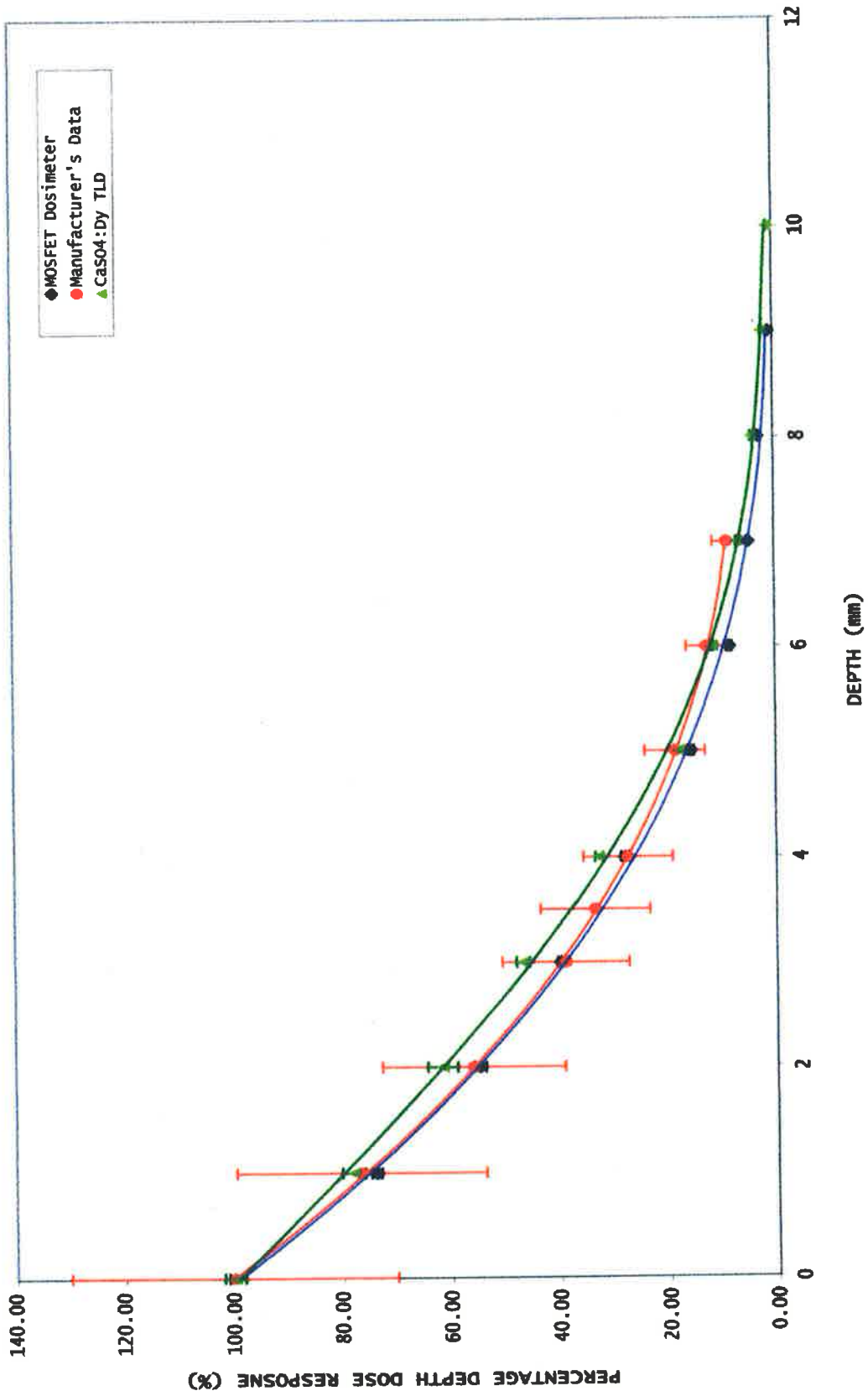

Figure 6.1 The on-axis percentage depth dose rate curves obtained from the measurements using small $CaSO_4$:Dy TLDs, MOSFET dosimeter and that provided by the manufacturer.

Appendix

Table 1 Measurement results of depth dose distribution of the 20-mm ruthenium-106 applicator.

Depth (mm)	Corrected relative dose rate (mGy/min)						Average relative Dose rate (mGy/min)
	1ST Measure-ment	2ND Measure-ment	3RD Measure-ment	4TH Measure-ment	5TH Measure-ment	6TH Measure-ment	
Position: Centre							
0	179.73	171.06	168.71	180.15	187.16	-	177.36
1	140.49	130.57	138.95	130.40	150.73	-	138.23
2	110.05	110.67	108.96	110.92	125.24	88.15	109.00
3	79.01	89.72	78.02	81.65	85.10	-	82.70
4	53.40	57.92	57.85	58.57	61.60	-	57.87
5	31.58	30.43	31.78	27.46	37.37	-	31.73
6	20.80	20.70	21.27	19.24	20.33	-	20.47
7	11.84	12.24	12.29	13.09	11.38	-	12.17
8	7.28	7.84	7.08	7.12	-	-	7.33
9	3.98	4.08	3.68	3.75	3.70	-	3.84
10	1.77	1.80	2.34	1.77	1.98	-	1.99
Position: Top							
1	162.04	146.73	165.26	131.31	154.40	-	151.95
2	138.43	139.22	104.48	122.47	106.30	83.42	115.72
3	66.06	74.62	67.26	64.58	73.69	-	69.24
4	44.50	43.78	45.90	47.60	50.40	-	46.44
5	22.49	21.48	21.50	21.20	26.53	-	22.64
6	12.57	13.50	15.13	12.59	14.14	-	13.59
7	9.21	7.71	9.93	8.94	7.76	-	8.71
8	4.55	5.54	4.72	4.75	-	-	4.89
9	2.65	2.72	2.30	2.81	2.66	-	2.63
10	1.33	0.90	1.40	1.07	1.11	-	1.27
Position: Right							
1	152.99	160.70	164.38	150.85	182.90	-	162.36
2	143.23	144.05	127.34	133.10	156.30	132.25	139.38
3	99.31	116.37	104.03	100.56	126.94	-	109.44
4	62.30	77.08	72.20	91.97	84.02	-	77.51
5	40.66	37.59	34.12	37.10	43.40	-	38.58
6	21.67	24.30	30.73	19.32	26.63	-	24.53
7	14.47	15.42	14.65	15.43	13.01	-	14.60
8	8.19	9.23	8.97	9.49	-	-	8.97
9	4.42	3.63	3.68	4.21	4.33	-	4.05
10	1.77	2.25	2.80	1.95	2.51	-	2.26
Position: Bottom							
1	173.67	141.92	138.95	147.64	157.16	-	151.87
2	98.26	98.81	138.10	129.86	142.71	113.93	119.94
3	98.01	122.59	104.92	106.55	110.77	-	108.57
4	70.76	79.81	71.24	92.09	83.71	-	79.52
5	38.07	40.73	42.53	39.50	49.29	-	42.02
6	28.60	30.61	30.26	27.83	27.85	-	29.03
7	18.41	17.69	16.07	16.94	16.16	-	17.05
8	11.38	9.69	10.85	10.44	-	-	10.59
9	5.30	4.99	5.52	5.15	5.92	-	5.38
10	3.10	3.61	3.74	3.52	3.55	-	3.30

Table 1 Measurement results of depth dose distribution of the 20 mm ruthenium-106 applicator (continue).

Depth (mm)	Corrected relative dose rate (mGy/min)						Average relative Dose rate (mGy/min)
	1ST Measure-ment	2ND Measure-ment	3RD Measure-ment	4TH Measure-ment	5TH Measure-ment	6TH Measure-ment	
Position: Left							
1	161.61	158.52	169.20	148.12	172.33	-	161.96
2	136.68	137.46	129.59	148.81	149.51	120.13	137.03
3	110.53	110.16	102.68	111.63	103.17	-	107.63
4	71.20	77.08	74.59	73.55	90.73	-	77.43
5	44.56	45.20	52.35	43.36	50.24	-	47.14
6	29.04	30.16	29.31	33.75	27.30	-	29.91
7	17.53	17.23	18.91	14.22	16.15	-	16.81
8	10.47	10.15	9.44	9.49	-	-	9.89
9	4.86	5.90	5.99	5.62	5.28	-	5.53
10	3.10	2.71	2.80	2.62	2.67	-	2.85
Position: Top-Right							
1	-	-	-	-	-	-	-
2	-	-	-	-	-	-	-
3	112.69	114.60	102.68	95.48	117.43	-	108.58
4	59.63	69.78	67.42	83.96	70.07	-	70.17
5	33.74	27.75	27.11	30.35	29.83	-	29.76
6	14.74	17.55	21.27	13.81	15.40	-	16.55
7	9.64	9.52	9.93	11.27	9.38	-	9.95
8	5.92	6.00	6.13	6.17	-	-	6.06
9	3.09	2.72	2.30	3.28	2.79	-	2.84
10	0.89	1.35	1.87	0.92	1.47	-	1.39
Position: Bottom-Right							
1	-	-	-	-	-	-	-
2	-	-	-	-	-	-	-
3	115.71	138.58	124.20	118.09	137.87	-	126.89
4	65.42	88.48	80.33	101.33	91.57	-	85.43
5	44.56	42.96	42.07	45.77	52.73	-	45.62
6	26.44	27.46	34.04	25.49	30.10	-	28.71
7	16.22	17.69	14.18	17.88	13.87	-	15.97
8	10.01	8.76	10.85	10.91	-	-	10.13
9	5.30	3.63	4.60	4.68	4.13	-	4.47
10	2.22	3.61	3.74	3.05	3.78	-	3.04
Position: Bottom-Left							
1	-	-	-	-	-	-	-
2	-	-	-	-	-	-	-
3	101.47	135.03	118.82	134.69	127.89	-	123.58
4	101.46	99.88	91.80	104.33	108.86	-	101.27
5	51.48	53.26	61.70	53.47	61.40	-	56.26
6	35.11	36.91	34.98	40.76	36.97	-	36.94
7	21.48	20.86	18.91	15.78	17.93	-	18.99
8	14.11	10.15	11.80	11.39	-	-	11.86
9	6.18	5.90	6.91	5.62	5.50	-	6.02
10	3.55	3.61	3.27	3.88	3.76	-	3.47

Table 1 Measurement results of depth dose distribution of 20 mm ruthenium-106 applicator (continue).

Depth (mm)	Corrected relative dose rate (mGy/min)						
	1ST Measure-ment	2ND Measure-ment	3RD Measure-ment	4TH Measure-ment	5TH Measure-ment	6TH Measurem ent	Average relative Dose rate (mGy/min)
Position: Top-Left							
1	-	-	-	-	-	-	-
2	-	-	-	-	-	-	-
3	131.69	115.49	109.86	119.01	105.55	-	116.32
4	86.33	85.74	75.54	85.00	96.94	-	85.91
5	43.26	42.96	46.74	40.95	38.50	-	42.48
6	21.24	23.40	25.53	25.48	22.22	-	23.57
7	15.34	12.70	15.13	11.48	11.36	-	13.20
8	6.83	6.92	7.08	7.12	-	-	6.99
9	3.53	3.63	4.14	4.21	3.58	-	3.82
10	1.77	1.35	1.87	1.62	1.50	-	1.81

References

Attix, F.H. (1986). *Introduction to Radiological Physics and Radiation Dosimetry*. John Wiley & Sons, Inc.: Toronto, Canada.

Barthe, J. (2001). Electronic Dosimeters Based on Solid State Detectors. *Nuclear Instruments and Methods in Physics Research*, **184,** 158-189.

Bilski, P., Olko, P., Burgkhardt, B. & Piesch, E. (1995). Ultra-thin LiF:Mg,Cu,P Detectors for Beta Dosimetry. *Radiation Measurements*, **24,** 439-443.

Chan, M.F., Fung, A.Y., Hu, Y.C., Hui, C.S., Amols, H., Zaider, M. & Abramson, D. (2001). The Measurement of Three Dimensional Dose Distribution of A Ruthenium-106 Ophthalmological Applicator Using Magnetic Resonance Imaging of BANG Polymer Gels. *Applied Clinical Medical Physics*, **2,** 85-89.

Cohen, G., Lovelock, M., Amols, H., Losasso, T., Zaider, M. & Abramson, D. (2000). Dosimetric Analysis of Ruthenium-106 Ophthalmic Applicators for The Treatment of Retinoblastoma and Ocular Melanoma. In *The 22nd Annual International Conference of The IEEE Engineering in Medicine and Biology Society*, Enderle, J.D. (ed), Vol. 4. pp. 2757-2760: U.S.A.

Contento, G., Malisan, M.R. & Padovani, R. (1984). Response of Thermoluminescence Dosemeters to Beta Radiation and Skin Dose Assessment. *Physics in Medicine and Biology*, **29,** 661-678.

Crawford, R.H. (1967). *MOSFET in Circuit Design*. McGraw-Hill Book Company: New York, U.S.A.

Cross, W.G., Hokkanen, J., Jarvinen, H., Mourtada, F., Sipila, P., Soares, C.G. & Vynckier, S. (2001). Calculation of Beta-Ray Dose Distributions from Ophthalmic Applicators and Comparison with Measurements in A Model Eye. *Medical Physics*, **28,** 1385-1396.

Daltro, T.F.L., Campos, L.L. & Perez, H.E.B. (1999). Thermoluminescence Dosimeter for Equivalent Dose Assessment in Mixed Beta and Gamma Field. *Radiation Protection Dosimetry*, **85,** 145-148.

Davelaar, J., Schaling, D.S., Hennen, L.A. & Broerse, J.J. (1992). Dosimetry of Ruthenium-106 Eye Applicators. *Medical Physics*, **19,** 691-695.

Deogracias, E.C., Wood, J.L., Wagner, E.C. & Kearfott, K.J. (1999). Polynomial Expressions of Electron Depth Dose As A Function of Energy in Various Materials: Application to Thermoluminescence Dosimetry. *Nuclear Instruments and Methods in Physics Research (A)*, **422,** 629-637.

Dimitrijev, S. (2000). *Understanding Semiconductor Devices*. Oxford University Press, Inc.: New York, U.S.A.

Edwards, C.R., Green, S., Palethorpe, J.E. & Mountford, P.J. (1997). The Response of a MOSFET, P-Type Semiconductor and LiF TLD to Quasi-monoenergetic X-Rays. *Physics in Medicine and Biology*, **42,** 2383-2391.

Fellinger, J., Schmidt, P. & Hubner, K. (1990). Beta Dosimetry Using Thin TL Dectectors. *Radiation Protection Dosimetry*, **34,** 135-136.

Francescon, P., Cora, S., Cavedon, C., Scalchi, P., Reccanello, S. & Colombo, F. (1998). Use of a New Type of Radiochromic Film, a New Parallel Plate Micro-chamber, MOSFETs and TLD 800 Microtubes in Dosimetry of Small Beams. *Medical Physics*, **25,** 503-511.

Francis, T.M. & Driscoll, C.M.H. (1985). Thermoluminescence Beta Dosimetry. *Radiological Protection Bulletin*, **65,** 26-29.

Francis, T.M., O'Hagan, J.B., Williams, S.M., Driscoll, C.M.H. & Barlett, D.T. (1989). Response Characteristics of Carbon-loaded TL Detectors to Beta Radiation. *Radiation Protection Dosimetry*, **28**, 201-205.

Gelev, M., Spurny, F. & Votockova, I. (1991). Measurement of Beta Radiation Using Graphite-mixed Thermoluminescence $CaSO_4$:Dy. *Nuclear Tracks and Radiation Measurements*, **18,** 355-356.

Gladstone, D.J. & Chin, L.M. (1991). Automated Data Collection and Analysis System for MOSFET Radiation Detectors. *Medical Physics*, **18,** 542-548.

Gladstone, D.J. & Chin, L.M. (1995). Real-time, *in vivo* Measurement of Radiation Dose During Radioimmunotherapy in Mice Using a Miniature MOSFET Dosimeter Probe. *Radiation Research*, **141**, 330-335.

Gladstone, D.J., Lu, X.Q., Humm, J.L., Bowman, H.F. & Chin, L.M. (1994). A Miniature MOSFET Radiation Dosimetric Probe. *Medical Physics*, **21,** 1721-1728.

Hjortenberg, P., Hansen, J.W. & Wille, M. (1989). Measurement of Dose Rate from $^{106}Ru/^{106}Rh$ Ophthalmic Applicators by Means of Alanine-Polymer Foils. *Applied Radiation and Isotope*, **40,** 997-1001.

Horowitz, Y.S. (1984a). *Thermoluminescence and Thermoluminescent Dosimetry*. Vol. I. CRC Press, Inc.: Boca Raton, U.S.A.

Horowitz, Y.S. (1984b). *Thermoluminescence and Thermoluminescent Dosimetry*. Vol. II. CRC Press, Inc.: Boca Raton, U.S.A.

Horowitz, Y.S. (1984c). *Thermoluminescence and Thermoluminescent Dosimetry*. Vol. III. CRC Press, Inc.: Boca Raton, U.S.A.

ICRU. (1988). Tissue Substitutes in Radiation Dosimetry and Measurement. In *International Commission on Radiation Units and Measurements (ICRU)* pp. 25, 27, 31. ICRU: Bethesda, Maryland.

Jain, V.K. (1978). Graphite-Mixed $CaSO_4$:Dy for Beta Dosimetry. *Physics in Medicine and Biology*, **23,** 1000-1001.

Jones, A.R. & Sanders, J.M. (1986). A New Solid State Beta Dosemeter. *Radiation Protection Dosimetry*, **17,** 105-109.

Josef Novotny, J., Spevacek, V., Dvorak, P., Novotny, J. & Cechak, T. (2001). Energy and Dose Rate Dependence of BANG-2 Polymer Gel Dosimeter. *Medical Physics*, **28,** 2379-2386.

Kaplan, G.I., Rosenfeld, A.B., Allen, B.J., Carolan, M.G. & Holmes-Siedle, A. (2000). Improved Spatial Resolution by MOSFET Dosimetry of an X-Ray Microbeam. *Medical Physics*, **27,** 239-244.

Kathren, R.L. (1987). External Beta-Photon Dosimetry for Radiation Protection. In *The Dosimetry of Ionizing Radiation*, Kase, K.R., Bjarngard, B.E. & Attix, F.H. (eds), Vol. II. pp. 321-363. Academic Press, Inc.: Orlando, Florida.

Kelly, M.T. & Beddoe, A.H. (1992). Beta Dosimetry at Surface of Cylindrical Container. *Physics in Medicine and Biology,* 37, 421-437.

Kron, T., Duggan, L., Smith, T., Rosenfeld, A.B., Butson, M., Kaplan, G.I., Howlett, S. & Hyodo, K. (1998). Dose Response of various Radiation Detectors to Synchrotron Radiation. *Physics in Medicine and Biology*, **43,** 3235-3259.

Kron, T. (1999). Applications of Thermoluminescence Dosimetry in Medicine. *Radiation Protection Dosimetry*, **85,** 333-340.

Lakshmanan, A.R., Popli, K.L. & Bhatt, R.C. (1979). Thermal History and Reuability of $CaSO_4$:Dy Teflon TLD Discs. *Physics in Medicine and Biology*, **24,** 999-1008.

Lakshmanan, A.R. & Madhusoodanan, U. (1998). Behaviour of $CaSO_4$:Dy Embedded Teflon Discs at High Annealing Temperatures. *Radiation Measurements*, **29,** 527-530.

REFERENCES

Luguera, E., Fernandez, F., Planas, J., Dahabi, K.E., Bruguier, G., Daoud, M. & Gasiot, J. (1990). Thin $CaSO_4$:Dy for Beta Dosimetry. Grain Size and Energy Dependence. *Radiation Protection Dosimetry*, **33,** 207-9.

Mathur, V.K., Lewandowski, A.C., Guardala, N.A. & Price, J.L. (1999). High Dose Measurement Using Thermoluminescence of $CaSO_4$:Dy. *Radiation Measurements*, **30,** 735-738.

McKeever, S.W.S. (1985). *Thermoluminescence of solids*. Cambridge University Press: Cambridge.

McKeever, S.W.S., Moscovitch, M. & Townsend, P.D. (1995). *Thermoluminescence Dosimetry Materials: Properties and Uses*. Nuclear Technology Publishing: England.

Mobit, P.N., Nahum, A.E. & Mayles, P. (1998). A Monte Carlo Study of The Quality Dependence Factors of Common TLD Materials in Photon and Electron Beams. *Physics in Medicine and Biology*, **43,** 2015-2032.

Oberhofer, M. (1991). *Advances in Radiation Protection*. Kluwer Academic Publishers: Dordrecht, Netherlands.

Peet, D.J. & Pryor, M.D. (1999). Evaluation of a MOSFET Radiation Sensor for the Measurement of Entrance Surface Dose in Diagnostic Radiology. *The British Journal of Radiology*, **72,** 562-568.

Piessens, M. & Raynaert, N. (2000). Verification of Absolute Dose Rates for Intravascular Brachytherapy Beta Sources. *Physics in Medicine and Biology*, **45,** 2219-2231.

Pradhan, A.S. & Bhatt, R.C. (1977). Graphite-Mixed $CaSO_4$:Dy Teflon TLD Discs for Beta Dosimetry. *Physics in Medicine and Biology*, **22,** 873-879.

Pradhan, A.S. (1993). Emission Spectra and Influence of Sunlight on Thermoluminescence of Dysprosium Doped $CaSO_4$ and CaF_2. *Radiation Protection Dosimetry*, **47,** 151-154.

Prokic, M.S. (1985). Beta Dosimetry with Newly Developed Graphite Mixed TL Detectors. *Physics in Medicine and Biology*, **30,** 323-329.

Ramani, R., Russell, S. & O'Brien, P. (1997). Clinical Dosimetry Using MOSFETs. *International Journal of Radiation Oncology, Biology, Physics*, **37,** 959-964.

Robertson, M.E.A. (1981). *Identification and Reduction of Errors in Thermoluminescence Dosimetry System*. D.A. Pitman Ltd.: Surrey, England.

Rosenfeld, A.B., Kaplan, G.I., Kron, T., Allen, B.J., Dilmanian, A., Orion, I., Ren, B., Lerch, M.L.F. & Holmes-Siedle, A. (1999). MOSFET Dosimetry of An X-Ray Microbeam. *IEEE Transactions on Nuclear Science*, **46,** 1774-1780.

Sanchez-Reyes, A., Tello, J.J., Guix, B. & Salvat, F. (1998). Monte Carlo Calculation of The Dose Distributions of Two Ruthenium-106 Eye Applicators. *Radiotherapy and Oncology*, **49,** 191-196.

Sarrabayrouse, G. & Siskos, S. (1998). Radiation Dose Measurement Using MOSFETs. In *IEEE Instrumentation & Measurement Magazine*, Vol. 1. pp. 26-34.

Shields, C.L., Shields, J.A., Cater, J., Gunduz, K., Miyamoto, C., Micaily, B. & Brady, L.W. (2000). Plaque Radiotherapy for Uveal Melanoma: Long-Term Visual Outcome in 1106 Consecutive Patients. *Archives of Ophthalmology*, **118,** 1219-1228.

Soares, C.G., Vynckier, S., Jarvinen, H., Cross, W.G., Sipila, P., Fluhs, D., Schaeken, B., Mourtada, F.A., Bass, G.A. & Williams, T.T. (2001). Dosimetry of Beta-Ray Ophthalmic Applicators: Comparison of Different Measurement Methods. *Medical Physics*, **16,** 902-904.

Souza, J.H., de Rosa, L.A.R. & Muaricio, C.L.P. (1993). On the Thermoluminescence Glow Curve of $CaSO_4$:Dy. *Radiation Protection Dosimetry*, **47,** 103-106.

Thomas, S.J. & Palmer, N. (1989). The Use of Carbon-Loaded Thermoluminescent Dosimeters for the Measurement of Surface Doses in Megavoltage X-Ray Beams. *Medical Physics*, **16,** 902-904.

Uchrin, G. (1986). Beta Dosimetry: Different Solutions. *Radiation Protection Dosimetry*, **17,** 99-104.

Vohra, K.G., Pradhan, A.S. & Bhatt, R.C. (1982). X- and Gamma Ray Response of a TLD Badge Based on $CaSO_4$:Dy Teflon TLD Discs. *Health Physics*, **43,** 391-397.

Vynckier, S. & Wambersie, A. (1986). Dosimetry of Beta Sources in Radiotherapy: Absorbed Dose Distribution around Plane Sources. *Radiation Protection Dosimetry*, **14,** 169-173.